

University of Nebraska - Lincoln

DigitalCommons@University of Nebraska - Lincoln

---

Mechanical (and Materials) Engineering --  
Dissertations, Theses, and Student Research

Mechanical & Materials Engineering,  
Department of

---

Spring 5-2012

## A Conductivity Testing System Coupled with a Tensile Testing Machine to Measure the Surface Properties of Polymer Specimens

Nguyen T. Nguyen

University of Nebraska-Lincoln, nguyenthaonguyen@gmail.com

Follow this and additional works at: <https://digitalcommons.unl.edu/mechengdiss>



Part of the [Applied Mechanics Commons](#), and the [Polymer and Organic Materials Commons](#)

---

Nguyen, Nguyen T., "A Conductivity Testing System Coupled with a Tensile Testing Machine to Measure the Surface Properties of Polymer Specimens" (2012). *Mechanical (and Materials) Engineering -- Dissertations, Theses, and Student Research*. 35.  
<https://digitalcommons.unl.edu/mechengdiss/35>

This Article is brought to you for free and open access by the Mechanical & Materials Engineering, Department of at DigitalCommons@University of Nebraska - Lincoln. It has been accepted for inclusion in Mechanical (and Materials) Engineering -- Dissertations, Theses, and Student Research by an authorized administrator of DigitalCommons@University of Nebraska - Lincoln.

A CONDUCTIVITY TESTING SYSTEM COUPLED WITH A TENSILE TESTING MACHINE TO MEASURE THE  
SURFACE PROPERTIES OF POLYMER SPECIMENS

by

Nguyen Thao Nguyen

A THESIS

Presented to the Faculty of

The Graduate College at the University of Nebraska

In Partial Fulfillment of Requirements

For the Degree of Master of Science

Major: Mechanical Engineering

Under the Supervision of Professor Carl A. Nelson

Lincoln, Nebraska

May, 2012

A CONDUCTIVITY TESTING SYSTEM COUPLED WITH A TENSILE TESTING MACHINE TO MEASURE THE  
SURFACE PROPERTIES OF POLYMER SPECIMENS

Nguyen Thao Nguyen, M.S.

University of Nebraska, 2012

Advisor: Carl A. Nelson

Polymers play an essential role in our everyday life due to their employment in a widespread range of applications. Polymers are used in industries such as space, biomedical, electronics, etc. in which their electrical and mechanical properties are major aspects which need to be investigated prior to implementation. When subjected to mechanical stimulations, polymers may exhibit changes in electrical conductivity which can vary locally within the specimens, especially in those of conducting polymers. In mechanical investigations a tensile testing machine is used to understand polymers' strength, elasticity or other mechanical properties. In electrical analysis, using a four-point probe to examine the electrical resistivity (conductivity) of a material is also frequently applied. However, no studies have been done to explore the relationship between mechanical manipulations and changes in electrical properties in situ. The current study explores this relationship.

An electrical conductivity testing system is designed and developed to couple with a tensile testing machine to measure the electrical conductivity of polymeric specimens while experiencing tensile loading. The system features a commercial four-point probe sensor, which is automatically controlled to approach a specimen and to measure the electrical conductivity of that specimen locally in two directions: longitudinally and transversely to the axis of stress. The method of testing is then

implemented to experiment on specimens of high density polyethylene. Other types of specimens such as carbon nanotubes/polyethylene composites and metallic surface layer deposited polyethylene are also tested. Descriptions of the development process of the robotic systems and results of the execution are presented.

## Acknowledgement

I would like to express my gratitude to the following persons for their constant support throughout this project:

Dr. Carl Nelson for his sincere support, encouragement, and supervision on this project. This project would not have been possible if there were not his constant guidance and thoughtful remarks.

Dr. Mohamed Benzohra for his support and time spent on this project. Throughout the process of synchronizing the CTS and Instron® system, he has helped constantly with technical difficulties and troubleshooting. He also has helped in data rationale and project strategy.

Dr. Jean-Marc Saiter for his thoughtful inputs and guidance. This project was possible because of his support for the project to be performed in his directed laboratory.

Dr. Mehrdad Negahban for his thoughtful comments from time to time.

Jeff Midday and S.G.M. Hossain for their help during the beginning of the project by mentoring, instructing in machining processes, preliminary data collection and their thoughtful inputs throughout.

Peter Pellegrino for his help in improving the codes for the Arduino board.

Eric Donzoff for his help in machining some additional hardware for the CTS, setting up the Instron® and manufacturing samples.

Members of Dr. Nelson's laboratory for help in brainstorming and always giving sincere suggestions and comments.

Members of LECAP laboratory for helping with experimental procedures.

UNL Machine Shop for machining of some parts of the CTS device.

Nan Rowe, Kathie Hiatt, and Alicia Harvey for material orders and other support.

EU-US Atlantis Program for the opportunity to collaborate with LECAP laboratory in Rouen, France.

NASA Nebraska Space Grant for funds supporting portions of this project.

Office of Graduate Studies, University of Nebraska-Lincoln for reviewing the thesis.

Family members and friends for their earnest encouragement all through the master's program.

## Table of Contents

Acknowledgement .....	iv
List of Figures .....	vii
List of Tables .....	x
CHAPTER 1: INTRODUCTION .....	1
CHAPTER 2: BACKGROUND .....	3
2.1 Understanding Fundamental Properties of Materials .....	3
2.1.1 Mechanical Properties of Materials.....	3
2.1.2 Electrical Properties of Materials.....	8
2.2 Materials, Applications, and Current Issues .....	9
2.2.1 Materials in Aerospace Applications.....	9
2.2.2 Materials in Biomedical Applications.....	11
2.2.3 Materials in Electronic Applications .....	14
2.3 Objectives.....	16
PART A: THE DESIGN .....	17
CHAPTER 3: DEVELOPMENT OF THE CONDUCTIVITY TESTING SYSTEM (CTS).....	17
3.1 Overview of the System Mechanics.....	17
3.1.1 Instron® 3365.....	17
3.1.2 The Conductivity Testing System (CTS).....	21
3.2 The Design.....	22
3.2.1 Overview .....	22
3.2.2 Material Selection .....	23
3.2.3 Linear Guide Carriage.....	23
3.2.4 Sensor Bracket .....	28
3.2.5 Plates.....	31
3.2.6 Clamping to Instron® 3365.....	35
3.3 Final Assembly.....	37
CHAPTER 4: SYSTEM CONTROL.....	39

4.1 Design Requirements .....	39
4.2 Microcontroller System.....	40
4.2.1 Ruggeduino .....	42
4.2.2 Motor shield.....	42
4.2.3 Power supply.....	43
4.2.4 Relay.....	44
4.2.5 Microswitches .....	44
4.2.6 Assembly.....	45
4.2.7 Programming.....	46
4.3. Data Acquisition System.....	47
4.3.1 Keithley 6415 Programmable Picoammeters .....	47
4.3.2 ELC DC Power Supply AL 991S.....	47
4.3.3 TestPoint™ .....	47
4.4 System Assembly .....	49
PART B: THE EXPERIMENT.....	51
CHAPTER 5: EXPERIMENTAL TESTING ON POLYMERS .....	51
5.1 Materials and Methods.....	51
5.1.1 Silicon wafers .....	51
5.1.2 High Density Polyethylene (HDPE) .....	53
5.1.3 Polyethylene/Carbon Nanotubes Composite .....	54
5.1.4 Polyethylene with metallic surface layers .....	55
5.2 Four-Point Probe Sensor .....	58
5.2.1 Four-Point Probe Characteristics .....	58
5.2.2 Four-Point Probe Theory.....	61
5.2.3 Experimental Setup.....	63
5.3 Results and Discussions .....	66
CHAPTER 6: CONCLUSION AND FUTURE WORK .....	84
REFERENCES.....	88
APPENDIX A:.....	95
Engineering Drawings .....	95
APPENDIX B:.....	107
Technical Details of Commercial Components .....	107

## List of Figures

Figure 2.1: Charpy and Izod test [69].....	4
Figure 2.2: A creep test diagram [70].....	5
Figure 2.3: A tensile test diagram [71].....	5
Figure 2.4: A common stress/strain curve [72].....	6
Figure 2.5: Transition from stable to sharkskin extrudate [4] .....	7
Figure 2.6: NASA composite pressure vessels in space applications [73] .....	10
Figure 2.7: A knee implant with plastic surface [76].....	13
Figure 2.8: Integrated circuit on a flexible plastic substrate [74] .....	14
Figure 2.9: Schematic of a top-contact PTV OFET [26] .....	15
Figure 2.10: Flexible and bendable plastic electronic [75] .....	15
Figure 3.1: Schematic of Instron® 3365 [33].....	18
Figure 3.2: Relevant dimensions of Instron® 3365 for design of CTS [33].....	20
Figure 3.3: Overview of CTS coupling with the Instron®21 .....	21
Figure 3.4: The conductivity testing system CTS .....	22
Figure 3.5: Linear guide model from McMaster-Carr [34].....	24
Figure 3.6: Design of linear guide (side view) .....	26
Figure 3.7: Design of linear guide (top view) .....	26
Figure 3.8: Design of linear guide (isometric view).....	26
Figure 3.9: Signatone four-point probe [35].....	28
Figure 3.10: Overview of the sensor bracket.....	29
Figure 3.11: Motor shaft coupler .....	30
Figure 3.12: Mounting base .....	30
Figure 3.13: Front plate .....	31
Figure 3.14: Back plate .....	32



Figure 3.15: Front and back plates when connected .....	32
Figure 3.16: Schematic of experimental setup (top view) .....	33
Figure 3.17: The plate system can be adjusted for specimens .....	34
Figure 3.18: The clamping system and its components .....	36
Figure 3.19: Final assembly of CTS .....	37
Figure 3.20: CTS coupled with Instron® 3365 .....	38
Figure 4.1: Circuit diagram of microcontrolling system .....	41
Figure 4.2: Ruggeduino [40] .....	42
Figure 4.3: Motor shield [42] .....	43
Figure 4.4: 5V Power supply [43] .....	43
Figure 4.5: LCA 710 Relay [44] .....	44
Figure 4.6: Relay wiring diagram [44] .....	44
Figure 4.7: Microswitch [45] .....	44
Figure 4.8: Assembly of microcontroller system .....	45
Figure 4.9: Flowchart of Arduino programming .....	46
Figure 4.10: Diagram of DAQ system .....	48
Figure 4.11: Complete assembly of the control system .....	49
Figure 5.1: Carbon nanotube composite manufacturing procedure .....	55
Figure 5.2: a) PEPP with chromium deposited surface; b) CERAC silver epoxy cement and catalyst .....	56
Figure 5.3: HDPE specimen with silver/ethanol evaporated coating .....	57
Figure 5.4: Four-point probe diagram [51] .....	59
Figure 5.5: FPP test results of silicon $0.0038\Omega\cdot\text{cm}$ .....	66
Figure 5.6: FPP test results of silicon $3.45\ \Omega\cdot\text{cm}$ .....	67
Figure 5.7: FPP test results of silicon $3000\ \Omega\cdot\text{cm}$ .....	68
Figure 5.8: a ) Stress/strain curve for a HDPE specimen and b) the specimen ruptured after 15% of deformation .....	69
Figure 5.9: Electrical resistivity of a composite with different content of CNTs [67] .....	70
Figure 5.10: Electrical resistivity with different content of CNTs [66] .....	71

Figure 5.11: Surface of chromium deposited specimen after FPP test under Optic Microscopy .....	73
Figure 5.12: Results for PEPP silver pasted surface .....	74
Figure 5.13: FPP test results for HDPE silver coated specimen .....	77
Figure 5.14: Specimen under FPP and tensile test .....	78
Figure 5.15: FPP test results of HDPE silver painted .....	80
Figure 5.16: Reload test for HDPE/Silver paint .....	81
Figure 5.17: Result of FPP for hysteresis loops .....	82

## List of Tables

Table 2.1: Common polymers and their applications in biomedical engineering [14].....	12
Table 3.1: Relevant dimensions of Instron® 3365 [33] .....	19
Table 5.1: Characteristics of silicon wafers .....	51
Table 5.2: recommended current inputs for FPP test [9] .....	52
Table 5.3: Silicon test parameters .....	53
Table 5.4: Configuration of the Signatone Four-Point-Probe [35] .....	61
Table 5.5: Reading ranges of ELC power supply [48].....	64
Table 5.6: Results of silicon wafers tests with FPP .....	68

## CHAPTER 1: INTRODUCTION

Polymers, when subjected to mechanical loading, exhibit change in morphological and structural molecular organization [1]. As a unidirectional stress is applied on a polymeric specimen under a tensile test, there is reorganization in the molecular structures which results in changes in morphology. For example, a stretch occurs to the polymer chain in the longitudinal direction while a compression occurs in the transverse direction to the axis of stress. Other modifications exerted on specimens can include fractures and also surface modifications. As these modifications begin to occur primarily at the molecular level, it is reasonable that measuring the surface properties of a loaded specimen would become a potential tool to analyze such structural modification, regarding polymeric materials commonly known as non-conductive or insulating materials.

Polymers have been widely used in many applications, such as biomedical applications, packaging, aerospace applications and many others [14-18]. Biomedical applications of polymers include uses in prosthetics, various implants, hydrogels in drug delivery and pharmaceuticals, scaffolds for tissue growth, etc. Polymers are also used in composites to manufacture different components in aerospace vehicles, including composite overwrapped pressure vessels for space vehicles. Recently, polymers are becoming incorporated widely in producing organic electronic devices such as organic transistors in electrical circuits. Although the polymers used in different applications are designed, synthesized, and manufactured using different methods to produce various configurations, compositions, and functions, the majority of these applications expose polymers to mechanical stimulation of some sort. For instance, polymers used in knee or hip implants are subjected to high stresses over a long lifetime. Polymers used in space applications (e.g., pressure vessels) can obviously undergo a significant stress history during long-term flights. Also, in plastic electronic devices, a thin film containing a circuit with a

polymeric component needs to be bendable and flexible to be incorporated into the devices. In short, mechanical stimulations to polymers are the norm. Moreover, mechanical stimulations in materials tend to generate changes in electrical properties of the materials as well; here the focus is on the electrical resistivity (conductivity) of the polymers.

Not many studies have been done to study the relationship between mechanical loading and electrical behavior of polymeric materials in real time. This thesis aims to introduce a pioneering method to study such relationships. A conductivity testing system is designed and built for synchronous use with a universal tensile testing machine to measure the electrical resistivity of polymeric specimens via a four-point-probe method while being loaded in situ. Experiments using this method are applied to different types of samples to understand the electrical-mechanical relationship.

This thesis presents the project in two different parts. Part A presents the design and manufacturing process of the conductivity testing system. This part consists of the development of the hardware system and the control system. The work for this part was mainly conducted at the University of Nebraska-Lincoln campus. After the hardware was built, integration with the universal testing machine was done at AMME – LECAP – UNL Laboratory.

Part B of the thesis was also performed at Rouen, France. This part begins with the introduction of materials selected to perform the experiments. It also includes description of the method of four-point-probe conductivity testing. Many different types of materials and surface preparations are also incorporated in this part. Experimental results and discussions of each test are the main focus for this part of the thesis.

## CHAPTER 2: BACKGROUND

### 2.1 Understanding Fundamental Properties of Materials

#### 2.1.1 Mechanical Properties of Materials

The mechanical properties of materials, their strength, rigidity and ductility, are very important in determining their fabrication and possible practical applications [2]. In every practical application, the questions about the materials being used are always among the first to be considered: how strong, stiff, ductile, tough, or hard does the material need to be to satisfy the functional needs? These types of questions need to be answered before the material is selected to service the functions required.

In order to understand the properties of each material prior to its usage, the results of mechanical tests of the materials must be obtained. There are many techniques available to discover the mechanical properties of each material. Each technique is different to appropriately match the type of material. Common techniques are classified into six categories: impact test, creep test, hardness test, fatigue test and tensile test [3]. To have a better understanding of each mechanical test, two common parameters should be mentioned. Engineering stress and engineering strain are defined by the following equations:

$$\text{Engineering Stress} = \sigma = \frac{F}{A_0} \quad (1)$$

$$\text{Engineering Strain} = \varepsilon = \frac{l - l_0}{l_0} \quad (2)$$

where  $A_0$  is the original cross-sectional area,  $l_0$  is the original length, and  $l$  is the length after the force  $F$  is applied.

The impact test is often used to evaluate the brittleness of a material under a sudden, intense blow in which the strain rate is extremely rapid. The two common impact tests are the Charpy test and the Izod test shown in Figure 2.1. In these tests, a heavy pendulum starts at an initial elevation and swings

through to break a specimen, and reach a lower final elevation. The difference in potential energy can be calculated, and the difference is the impact energy absorbed by the specimen. From there, one can understand the toughness of the material, which is the ability of the material to absorb energy in an impact.

Fatigue testing is used to characterize the mode of failure known as fatigue in a material. A common fatigue test involves a specimen being subjected to repeated stress which is below the yield strength of

the material. Even though the stress is below the yield

strength, the material may fail after many cyclic recurrences of the application of stress, which can be in the form of rotation, bending, or even vibration.

Plastic deformation of a material at high temperatures is known as creep. In Figure 2.2, a creep test usually involves a constant stress applied to the specimen. The resulting combination of elastic and plastic stretch depends on the applied stress and the modulus of elasticity of the material. The creep test can be used to estimate the expected lifetime of a component or a composite under particular combinations of stress and temperature.

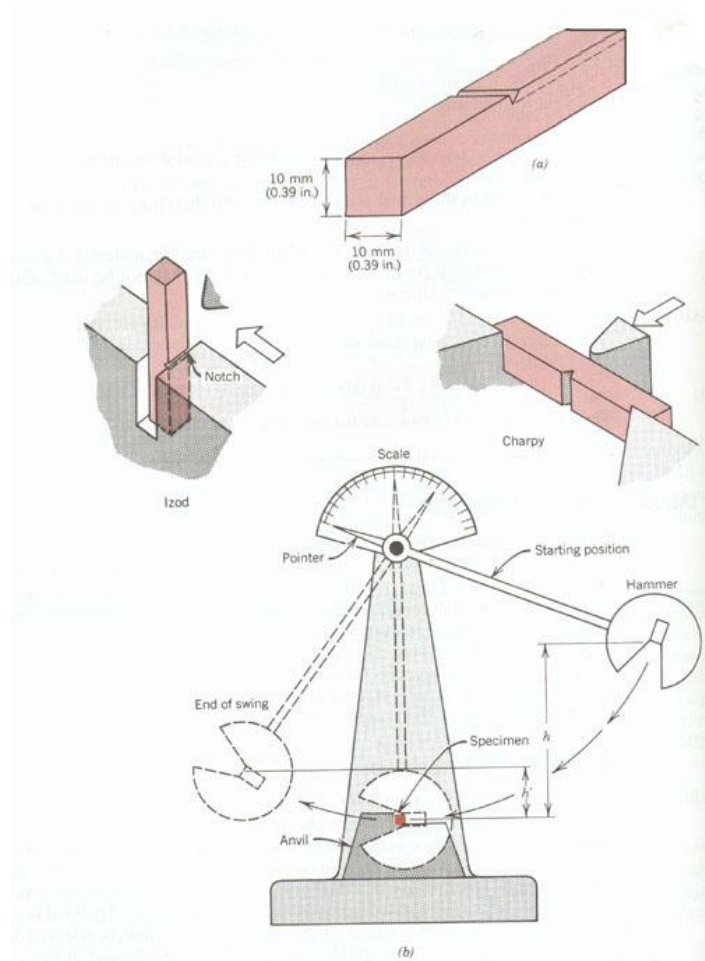


Figure 2.1: Charpy and Izod test [69]

Hardness can be described as the resistance of the material to wear, cutting, machining, or scratching, etc. Hardness is not an invariant property of a material since the result is different for each method of testing. However, using one method of hardness testing on different materials, one can compare the materials and provide recommendations for manufacturing, heat treatment or quality controls. It can be observed that polymer materials are typically soft, metals have an intermediate hardness, and ceramics are exceptionally hard.

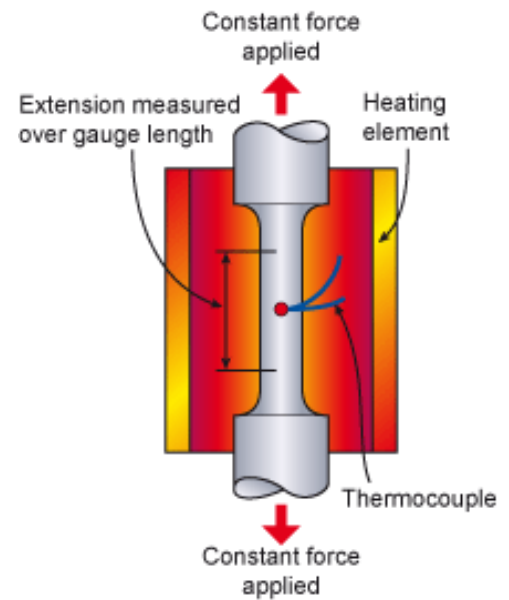


Figure 2.2: A creep test diagram [70]

Finally, tensile testing is the most common mechanical test and is done with many types of materials. The results of this type of test also provide a wide range of knowledge about the tested material. For the purpose of this project, the tensile test plays a very important role and is described in detail below.

A tensile test is performed as a normal stress is applied to a specimen and the resistance of the material to this stress is measured. The test is commonly executed as shown in Figure 2.3:

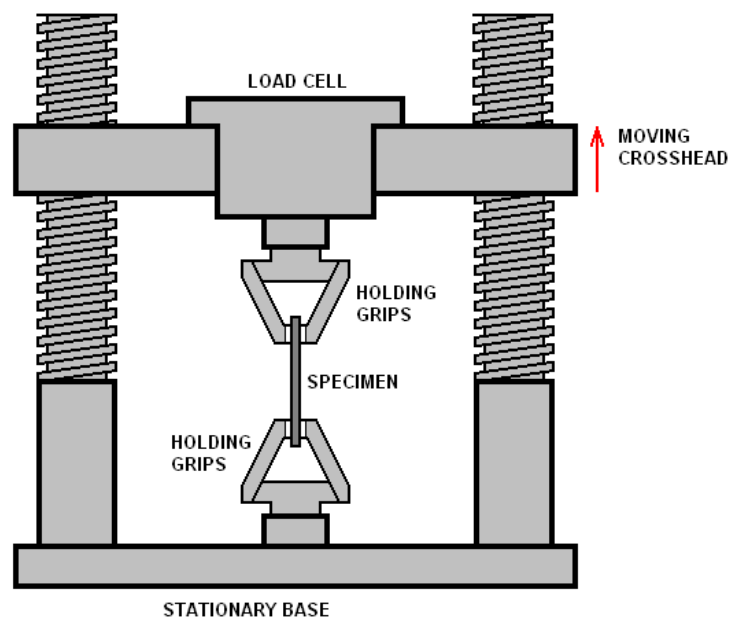


Figure 2.3: A tensile test diagram [71]



A force  $F$  is applied unidirectionally to the specimen. The force is known and monitored to obtain the stress rate. A strain gauge or an extensometer is used to measure the displacement of the specimen to obtain the strain rate. A stress-strain curve is then generated. This curve is a very crucial tool to understand the behavior of a material under loading conditions. The typical stress-strain curve for ductile elastic materials looks as follows:

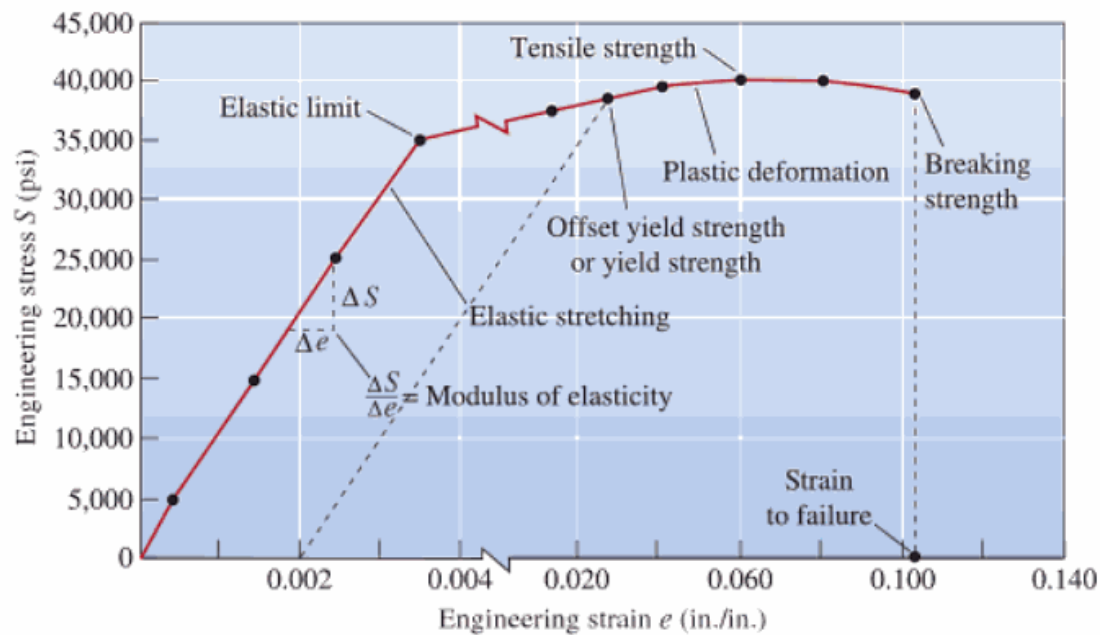


Figure 2.4: A common stress/strain curve [72]

Important properties regarding the material being tested can be obtained by this curve.

Modulus of elasticity is a fundamental property for each material, commonly known as Young's modulus  $E$ . It is used to describe how stiff a material is. The Young's modulus is defined as the stress divided by the strain at the elastic limit, and thus it is also the slope of the stress-strain curve in the elastic region.

$$E = \frac{\sigma}{\varepsilon}$$

(3)

The higher the modulus  $E$ , the steeper the slope, and the stiffer the material is. By understanding the stiffness of each material, one can use the material properly to acquire the desired functionality, especially in terms of force-deflection behavior of components on the macro scale.

Another important property that can be obtained by the tensile test is yield strength. Yield strength is the stress where the strain rapidly increases with increasing stress. The slip in the (crystalline) material structure becomes noticeable and irreversible. This is also entering the plastic region. In engineering applications, yield strength is often considered the static stress limit that a material can handle.

Depending on the deformation speed, a phenomenon called sharkskin can occur on the surface of the sample, generally during the extrusion process [4] shown in Figure 2.5. During

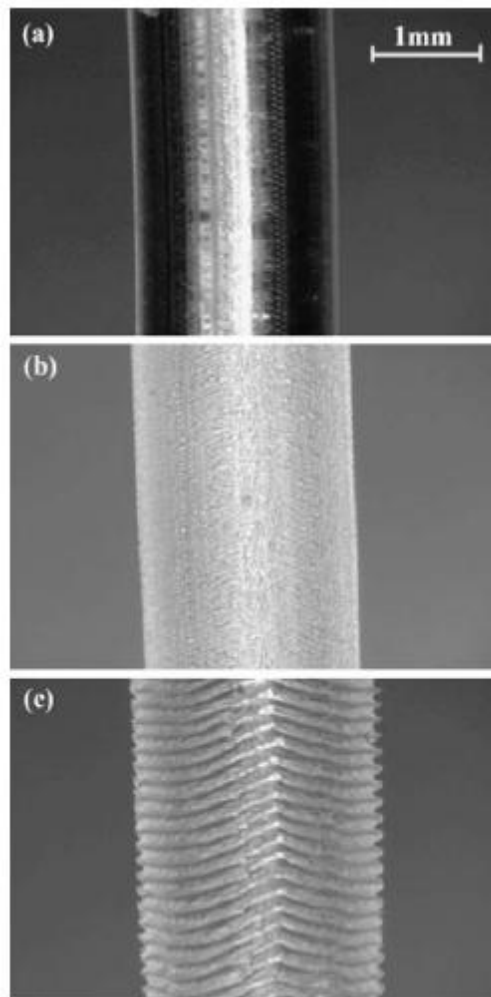


Figure 2.5: Transition from stable to sharkskin extrudate [4]

the extrusion of melted polymer through a capillary, a transition from a smooth surface to a nearly periodic ridge-like surface distortion has been observed at a critical shear rate or wall shear stress; these surfaces distortions are known as sharkskin.

Figure 2.5 shows an example of a surface deformation of a LLDPE specimen extruded at bulk temperature of  $140^{\circ}\text{C}$  [4]. This is an example of a surface effect that can potentially be detected using the method described in this thesis.

### 2.1.2 Electrical Properties of Materials

To use a material for electrical or electronic applications, one must clearly understand the electrical properties of the material, or how the material behaves electrically in given conditions. One of the most important electrical properties of a material is its electrical resistance  $R$ , or expressed in a geometry-independent way, the resistivity  $\rho$ .

Electrical resistance of a material is a characteristic of the physical properties of the material (size and shape). Electrical resistance is defined as [6]:

$$R = \rho \frac{l}{A} = \frac{l}{\sigma A} \quad (4)$$

where:

$R$  is the electrical resistance ( $\Omega$  ohms)

$A$  is the cross-sectional area ( $\text{m}^2$ )

$\rho$  is the electrical resistivity ( $\Omega \cdot \text{m}$ )

$\sigma$  is the electrical conductivity, or the reciprocal of  $\rho$  ( $\Omega^{-1} \cdot \text{m}^{-1}$ )

Ohm's law is an experimental observation relating the resistance of a material to voltage across and current through the material:

$$V = IR \quad (5)$$

where:

$V$  is the voltage or potential across the material (V, volts)

$I$  is the current flowing through the material (A, amperes)

Based on the electrical resistance of the material, among other properties, one can determine what applications the material can be used for. The spectrum of conductivity of solids is remarkably wide, spanning about twenty-three orders of magnitude [10-11]. Copper and silver have a conductivity of  $10^8 \Omega^{-1}\text{m}^{-1}$ . They are the best metallic conductors, and are widely used in manufacturing electrical wires and contacts. On the other hand, polymers such as polystyrene with a conductivity of  $10^{-15} \Omega^{-1}\text{m}^{-1}$  are commonly used as electrical insulators.

Techniques used to measure the electrical conductivity of materials are chosen depending on the physical characteristics of materials being tested. For materials in liquid form, techniques based on five electrode designs are often used [7]. In this study, we are focusing in solid materials such as polymers or conducting polymers, and also thin films. There are several techniques available to measure the resistivity of a material. For highly resistive materials, advanced equipment such as a resistivity cell is desired. Using this equipment, it is possible to measure the resistivity/volume resistance up to  $4.0\text{E}+15 \Omega\cdot\text{cm}$ , or and surface resistivity up to  $4.0\text{E}+15 \Omega$  [8]. The other method which is more widely used is the four point probe (FPP) method. The more detailed description of how FPP works is included in Section 5.2 of this thesis. In general, FPP is a technique consisting of four pins in line and in contact with a specimen, a direct current is passed through the two outer pins and the resulting potential difference is measured between the inner pins. The resistivity of the specimen is essentially calculated based on the measured current and potential values using factors appropriate to the geometry [9]. Due to its simplicity and cost effective nature, the FPP will be tried to measure the conductivity of materials in this study.

## **2.2 Materials, Applications, and Current Issues**

### **2.2.1 Materials in Aerospace Applications**

Kevlar® Composite Overwrapped Pressure Vessels (COPV) are widely used in space vehicles, and require monitoring to ensure safety in long-term use [12]. Although strain gauges can be used to detect increased stress related to either over-pressurization or age-related material weakening, we hypothesize that changes in surface electrical conductivity could provide a more information-rich and less energy-consumptive approach. These

pressure vessels in Figure 2.6 have undergone numerous tests and experiments to improve safety and reliability of space vehicles. Significant COPV tests were performed at Lawrence



Figure 2.6: NASA composite pressure vessels in space applications [73]

Livermore National Labs and NASA White Sands Test Facility

including morphological changes of the composite fibers under stress, manufacturing changes and their effects on tensile strength, epoxy resin strain, composite creep, degradation of polyurethane coatings, and titanium yield characteristics. However, none of the above tests were performed to investigate the surface electrical conductivity of the composite material, which is potentially related to the aging issue of the pressure vessels. Therefore, this project addresses goals in NASA's 2011 Strategic Plan [13] regarding space technology innovation, particularly in this case new techniques to study and track aging of space structures.

The study is to examine the surface properties, particularly electrical conductivity, of polymer composites under loading conditions to understand the characteristics of the material using a new and different approach. The study also aims to characterize aging through surface electrical conductivity by comparison of the properties of non-aged composite samples and long-term aged samples where fiber

strands are already disrupted. This approach addresses three basic objectives – identifying performance characteristics, obtaining material property data and performing data validation – recommended in a NASA 2006 Material Issues In Space Shuttle Report [12] on pressure vessels used in space vehicle applications. This study will benefit future aerospace programs as pressurized tanks of this type are common to practically all space vehicles and aviation safety remains an omnipresent priority issue.

### **2.2.2 Materials in Biomedical Applications**

Polymers and polymer composites have been commonly used as biomaterials in recent decades. They can be used as biomaterials because of their ability to provide appropriate host responses within the biological environment.

There are five different groups of biomaterials commonly used: natural materials, metals, ceramics, polymers, and composites of the other four material classes. A large number of polymers are widely used in many different biomedical applications because they can be tailored to have a variety of forms and properties. They can be in solids, fibers, fabrics, films or gels. Polymers are more conducive to manufacture than the other groups of materials in the sense that they can be easily molded and formed into complex shapes and structures. However, polymers are much more flexible and weak compared to metals and ceramics. Therefore, most polymers are rarely seen in orthopedic applications because of the mechanical demands. Certain polymers can also absorb liquid and swell, and/or leach undesirable products such as monomers, fillers, plasticizers, and sometimes undesired antioxidants [14]. Sterilization processes can also affect the properties of polymers. This is why the use of polymer composites is considered preferable. Polymer composites can be combinations of polymers and metals, polymers and ceramics, etc., since in this way the shortcomings of each homogenous material can be overcome. Polymer composites can be seen in applications such as hip and knee implants, dental

applications, ureter prostheses, catheters, vascular grafts, tissue engineering devices, and much more as shown in Table 2.1 [14-18].

**Table 2.1: Common polymers and their applications in biomedical engineering [14]**

<b>Polymer</b>	<b>Application</b>
<b>Poly(methyl methacrylate)</b>	Intraocular lens, bone cement, dentures
<b>Poly(ethylene terephthalate)</b>	Vascular graft
<b>Poly(dimethylsiloxane)</b>	Breast prostheses
<b>Poly(tetrafluoroethylene)</b>	Vascular graft, facial prostheses
<b>Polyethylene</b>	Hip joint replacement
<b>Polyurethane</b>	Facial prostheses, blood/device interfaces

A biomaterial has to be determined to be biocompatible with the living environment before it can be approved for contact with that environment. The biocompatibility characterization of a biomaterial is very crucial and is among the most important processes in developing any biomedical application. The biocompatibility can be categorized into two definitions: surface compatibility and structural compatibility [17].

Surface compatibility is the suitability of the implanted surface to the host tissues. Surface compatibility reflects the chemical, biological, and physical properties of the biomaterial, and can be characterized by hydrophilicity, protein immobilization, thickness and molecular weight of polymer layer, functional group density, and cell analysis including surface energy and probability of bacterial attachment on the surface. One useful parameter for characterizing the surface compatibility is the electrical



conductivity of the surface. Different methods to obtain the electrical conductivity properties of the surface of a biomaterial will be discussed in detail later.

Structural compatibility relates to the material's adaptation to the mechanical behaviors of the host tissues. The structural compatibility of a material is characterized by its mechanical properties such as bulk strength, ductility and load transmission at the interface area. A useful method to obtain most of the important mechanical properties related to structural compatibility is the tensile test. As discussed above, a tensile test can provide information about the stiffness and strength of a material. A simple tensile test using a universal testing machine is commonly performed to obtain this information.

Many methods have been introduced for measuring the surface electrical conductivity of a biomaterial. The conductivity of the surface controls the reactions across the interface with biomacromolecules of the biological system [14]. This phenomenon is extremely important to determine the duration that a biomaterial can be safely implanted inside a biological environment. One example is the polymer composite used as bone replacement material shown in Figure 2.7. There have been many studies of microbial adhesion on the surface of replacement materials, and it has been found that the adherence rate of pathogens to the biomaterials is very high [18]. Although the explanations of the different



adherence densities of microbes on different polymers have not been discovered thoroughly, the theory that is used to explain the microbial adhesion on material surfaces was studied by Coquet et al. in 2002 [19]. The result showed the relation of bacterial adhesion to the level of surface energy, which again relates to electrical conductivity of the surface of the material. Therefore, the study of surface electrical conductivity of biomaterials is important to provide strategies in decreasing microbial adherence to prevent infection in implants.

### 2.2.3 Materials in Electronic Applications

One other field in which polymers are now becoming a major studied material is the field of plastic electronic devices. Plastic or organic electronic devices such as the one in Figure 2.8 have attracted tremendous scientific attention due to their characteristics of being low-cost, mechanically flexible and bendable, and easily fabricated at ambient conditions over large areas. Therefore, organic electronics have been investigated for use as backplanes to power flexible

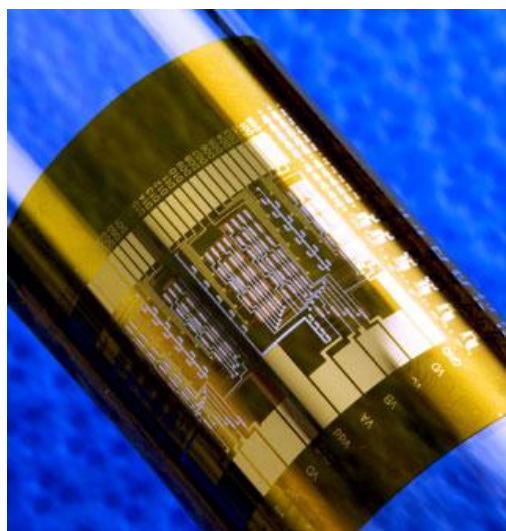


Figure 2.8: Integrated circuit on a flexible plastic substrate [74]

displays, circuitry in low-cost radio frequency identification tags, and photovoltaic devices in large-area plastic solar modules [25-29].

The most widely used organic electronic component nowadays is the organic field-effect transistor (OFET). OFETs have been proposed for applications such as display switches, display drivers, radio frequency identification tags, and sensors [27]. OFETs are based on processible polymeric solution as well as small molecular semiconductors [26]. The first organic transistor based on an organic semiconductor was reported in 1986 [28]. The device was made on an electrochemically grown

polythiophene film. Polythiophene is in the family of conducting polymers. Currently, a thin-film transistor is composed of three basic elements: a thin semiconductor film, an insulating layer, and three electrodes. With the same principles, OFETs have been fabricated with various device geometries, which depict different placements of a substrate, dielectric, and semiconducting layers with respect to each other. For the purpose of an overview of how polymers are used in organic electronics, a common poly(2,5-thienylene vinylene) (PTV) OFET is shown in Figure 2.9 [26]:

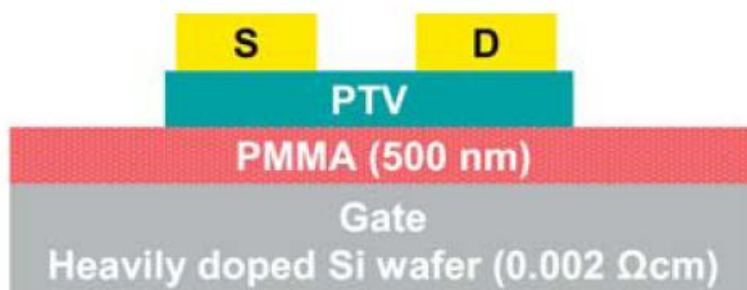


Figure 2.9: Schematic of a top-contact PTV OFET [26]

In this configuration PTV acts as the semiconductor, 500nm spin-coated polymethyl-methacrylate PMMA as the gate insulator on top of a heavily doped silicon substrate as the gate electrode, and gold as source and drain electrodes. This is also called the OFET top contact geometry. To characterize the OFET, a standard I-V graph is obtained to show the drain current versus drain voltage at various gate voltages.

As mentioned above, one of the advantages of plastic electronics is their flexibility to bend as an example displayed in Figure 2.10. As the devices are more widely manipulated in current technologies, the possibility of these devices being subjected to loading and bending will

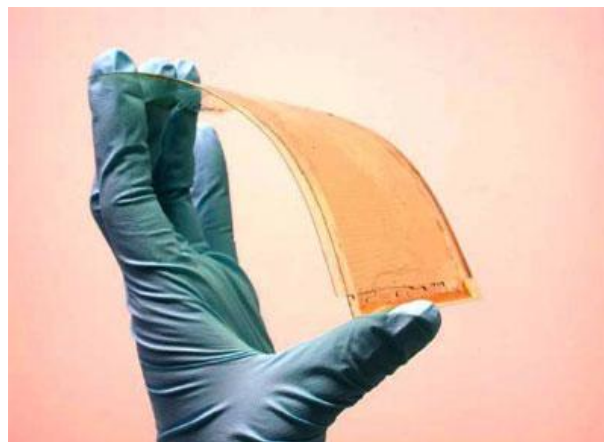


Figure 2.10: Flexible and bendable plastic electronic [75]

surely increase. However, since the field is newly developed, studies made on the characteristics of these devices are not yet abundantly carried out. In particular, it would be insightful to understand the behaviors of the electrical properties of plastic electronics while being subjected to loading or bending. This is also another motivation for our study to discover the relationship between electrical conductivity of materials during mechanical stimulations, in particular the materials used in plastic electronics where electrical properties are of highest importance.

### 2.3 Objectives

Understanding the current issues of polymeric materials in several applications such as in space, biomedical and electronic applications, in which an innovative method that allows a different vision in the relationship between mechanical stimulations and exerted electrical properties on polymers is desirable. Therefore, the objectives of our study are:

- To design a robotic system that is able to measure surface conductivity of materials under loading using a tensile testing machine.
- To test the robotic system on different polymeric specimens under dynamic stimulations.

## **PART A: THE DESIGN**

### **CHAPTER 3: DEVELOPMENT OF THE CONDUCTIVITY TESTING SYSTEM (CTS)**

#### **3.1 Overview of the System Mechanics**

The desired conductivity testing system (CTS) is to be coupled with a tensile testing machine, particularly Instron® 3365 (Instron®). The system is mounted to the Instron® machine as an accessory and performs its test on the sample while mounted on the Instron®. The following description presents the integration of the Instron® and CTS.

##### **3.1.1 Instron® 3365**

Tensile testing is a fundamental materials test in which a sample is subjected to uniaxial tension or compression until failure [30]. The test can provide much important information about the material of the sample, such as the amount of force required to break a material, modulus of material, the point of permanent deformation, stress-strain curves, etc. The information can be used to present a better understanding of known materials, to develop new materials, or to monitor/maintain the quality of materials [31]. A common piece of equipment used for tensile testing is the universal testing machine, which tests materials in tension, compression, or bending. There are both hydraulic powered and electromagnetically powered (electromechanical) testing machines.

The Instron® 3365 is a universal testing machine which is powered electromagnetically. This electromechanical machine uses a combination of a motor and gear reduction system to move a crosshead up and down to provide force to the sample. The speed of the motor controls the speed of

the crosshead. The following figure shows an overview of the Instron® 3360 Series and its major components. The 3360 series includes models 3365, 3366, 3667, and 3369 [32].

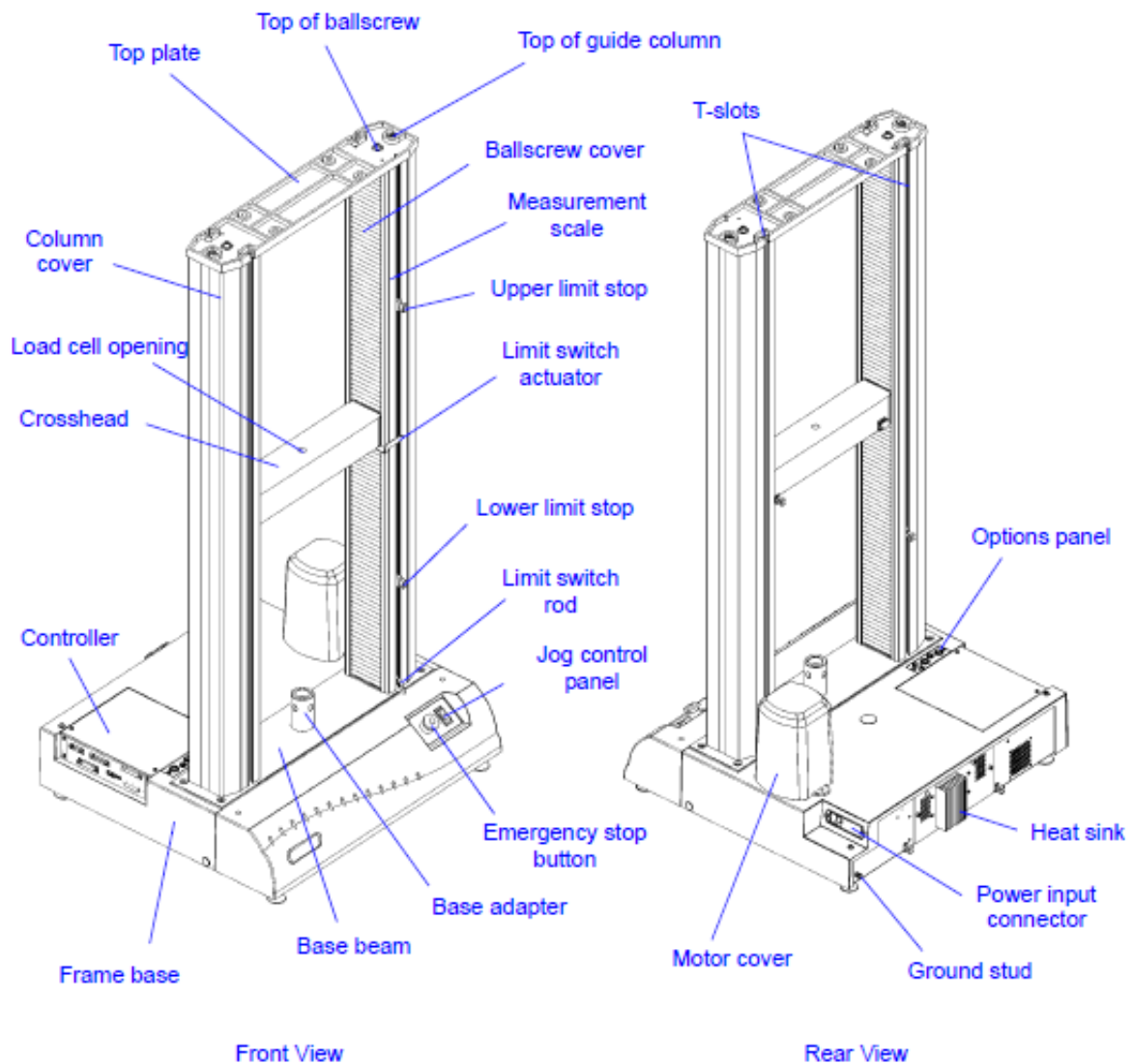


Figure 3.1: Schematic of Instron® 3365 [33]

Load cells with different grips are attached to the crosshead. Depending on the material, geometry, and the strength of test specimens, grips are selected accordingly. In tensile testing, the specimen is held securely in the jaws of the upper and lower grips. The upper grip is attached to the load cell that is mobile in the vertical direction, and the lower grip is attached to the fixed base plate of the load frame.

In compression testing, an anvil is used. The anvil is coupled with the load cell to apply loads to the specimen which is placed on a table. The diameter and loading capacity of the anvil is important in compression testing [33].

For the purpose of designing CTS to integrate with the Instron® system, the dimensions of the testing machine are acquired as shown in Figure 3.2 and Table 3.1.

**Table 3.1: Relevant dimensions of Instron® 3365 [33]**

<b>Letter Designation</b>	<b>Description</b>	<b>Dimension - mm</b>
<b>B</b>	Overall width	756
<b>C</b>	Overall depth	707
<b>D</b>	Horizontal test daylight	420
<b>E</b>	Vertical test daylight	
	Maximum	1193
	Minimum	71
<b>G</b>	Base platen to coupling pin	59
<b>P</b>	Column cover depth	113
<b>Q</b>	Column cover width	128

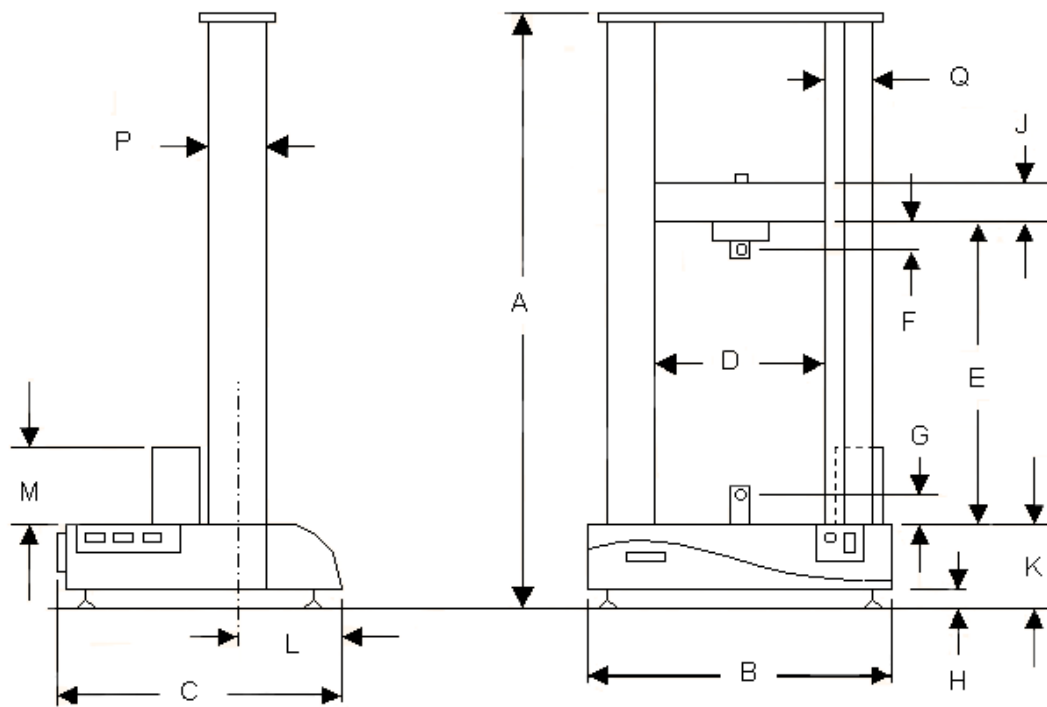


Figure 3.2: Relevant dimensions of Instron® 3365 for design of CTS [33]

Understanding the functionality and features of the Instron® machine, CTS was designed and developed as described below.

### 3.1.2 The Conductivity Testing System (CTS)

CTS is designed as a detachable tool used with the Instron® machine. The system has a site for attachment to the tensile machine when the electrical conductivity testing is needed for the loading samples, and can be easily removed when the test is done. Below is the overview of CTS when used with the Instron®.

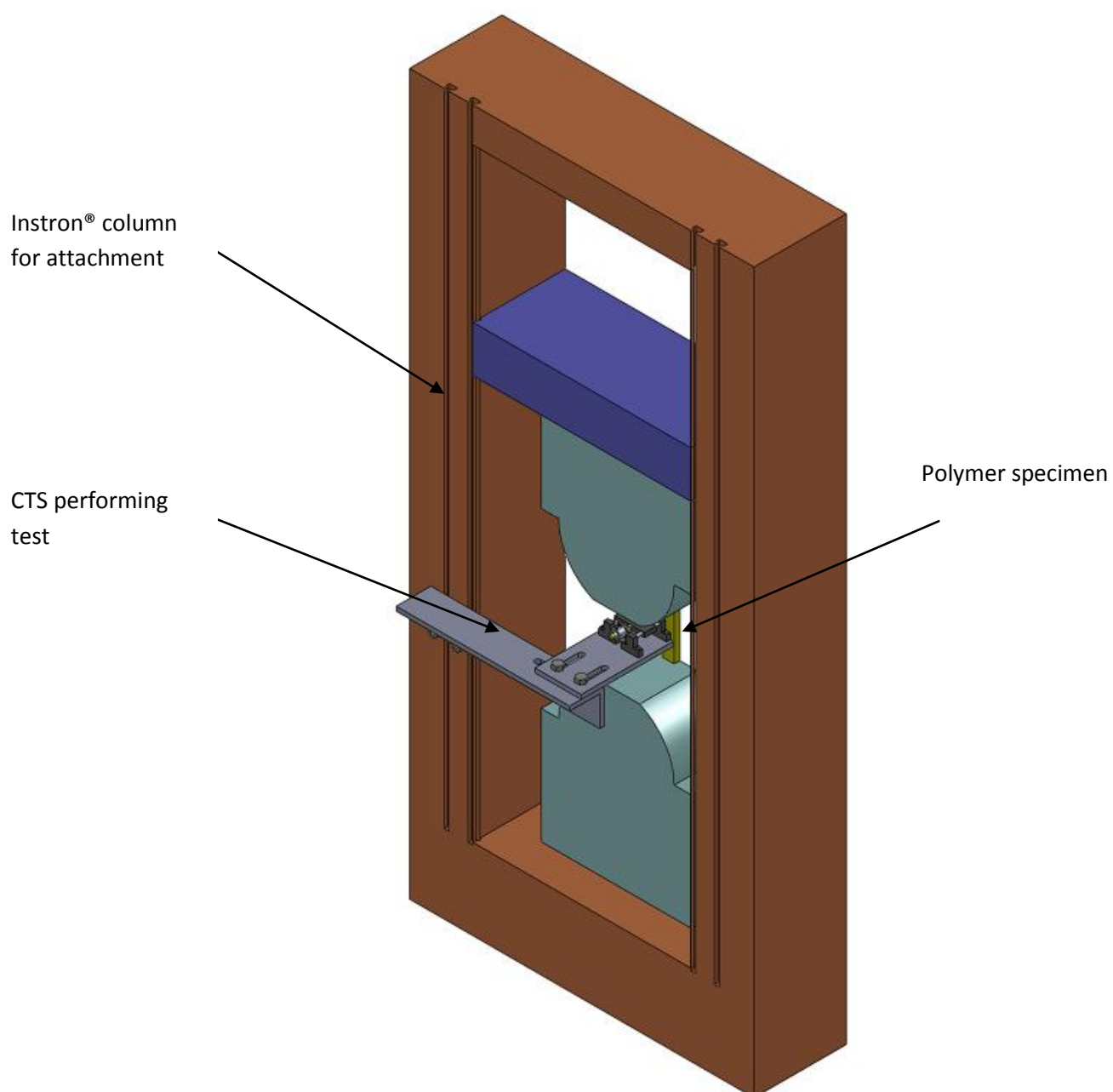


Figure 3.3: Overview of CTS coupling with the Instron®



As shown in the figure above, the mounting arm is customized to attach to the left column of the Instron® with a 90-degree angle aiming toward the load cell area. At the tip of the arm, a resistivity sensor is mounted to linearly approach the sample and perform its resistivity test.

CTS is designed to operate in a synchronized manner with the tensile machine. In general, while the sample is being loaded with a given strain rate, the resistivity sensor will be controlled to perform the resistivity test on that particular sample. The details of how the system functions and how the test is done will be discussed in depth in the next section.

## 3.2 The Design

### 3.2.1 Overview

CTS is designed to be attached with the Instron® and to coordinate with the machine. CTS consists of four main parts: linear guide carriage, sensor bracket, front plate, and attachment fasteners. Below is an overview figure of the designed system.

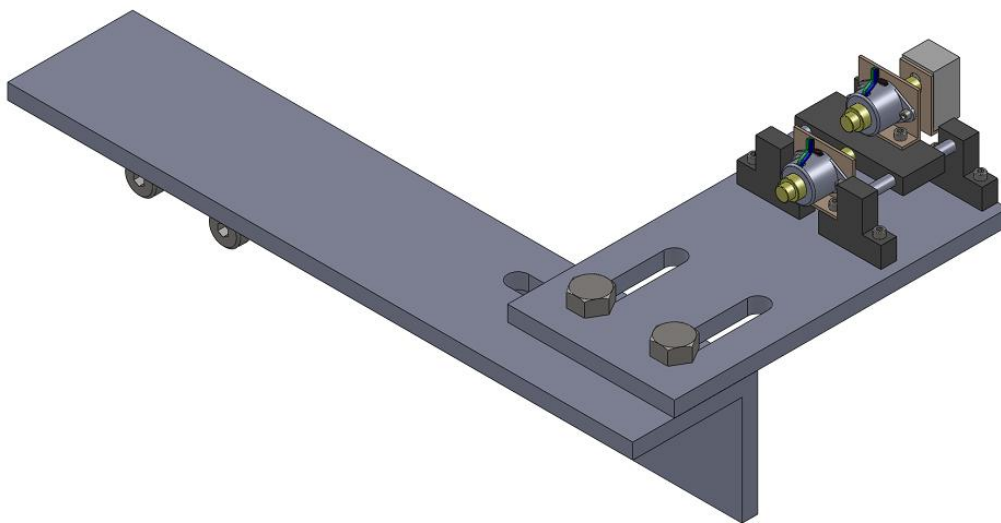


Figure 3.4: The conductivity testing system CTS

The following sections will describe in detail the four main parts of CTS. Also included are the analysis of the design and material selection process for each part. The complete assembly of CTS integrating all the system components with the Instron® machine will be presented.

### **3.2.2 Material Selection**

Since the sensor bracket has to fit the configuration of a chosen motor shaft and support a particularly non-standardized type of sensor, it is determined that the sensor bracket should be customized in-house. Aluminum alloy was chosen to fulfill this task. The technical drawing of this sensor bracket is shown in Appendix A.

Since the plates have to fit the configuration of the Instron® 3665, it is determined that the plates should be customized in-house. Again, aluminum alloy was chosen to fulfill this task. The technical drawings of the plates are shown in Appendix A.

Due to the requirements that the clamping system must fit the configurations of the Instron® 3365 and the designed CTS, it was determined that the clamping system should be customized in-house to satisfy the criteria.

### **3.2.3 Linear Guide Carriage**

#### ***3.2.3.1 Design Requirements***

The linear guide must:

1. Be lightweight, but strong and stiff for being suspended 20 cm above the table surface.
2. Provide a carriage/base to mount motors.
3. Provide mobility to the resistivity sensor.
4. Actuate the sensor in one linear degree of freedom.

5. Translate accurately the base in a straight-line configuration.
6. Remain steady while operating to prevent any vibration which can affect the measurements.

### 3.2.3.2 Components

#### First solution:

Figure 3.5 shows a configuration that was selected to build the linear guide carriage.

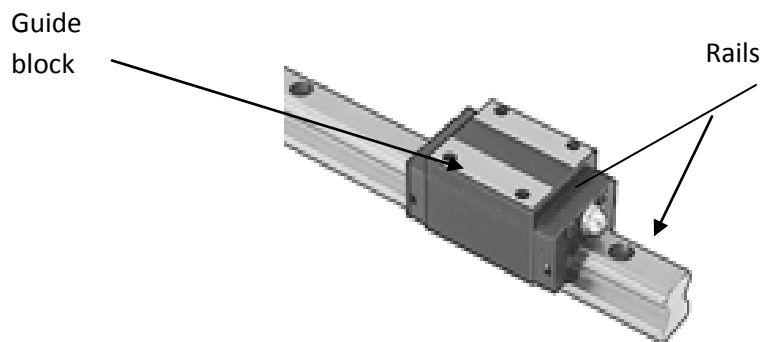


Figure 3.5: Linear guide model from McMaster-Carr [34]

This particular linear guide is composed of a steel guide block and rails, with the rails being ground and hardened. There are seals on both ends of the block which are made of resin with H-NBR rubber. The seals function to keep dirt out of the lubricants. There are two rails, one on each side, that help to keep the guide block traveling steadily and accurately without any vibration or disruption created by contact between the components. The advantages and disadvantages of this configuration were considered:

#### 1) Advantages:

- Provide a good base for mounting the sensor
- High accuracy in mobility

- Steady and no vibration in contact

2) Disadvantages:

- Expensive
- Heavy

One of the design requirements for the linear guide mentioned above is that the linear guide must be lightweight to be suspended about 20cm above a reference surface. This particular linear guide is made of steel so it is heavy in weight . Also, the total cost of the block and the complementary rails is about \$180. These two shortcomings of weight and cost have potential for improvement. Therefore, another solution has been found to meet the requirements better and to be more cost effective.

*Final solution:*

Below is the final design to serve as a linear carriage guide that is used in the final CTS assembly. Based on the same design requirements, a customized linear guide was designed and manufactured in-house which can satisfy all the criteria without excessive cost.

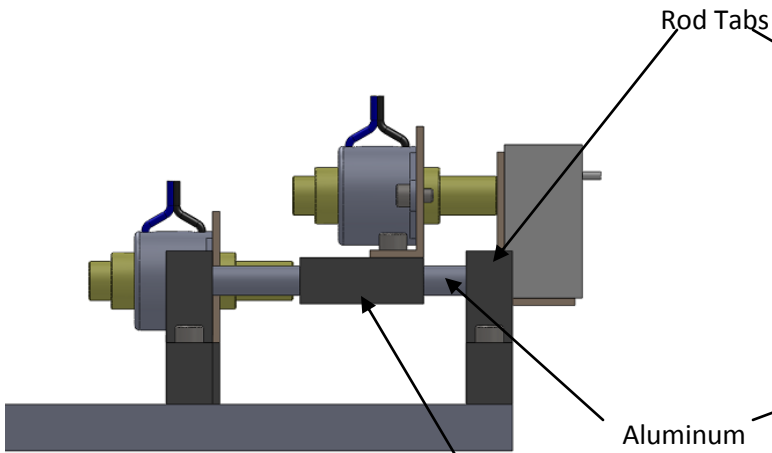


Figure 3.6: Design of linear guide (side view)

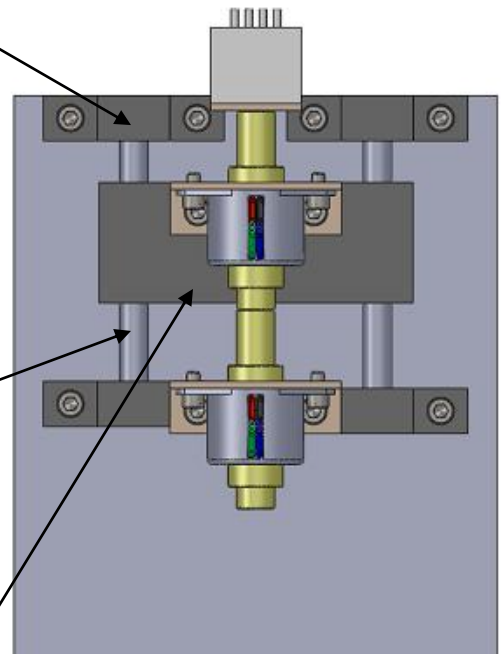


Figure 3.7: Design of linear guide (top view)

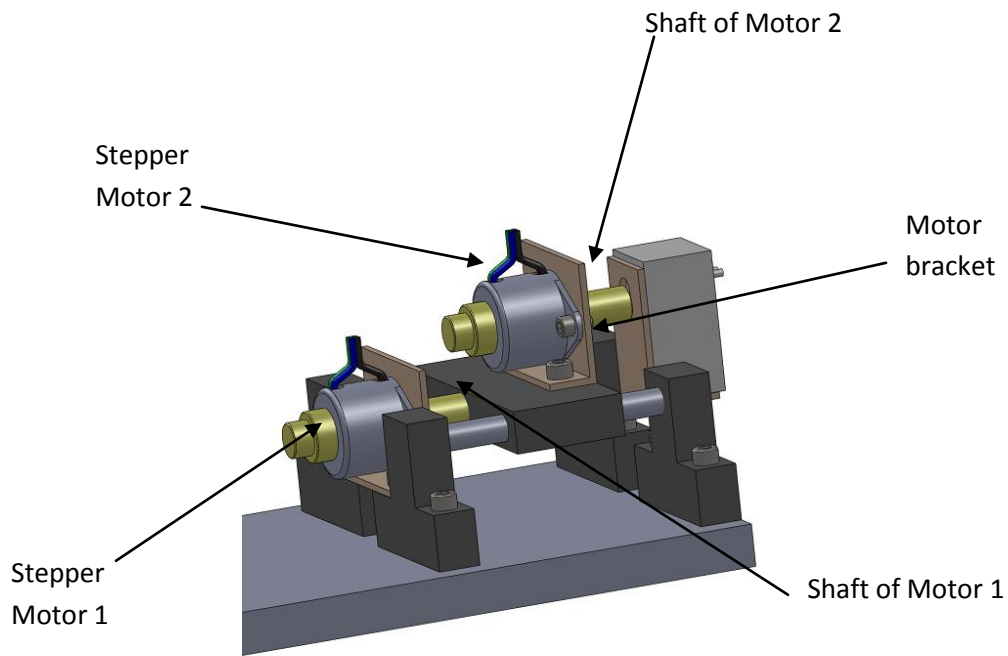


Figure 3.8: Design of linear guide (isometric view)

In this particular design, there are four major components: 4 rod tabs, 2 rods, 1 carriage block, and 1 motor bracket shown in Figure 3.6 to 3.8. All of these components are made of 6061-T6 aluminum. This material is known to have high strength, low cost (\$14 for a plate of 0.95 cm × 20cm × 20cm), and low density (weight of 4.8kg per square meter of 0.95cm aluminum alloy plate).

The 4 rod tabs are mounted on the surface of an aluminum plate (the design of this plate is described in a later section). Each tab is in the shape of a T with a countersink in the middle so that the end of each rod is accurately located inside each hole. The rod tabs are to secure the rods and keep them steady and level as the carriage block translates.

The 2 rods are 70mm aluminum cylinders. Each end of the rod is secured by the rod tabs as described above. The rods are polished to minimize friction while the carriage block slides along them.

The carriage block is a rectangular block with two holes for the rods to pass through. The block is designed to be in contact with the shaft of a linear stepper actuator, which provides the block linear motion to translate along the rods. On top of the block is a mount point for a motor bracket.

The motor bracket sits on top of the carriage block and provides a mount point for another stepper motor to provide the four-point probe sensor another degree of freedom, which will be discussed in a later section. The motor bracket is an L-shaped component and moves with the carriage block as one entity.

This final design has been built in-house with a total material cost of \$14.83. The design fulfills its design requirements in a cost-effective way.

### 3.2.4 Sensor Bracket

#### 3.2.4.1 Design Requirements

The sensor bracket must:

1. Be lightweight and tolerate a minimum force of 5 N (which is equivalent to the weight of the sensor attached to the bracket)
2. Support the sensor steadily while operating to prevent any vibration affecting the measurements.
3. Provide 360 degrees of rotation
4. Provide a base to mount the sensor
5. Fit the configuration of a chosen motor shaft

#### 3.2.4.2 Components

The mechanical analysis of the sensor is presented in this section.

The sensor bracket serves as a mounting base for the four-point probe sensor, which is then translated and rotated to contact a sample under loading in a tensile testing machine. The four-point probe sensor has a configuration as shown in Figure 3.9:

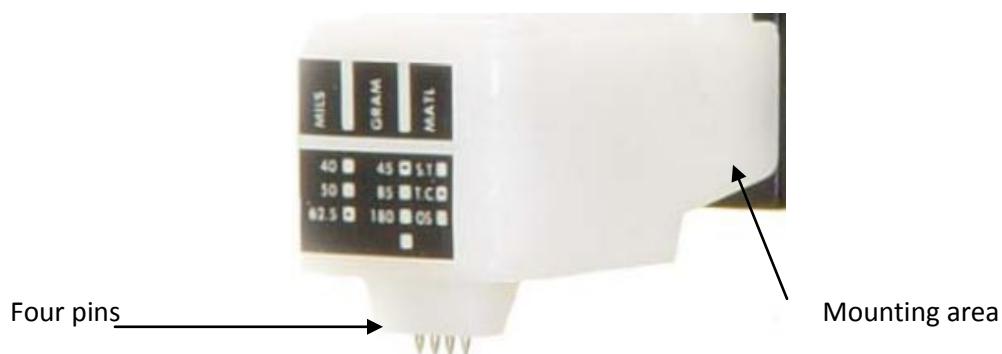


Figure 3.9: Signatone four-point probe [35]

This four-point probe sensor is mounted upright on the sensor bracket so that the four pins of the probe are perpendicular to the surface of the loading sample. (A more detailed explanation of the setup will be discussed in later sections).

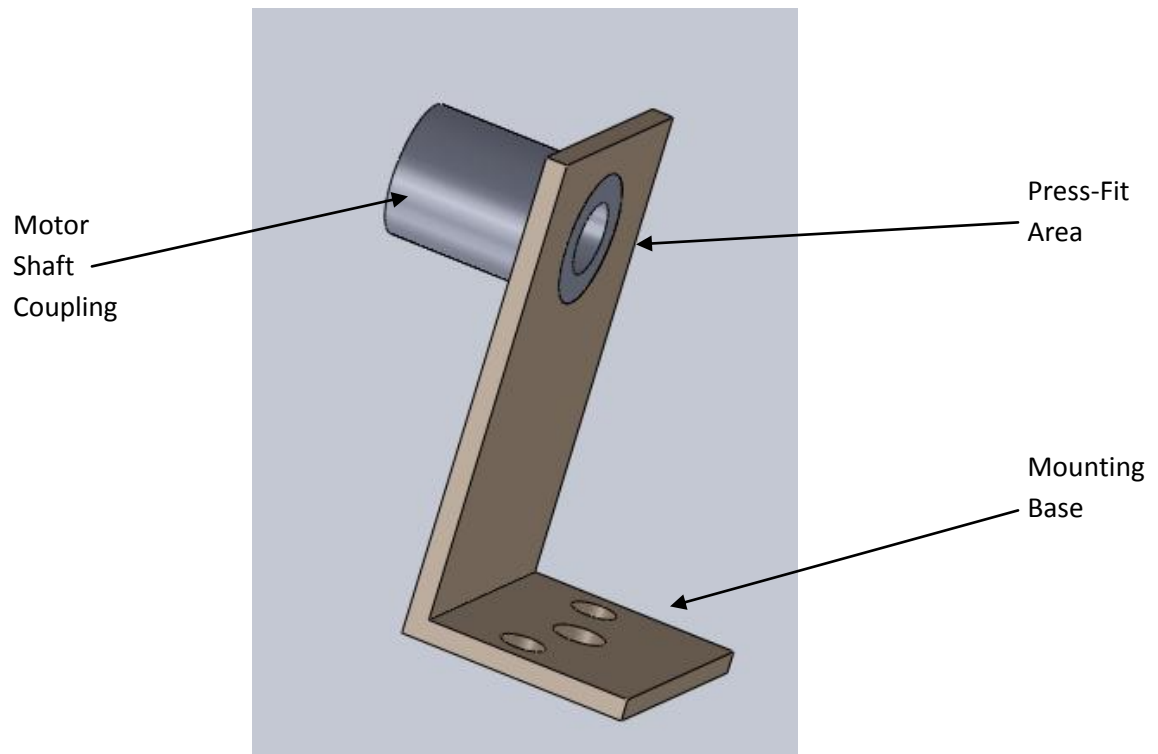


Figure 3.10: Overview of the sensor bracket

There are two separate parts that make up the sensor bracket in Figure 3.10. The first part is the motor shaft coupling in Figure 3.11. The coupler has an outer diameter of 9mm and an inner diameter of 5mm. The shaft of motor 2 is completely inserted through the cylinder, and then fasteners are inserted through the through hole to provide more stability to the motor shaft and the rest of the bracket.



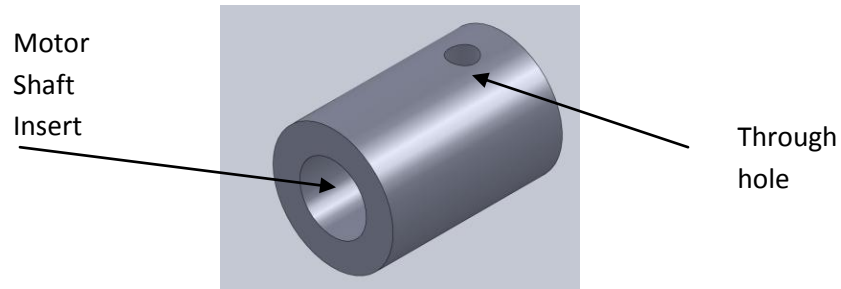


Figure 3.11: Motor shaft coupler

The second part of the bracket is the mounting base in Figure 3.12. The mounting base is connected rigidly with the coupling using a press fit. The mounting base supports the sensor via two mounting holes underneath the sensor. The middle hole is to run the electrical wires from the sensor to the corresponding system.

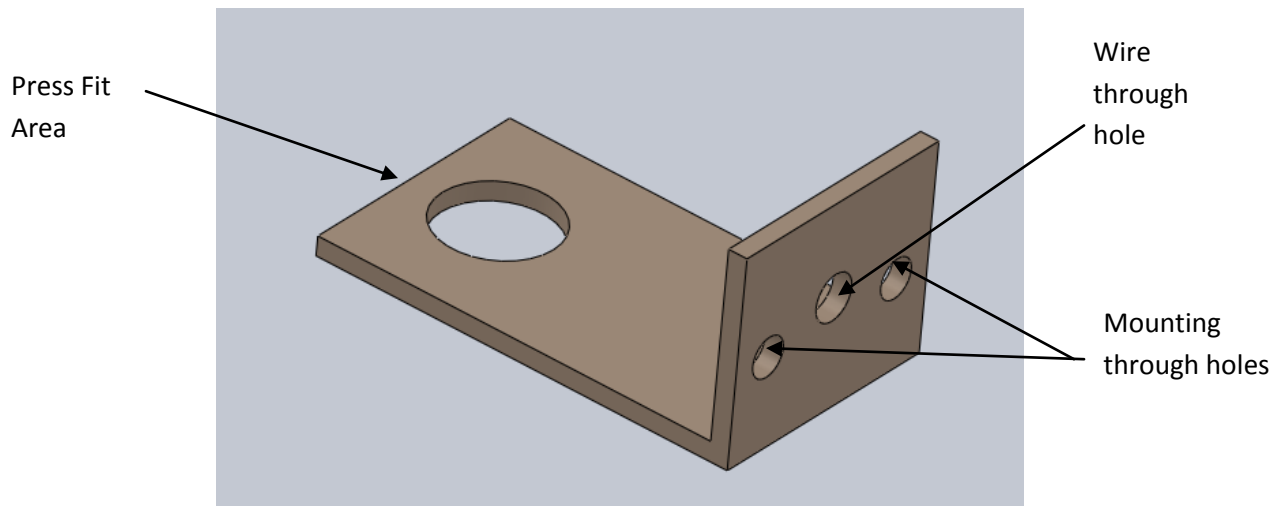


Figure 3.12: Mounting base

This entire sensor bracket is then connected to motor 2, which imparts its rotating motion. This completes the second degree of freedom that the CTS requires. Motor 1 in the linear guide provides the first (translation) degree of freedom to the carriage block which carries motor 2, which is serially connected to the sensor bracket to provide the final rotational degree of freedom.

## 3.2.5 Plates

### 3.2.5.1 Design Requirements

The plates must:

1. Be lightweight but strong and stiff enough to be suspended 20cm above the table
2. Fit the configuration of Instron® 3365
3. Provide a base for the linear guide to be mounted
4. Support steadily other components while operating to prevent any vibration affecting the measurements
5. Provide easy adjustment to adapt to different sizes of the loading specimens.

### 3.2.5.2 Components

There are two main parts that make up the plate system: the front plate and back plate (as shown in Figures 3.13 and 3.14). Each is made of 6061-T6 aluminum alloy with a thickness of 9.5mm. The front plate was customized with two slots that are used to connect with the back plate perpendicularly. They also have mounting holes so that the rod tabs and the linear guides can be mounted securely on top of the plate.

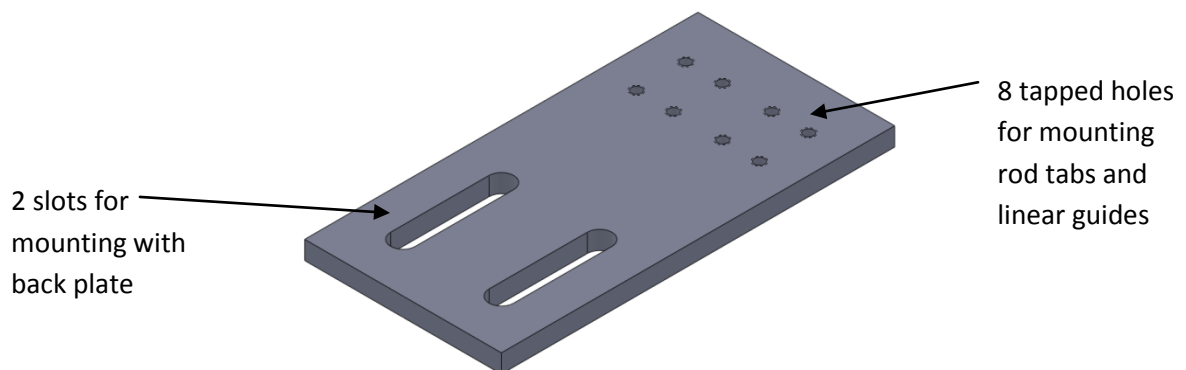


Figure 3.13: Front plate

The back plate is a bare extruded angle with an L-shaped configuration. The purpose of the angle is that the top surface of the plate is connected with the front plate, while the other surface is mounted upright flush with the Instron® machine's vertical rails. There is a slot on the top surface corresponding with the two slots on the front plate, and there are four through holes on the other surface so it can be fastened to the Instron® system.

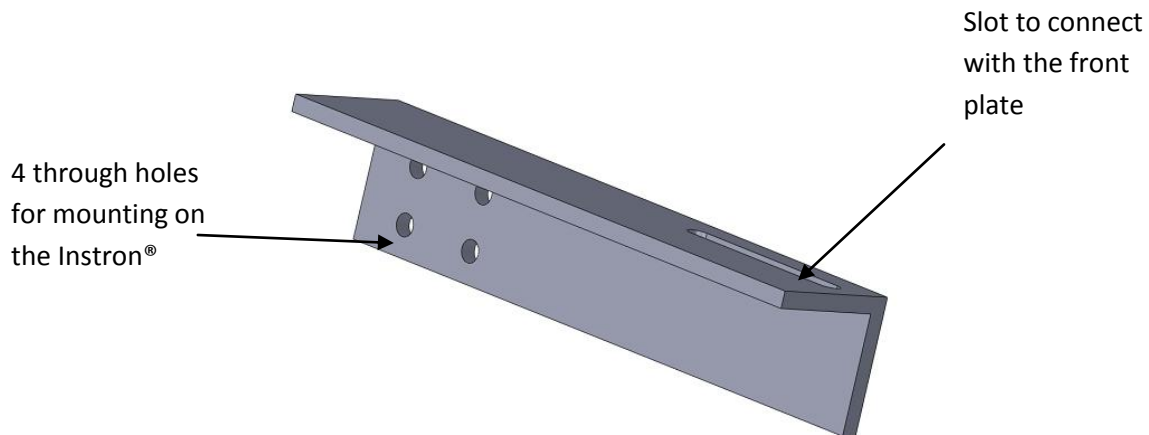


Figure 3.14: Back plate

The front and back plates are connected simply with two fasteners in Figure 3.15. These fasteners provide a strong connection between the two plates, but also act as quick release so that the plates can easily be adjusted accordingly to the sizes of the specimens.

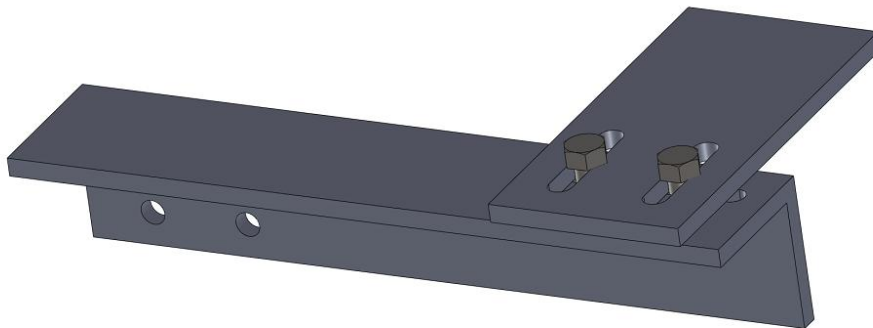


Figure 3.15: Front and back plates when connected

The plates are connected using a slot system so that the configuration can be adapted according to the geometry of the loading specimens. Specimens being loaded on the tensile testing machine can come in a variety of shapes and sizes. The details of the physical properties of the specimens will be discussed in the experimental sections. However, a general schematic of where the plate system and sensor are placed with respect to the specimen is presented in Figure 3.16.

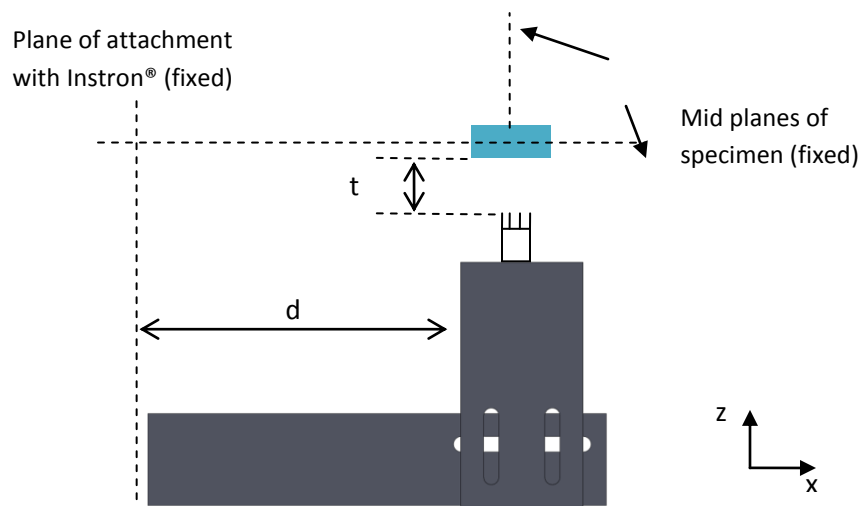


Figure 3.16: Schematic of experimental setup (top view)

Two parameters that can be manipulated are  $d$  and  $t$ . The parameter  $d$  can be changed by shifting the front plate in the  $x$  direction. This action is to complement the width of the specimen. In the same manner, the parameter  $t$  can be controlled by shifting the front plate in the  $z$  direction. This ensures the tip of the sensor reaches the surface of the specimen, despite the range of different thicknesses that specimens may have.

It is important that the sensor is situated in an appropriate position with respect to the specimen (i.e., the sensor should be centered along the line of symmetry of the specimen for better measurement). Adjustment of the plate system is shown in Figure 3.17.

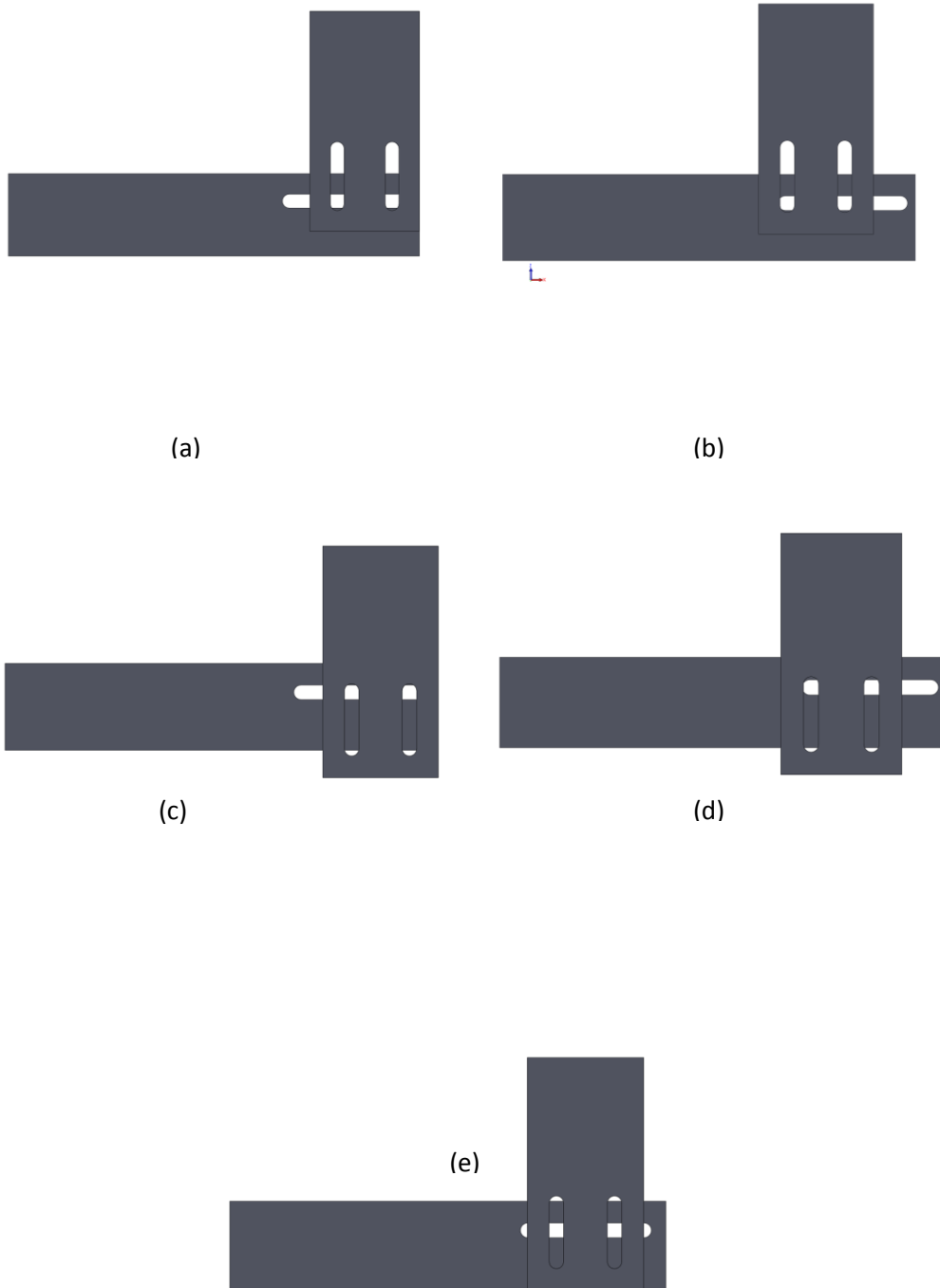


Figure 3.17: The plate system can be adjusted for specimens with: (a) min thickness, min width; (b) min thickness, max width; (c) max thickness, min width; (d) max thickness, max width; (e) average thickness, average width.

## 3.2.6 Clamping to Instron® 3365

### 3.2.6.1 Design Requirements

The clamping system must:

1. Adapt to the configurations of the Instron® and the plate system
2. Securely attach the plate system to the Instron® 3365
3. Prevent vibration during operation that can affect the measurements
4. Be easily detachable to modify the position of the system as needed

### 3.2.6.2 Components

As described in section 3.2.5.2, the back plate is right-angled. One surface of the angle structure is attached to the Instron® 3365; therefore four through holes are drilled for this attachment. Since the upright support column of the Instron® 3365 has two T-slots for accommodating accessories, matching standard T-keys from a commercial supplier (McMaster-Carr) allow attachment to the existing T-slots. Shoulder bolts are used as fasteners to securely attach the back plate to the Instron® system (i.e., the T-keys) and to ensure appropriate clearance between the bolts and the through holes.

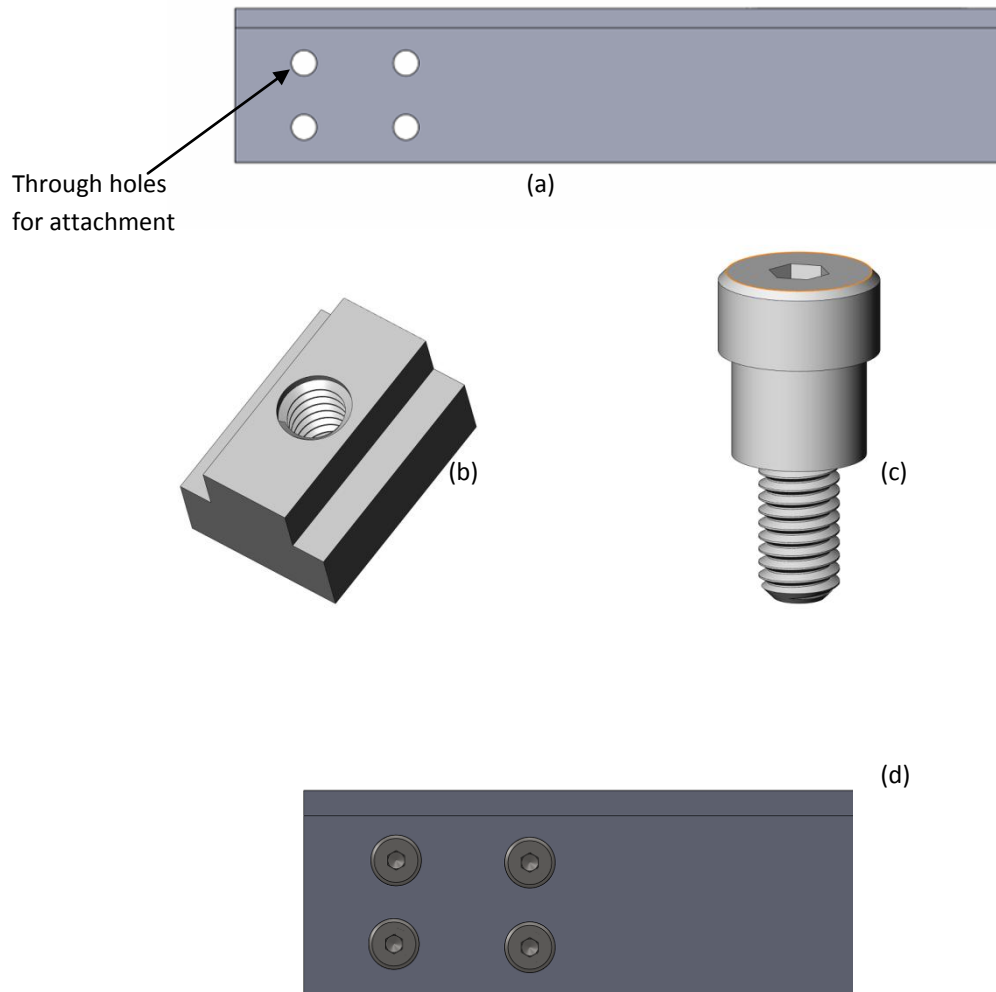


Figure 3.18: The clamping system and its components: (a) back plate with through holes; (b) T-Key inserted to the Instron® upright column [38]; (c) shoulder bolt for fastening [39]; (d) assembled clamping system

### 3.3 Final Assembly

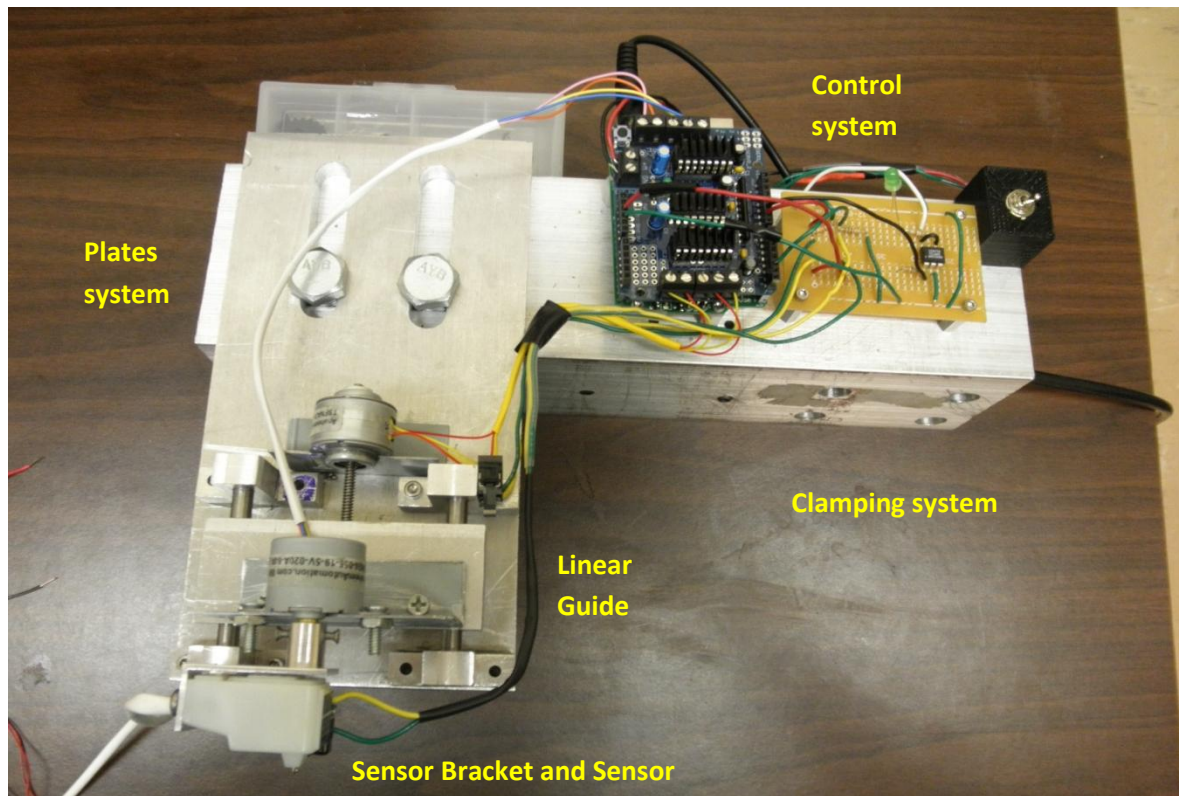


Figure 3.19: Final assembly of CTS.

The first prototype of CTS has been built to meet all the given requirements shown in Figure 3.19. The linear guide was the most complex component overall. The final assembly of the linear guide served as a site for attaching the motors and the sensor bracket, and most of all gave the required degrees of freedom to the carriage to satisfy the criterion of mobility. The plates and clamping system are more straightforward and were easily implemented as described in the preceding sections. (The control system will be described in detail in the following chapter.) The completed system after assembly weighs 4.5kg. With CTS attached to the Instron® 3365 shown in Figure 3.20, it successfully matches the configuration of the Instron® as seen in Figure 3.20. Moreover, CTS exhibits no noticeable vibration or interruption while operating with the Instron® machine.



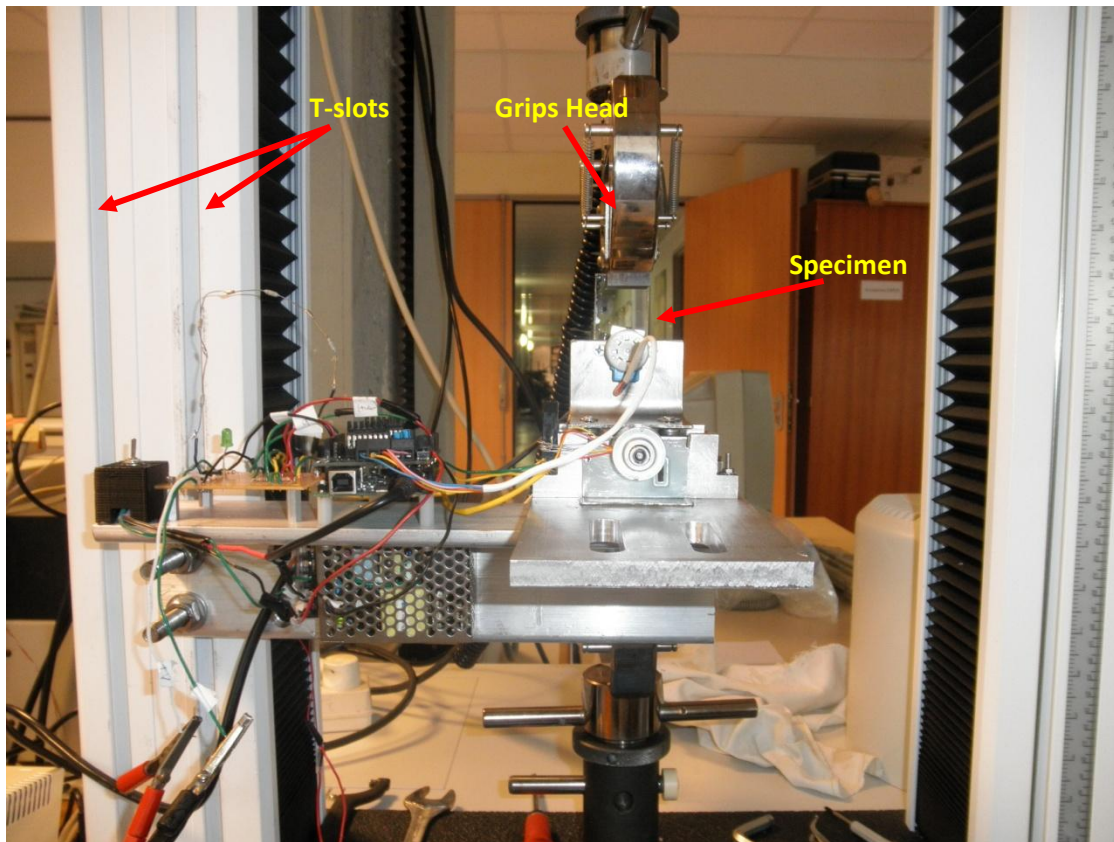


Figure 3.20: CTS coupled with Instron® 3365

## CHAPTER 4: SYSTEM CONTROL

### 4.1 Design Requirements

CTS has to meet several requirements to achieve functionality, usability, and reliability. A comprehensive list of specific requirements was compiled before the design work could begin. The list is as follows:

1. The system must synchronize its operations with the Instron® 3365.
2. The four-point probe sensor must measure the electrical conductivity on the surface of specimens gripped in the Instron® 3365.
3. The entire system must be automatically controlled by a microcontroller.
4. The system must provide input voltage to the sensor only when the sensor is in contact with the loaded specimen.
5. The system must terminate input voltage to the sensor before the sensor breaks contact with the specimen.
6. The input voltage or input current to the four-point probe must be regulated closely so that the probe is protected from any damage such as burns from electrical arcing (which may be caused by malfunction of the probe's internal springs).
7. The system must provide a safety operation which allows every component of the system (motors, sensors, switches, etc.) to return to their original positions to prevent any damage to the system and the specimen.

8. The data acquisition system must capture the measurements from the four-point probe in real time.
9. The data acquisition system must allow data to be recorded in formats compatible with common data analysis programs such as Microsoft Excel.

## 4.2 Microcontroller System

The microcontroller system functions as the principal controller to automate the hardware of CTS according to its stated requirements. To serve this objective, the microcontroller system consists of six main components: a Ruggeduino board, a motor shield, a power supply, a relay, microswitches, and controlling software. Each component will be discussed in detail in the following section; however, the overall connections are shown in a basic diagram below.

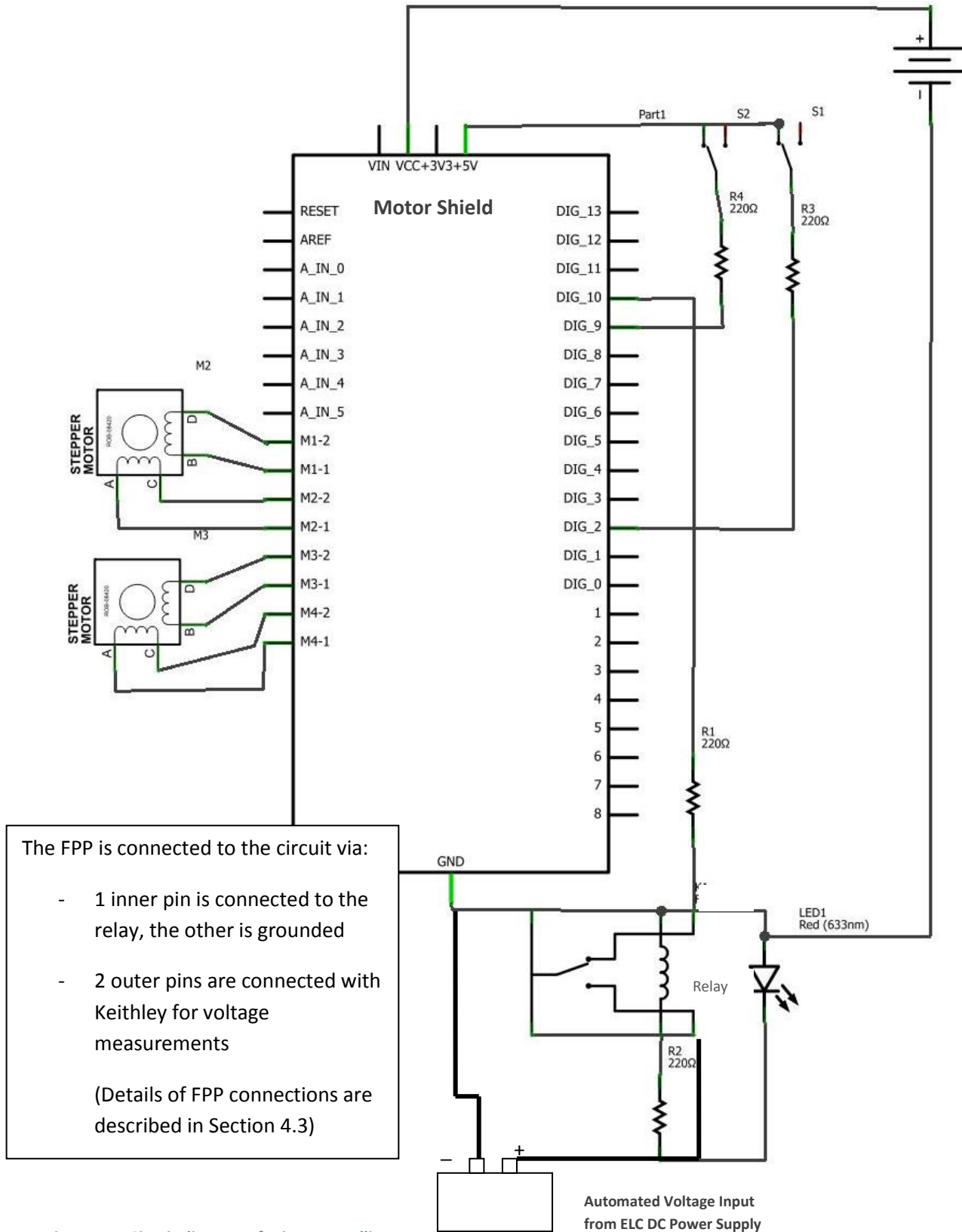


Figure 4.1: Circuit diagram of microcontrolling system

### 4.2.1 Ruggeduino

Ruggeduino [40] is a ruggedized Arduino-compatible microcontroller board (ruggedcircuits) purchased from Rugged Circuits LLC, Michigan. A regular Arduino board is an open-source physical computing platform based on a simple microcontroller board, and a development environment for writing software for the board (Arduino.cc)

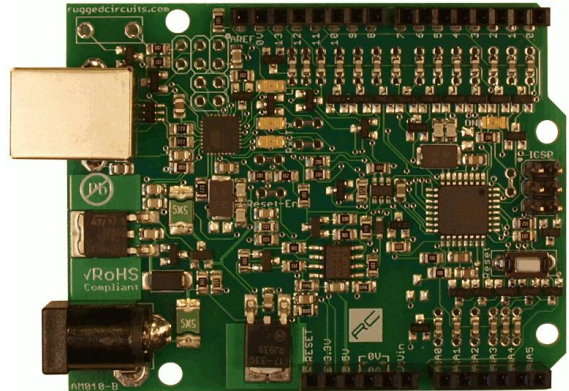


Figure 4.2: Ruggeduino [40]

[41]. The Arduino board can be used to take inputs from a variety of switches and sensors, and control a variety of lights, motors and other physical outputs. The Ruggeduino is an Arduino board but includes overcurrent and overvoltage protection on all input and output pins.

In this study, the Ruggeduino is used to take inputs from microswitches and to drive one linear stepper motor, one rotational stepper motor, and a relay. The power input is +5V from a DC power supply. The Ruggeduino then supplies power to the motor shield, the two stepper motors, the relay, and the microswitches. A +5V output is supplied to each connector pin on the microcontroller. The language used to program the board is C++. Programming of the Ruggeduino is the same as for the Arduino Uno, so the connections between the board and its external circuits are the same as that of the Arduino Uno. For circuit diagrams, images of the Arduino Uno will be used to replace the Ruggeduino (for simplicity).

### 4.2.2 Motor shield

A motor shield is a full-featured motor board that can power many simple- to medium-complexity projects for the Arduino board. The motor shield can be used to power up and control different types of motors such as servos, bi-directional DC motors, and stepper motors. The motor shield is obtained from Adafruit Industries, New York [42].

The motor shield is stacked on top of the Ruggeduino through the 8-pin and 6-pin headers. After the motor shield and the Ruggeduino are connected, the stepper motors, switches, and relay are connected to the motor shield.

The linear stepper motor is connected to the DC motor 1 screw terminal, and the rotational stepper motor is connected to the DC motor 2 screw terminal. No servo motors are used in this study. The switches and the relay connections are described in later sections.

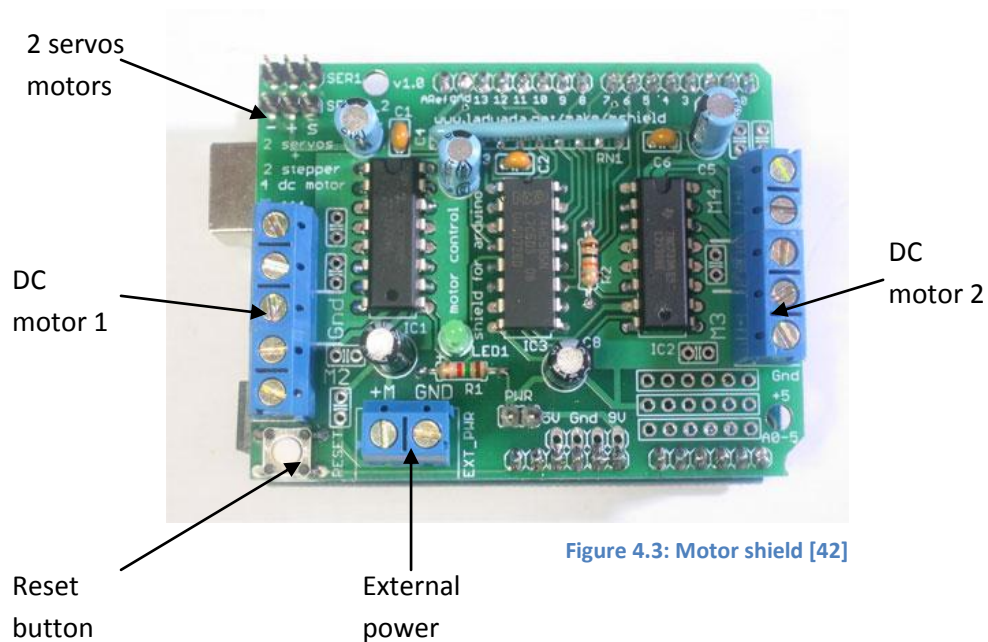


Figure 4.3: Motor shield [42]

### 4.2.3 Power supply

This is a 25W single output switching power supply.

This power supply is a universal AC input with a voltage range of 88-230VAC and output DC voltage of 5V. In

this study, the power supply is used to power the

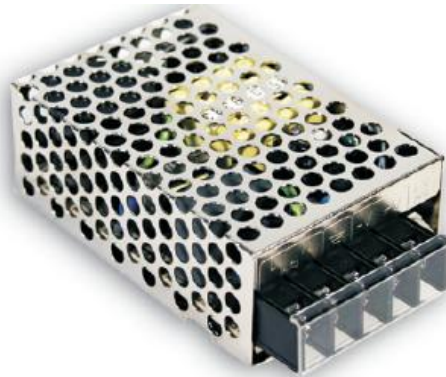


Figure 4.4: 5V Power supply [43]

Ruggeduino and the motor shield. It also powers the relay with its 5VDC output. The power supply was obtained from Mean Well USA, Inc., California [43].

#### 4.2.4 Relay



Figure 4.5: LCA 710 Relay [44]

The four-point probe sensor, with its characteristics described in Section 5.2, has two pins provided with voltage and two other pins for measuring output

current, or vice versa. The most important point of note when using the four-point probe is that the voltage or current input should be provided only after the spring-loaded pins are in contact. This is to prevent any electrical arc that can damage the probe tips.

Therefore, the relay obtained from IXYS – Clare, Massachusetts [44] is incorporated into the circuit of the Ruggeduino and microswitches to give control in voltage output to the probe. This particular LCA710 relay can block voltage up to 60V. It has a pin configuration as shown in Figure 4.6.

Pin 1 is connected to the Ruggeduino as the control pin so that the output voltage can be controlled via the Ruggeduino coding. Pin 6 is connected to the voltage supply which is blocked prior to transferring. Pin 5 is connected to the voltage input pins of the four-point probe.

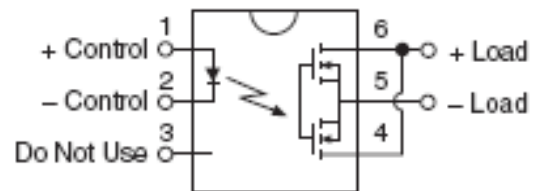


Figure 4.6: Relay wiring diagram [44]

#### 4.2.5 Microswitches

There are two microswitches from Honeywell, New Jersey used in this circuit. The first microswitch is used to signal the relay that the springs of the four-point probe



Figure 4.7: Microswitch [45]

are now in contact, so the voltage can be unblocked and transferred to the probe.

An identical microswitch is used to signal when the linear guide has reached the end of its travel.

The two microswitches are connected to the Ruggeduino via output pins, and are mounted on the mechanical hardware of CTS.

#### 4.2.6 Assembly

The overview electrical assembly of the microcontroller system is shown in Figure 4.8.

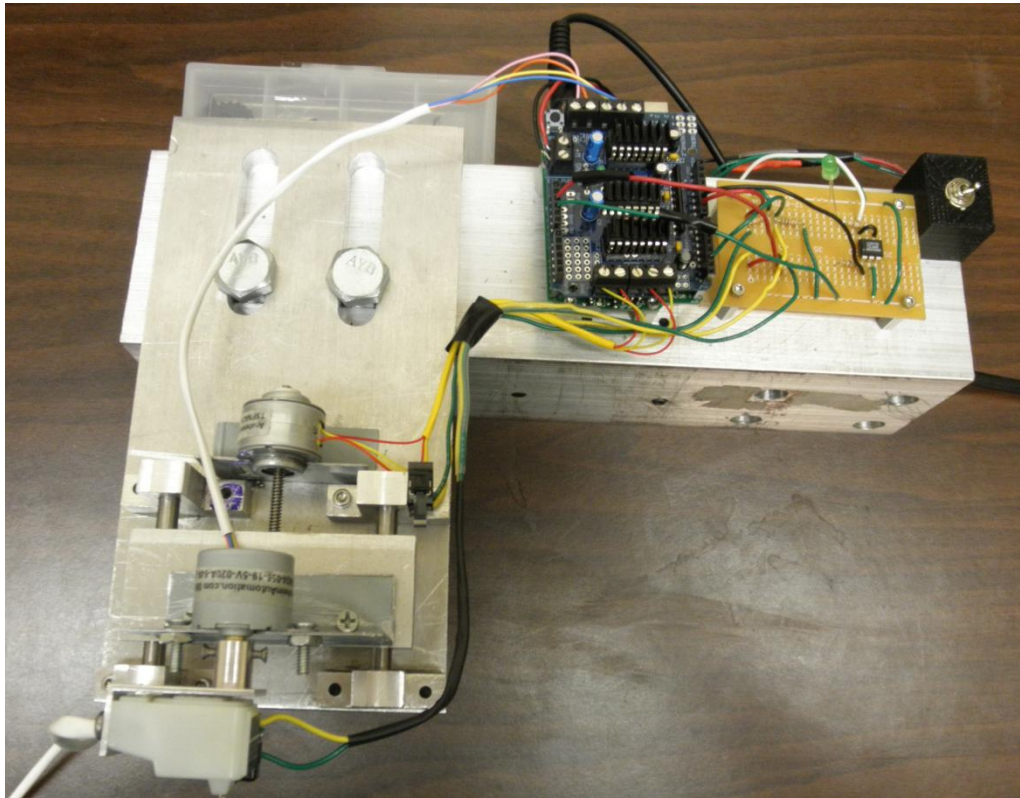


Figure 4.8: Assembly of microcontroller system



#### 4.2.7 Programming

The following schematic describes the logic behind programming of the microcontroller. Stepper motor 1 operates to carry the FPP sensor to approach a loaded specimen. When the sensor is in contact with the specimen, microswitch 1 signals to return stepper motor 1 to the original position indicated by microswitch 2. Once FPP sensor is back to the original position, stepper motor 2 rotates the sensor in 90 degrees increment (clockwise or counterclockwise depending on the order of the loop). After that, the same operation is then carried.

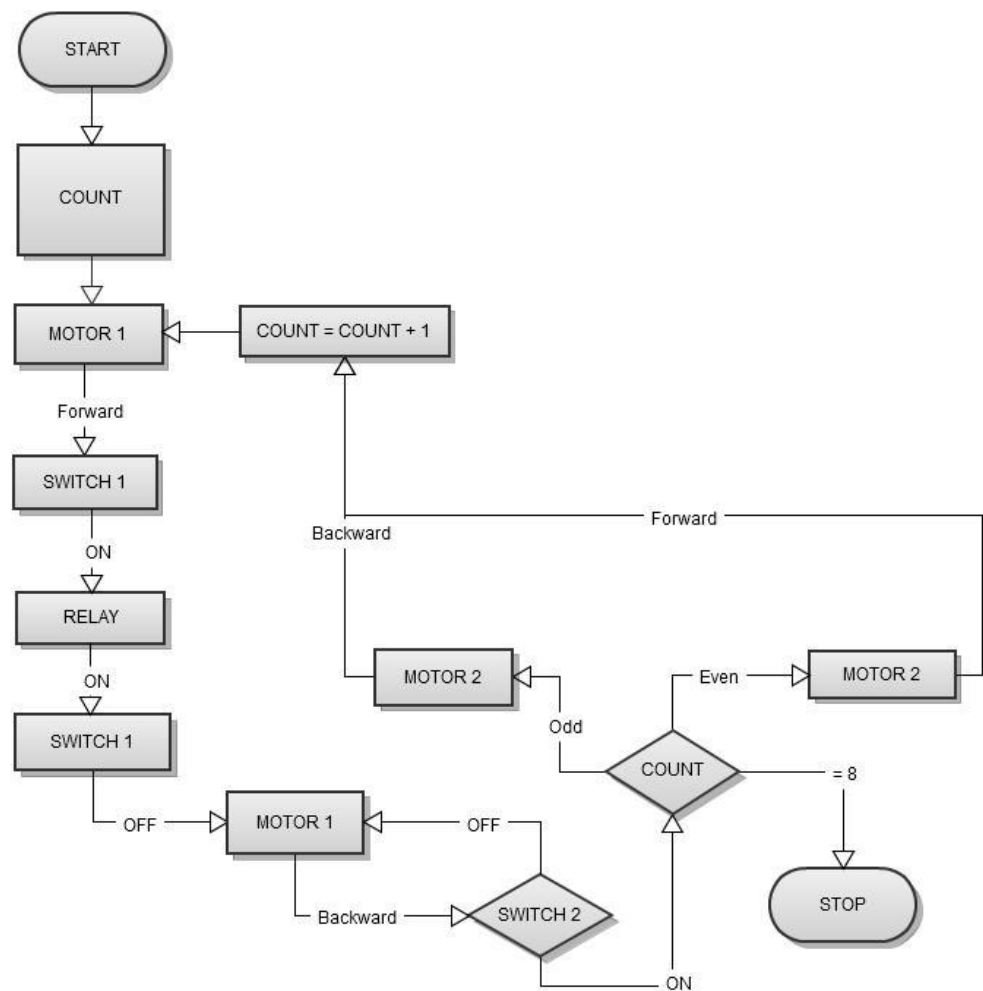


Figure 4.9: Flowchart of Arduino programming

## 4.3. Data Acquisition System

### 4.3.1 Keithley 6415 Programmable Picoammeters

The Keithley 6415 picoammeter [47] is a high-performance system which can measure voltage, current, resistance and charge. For this study, a Keithley 6415 is used to measure either current or voltage output from the four-point probe. The Keithley 6415 can also be controlled using the RS-232 interface, which is convenient to interface with TestPoint™ software.

### 4.3.2 ELC DC Power Supply AL 991S

The ELC DC Power Supply AL 991S [48] is a digital regulated power supply. It can be regulated with system designed platforms such as TestPoint™ or LabVIEW. The power supply can provide up to  $\pm 15\text{VDC}$  via three different channels. In this study, the power supply inputs voltage to the four-point probe via digital commands from TestPoint™. It is also compatible with the RS-232 interface.

### 4.3.3 TestPoint™

The main software that is used for data acquisition is TestPoint™ [49]. It is a software package for designing test and measurement applications. The use of TestPoint™ in this study is to control the DC power supply and a picoammeter. TestPoint™ monitors the voltage of the power supply, and when the program receives data from the picoammeter, it collects and imports the data in Microsoft Excel spreadsheet format. The schematic of how TestPoint™ is connected with the power supply and the picoammeter is shown in Figure 4.10.

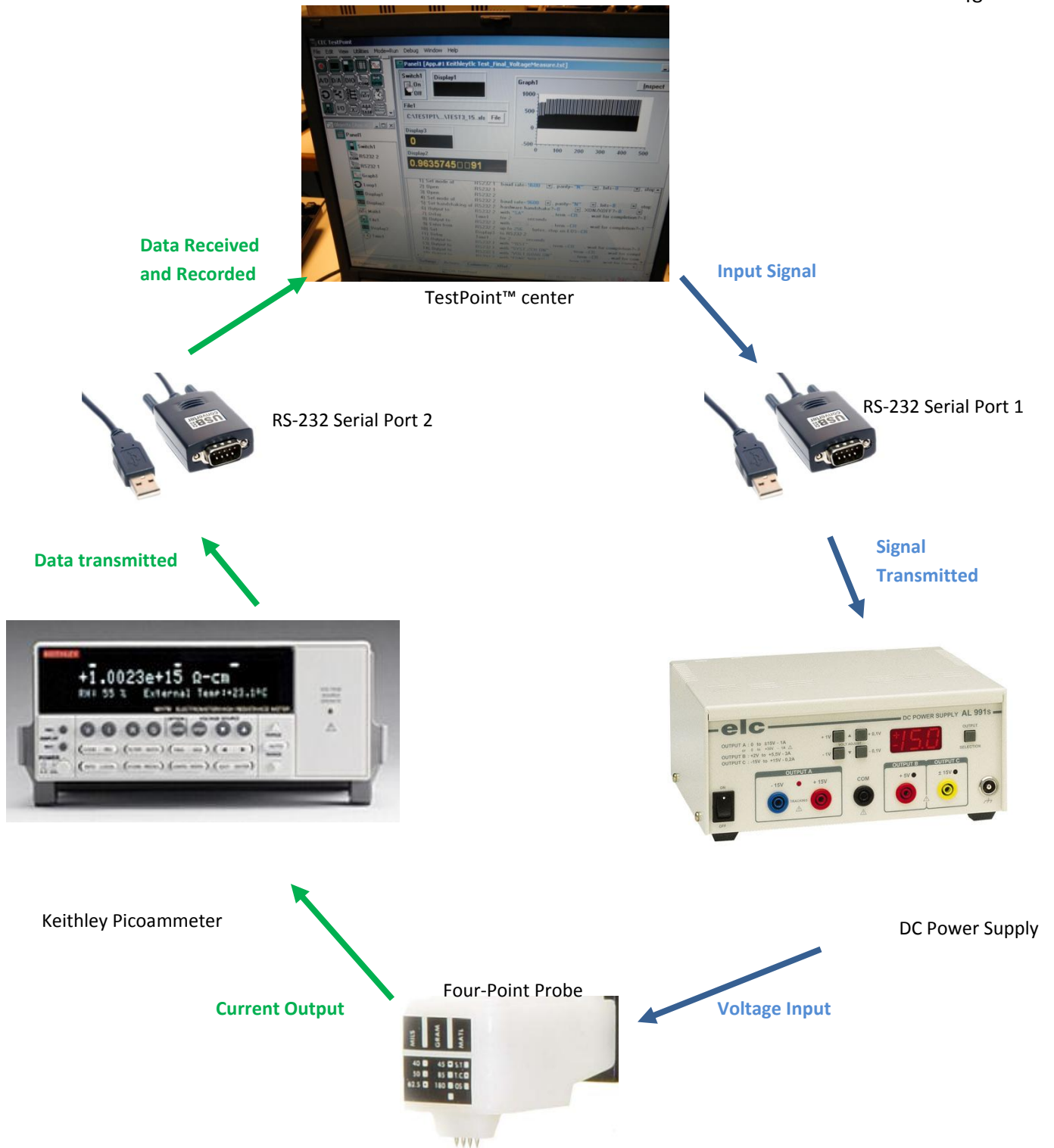


Figure 4.10: Diagram of DAQ system

## 4.4 System Assembly

The complete assembly of the control system is shown in Figure 4.11.

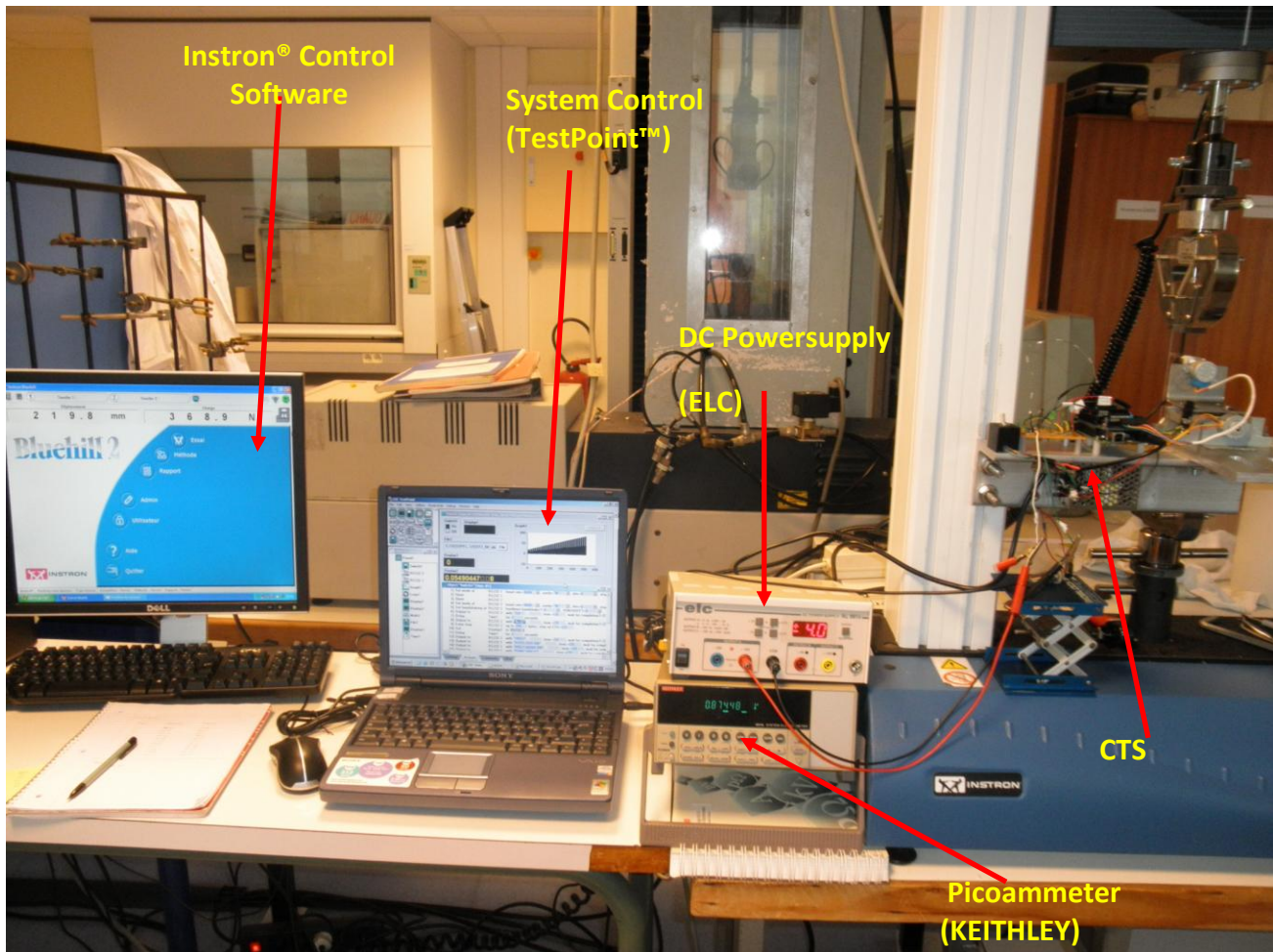


Figure 4.11: Complete assembly of the control system

CTS and its control system operate synchronously with the Instron® 3365 and its Bluehill® control software. The primary intention for the synchronization between the TestPoint™ and Bluehill® software was to collect data from both systems and to store them in the same spreadsheet file for processing. TestPoint™ exports the data obtained from the picoammeter in an Excel worksheet. Bluehill® also collects information such as time, deformation rate, displacement rate, etc., and stores these data in an Excel file. However, as Bluehill® controls the actuation of the Instron®, data obtained from Bluehill® do

not get exported into a file until the routine is completed and terminated. After that, the Excel file that contains raw data from the mechanical test is then free for access. This circumstance leads to the lack of a destination file for inputs from TestPoint™. While CTS is working during the mechanical manipulation, TestPoint™ is trying to find an Excel file to save its data, but the file does not exist until the test is completed. Therefore, the ideal implementation of file synchronization cannot be performed.

A second approach, which is also easier and is the approach ultimately adopted, is to use time synchronization. In time synchronization, Bluehill® and TestPoint™ collect and store data individually. By enforcing that the two data files include time and sampling rate information, the desired data can be copied to a common Excel file and synchronized in a post-processing step.

## PART B: THE EXPERIMENT

### CHAPTER 5: EXPERIMENTAL TESTING ON POLYMERS

#### 5.1 Materials and Methods

The next objective of this study is to employ CTS and FPP method on materials of interest while being tested under the Instron®. As we have presented our motivation in Section 2.2, we are interested in polymeric materials which are commonly used in applications such as space vehicles, biomaterials, or plastic electronics. Whereas mechanical stimulations are not dramatically difficult to perform, electrical resistivity testing is more complex. Therefore, prior to implementation on polymeric specimens, calibration process was carried out using semiconductive silicon wafers as subjects.

##### 5.1.1 Silicon wafers

Silicon wafers were chosen to be the first samples to be tested under FPP test because they are semiconductive with known resistivity values. Therefore, silicon wafers are good candidates to characterize the accuracy of the FPP sensor. Silicon wafers were supplied by the Université de Toulouse with three different types as shown in Table 5.1.

**Table 5.1: Characteristics of silicon wafers**

Type	Resistivity ( $\Omega \cdot \text{cm}$ ) = $\rho$	Thickness ( $\mu\text{m}$ ) = $t$	Length (cm) = $l$	Width (cm) = $w$
1	3.8 E-3	500	1.72	1.65
2	3.45	722	1.42	1.29
3	3000	372	1.11	0.98

Type 1 and 2 wafers are from ePAK, Austin, Texas, and type 3 is from Fluoroware, Inc., Minnesota. The wafers are always protected in wafer boxes to prevent any undesired oxidation or contamination.

Three different samples of wafers were subjected to static FPP tests. The purpose of silicon wafer testing is to determine whether the FPP sensor works appropriately, not to obtain the relationship between their electrical and mechanical behaviors; thus no mechanical stimulation was needed. Samples were placed on a clean, flat insulating surface. The FPP sensor was connected to the DC power supply via a  $470\Omega$  resistor for current input, and to the ammeter for voltage measurement (see Chapter 4 and Figure 5.4). The FPP sensor was hand-held during these tests for simplicity.

According to ASTM-F84 [9], there are recommended nominal current values for different types of resistivity. These are shown in Table 5.2. The recommended current values are based on achieving 10mV of specimen voltage between two inner probes with specimen thickness of 0.5mm.

**Table 5.2: recommended current inputs for FPP test [9]**

<b>Resistivity (<math>\Omega\cdot\text{cm}</math>)</b>	<b>Current</b>
<b>&lt;0.03</b>	100mA
<b>0.03 to 0.3</b>	25mA
<b>0.3 to 3</b>	2.5mA
<b>3 to 30</b>	250 $\mu\text{A}$
<b>30 to 300</b>	25 $\mu\text{A}$
<b>300 to 3000</b>	2.5 $\mu\text{A}$
<b>&gt;3000</b>	0.25 $\mu\text{A}$

To achieve the recommended values of current, a different resistor is used to control the input current to the outer pins of the FPP sensor. The values of voltage and resistance are as indicated in Table 5.3.

**Table 5.3: Silicon test parameters**

<b>Resistivity (<math>\Omega \cdot \text{cm}</math>) = <math>\rho</math></b>	<b>Input Voltage (V)</b>	<b>Via Resistance</b>	<b>Current Expected</b>
<b>3.8 E-3</b>	1-15	110 $\Omega$	9mA to 136mA
<b>3.45</b>	1-15	12 k $\Omega$	82 $\mu$ A to 1.2mA
<b>3000</b>	1-32	2.5M $\Omega$	0.4 $\mu$ A to 13 $\mu$ A

As shown in Table 5.1, the dimensions of the silicon wafers matched the criteria for equation 11, and thus the bulk resistivity  $\rho$  was calculated using equation 11. The reported result is calculated as an average value of bulk resistivity  $\rho$  from the obtained data. The confidence interval  $\Delta \rho$  of the mean conductivity value was calculated using the confidence coefficient of  $1-\alpha = 0.95$ . The coefficient of variation  $\gamma$  was calculated as  $\gamma = \Delta \rho / \rho$ , and along with  $\Delta \rho$ , was used as an evaluation of random measurement error.

### 5.1.2 High Density Polyethylene (HDPE)

The first polymeric material was used for the experiment was high density polyethylene (HDPE) from Polimeri Europa, Italy. PE is the most widely used mass-produced plastics and is incorporated in tremendous amount of applications. The target materials used in this study are common polymers, such as polyethylene (PE). Specimens of PE were prepared in the typical dog-bone shape with dimensions of 110mm X 10mm X 4mm subjected to tensile testing using the Instron® 3365 via Bluehill® testing software. The specimen is subjected to a tensile test with a deformation rate of 5mm/minute. The information logged in the Bluehill® software regarding the tensile test includes time, load, displacement, and deformation percentage (strain). Concurrently, the specimen is subjected to FPP testing via TestPoint™ software to measure the voltage output as a function of time. Results from both software packages were then synchronized to develop the relation between the electrical and mechanical behavior of the specimen.



For highly resistive materials such as PE, it is recommended to have a very low current input, approximately  $1\mu\text{A}$  or smaller to make sure not too much voltage potential is induced on the inner pins. Therefore, the minimum voltage that the power supply can provide ( $0.1\text{V}$ ) and a very large resistor ( $1\text{M}\Omega$ ) were coupled to provide a constant current of  $0.1\mu\text{A}$  input to the two outer pins of the FPP.

### 5.1.3 Polyethylene/Carbon Nanotubes Composite

Depending on their chemical characteristics, carbon nanotubes with a small diameter are either semi-conducting or metallic [63]. Recently, carbon nanotubes have been widely used as conductive fillers for fabricating conductive polymer composites based on both thermoplastic and thermosetting polymers. Also, one of exciting features of CNTs is that their volume electrical conductivity can be estimated in longitudinal and transverse directions for molded conductive polymer composites [59]. This particular feature makes CNTs a suitable candidate for this study because we are interested in examining the electrical conductivity of polymers in both longitudinal and transverse directions with respect to the polymer fibers.

299.25g of HDPE was mixed with 0.75g of CNTs and placed inside the extruder to produce a 0.25%wt of CNTs composite sample as shown in Figure 5.1.



Figure 5.1: Carbon nanotube composite manufacturing procedure: raw materials of CNTs (a) and small beads HDPE (b) are proportionally determined and mixed together (c) prior to transfer to a plastic extruder (c). The melted compound is then pushed through the barrel and collected to continue on the press molding process (d) to produce the final product of CNTs/HDPE plastic sheet (e) which can be cut into desired specimen shapes.

#### 5.1.4 Polyethylene with metallic surface layers

A specimen of polyethylene and 5% polypropylene (PEPP) with dimensions of 123 x 34 x 3.3mm was prepared to have a surface deposit. A 3 x 3 cm area on the surface of the specimen was polished and deposited with a 10nm layer of chromium. Another similar sample was deposited with a 200nm chromium layer. The specimens underwent the FPP test to measure the electrical potential with a constant current input of 21.3mA.



Figure 5.2: a) PEPP with chromium deposited surface; b) CERAC silver epoxy cement and catalyst

A specimen of PEPP 5% with dimensions of 123 x 34 x 3.3mm was prepared to have a surface deposit. Silver-filled epoxy cement was obtained from CERAC Inc., Milwaukee, WI. The silver-filled epoxy cement is a silver-colored thick paste containing the optimum ratio of silver powder to epoxy resin for maximum thermal and electrical conductivity. There are two components in the paste: the epoxy cement and catalyst [68]. The typical volume resistivity given by the manufacturer is less than  $0.001 \Omega \cdot \text{cm}$ .

A small quantity of catalyst and epoxy cement were added together and mixed thoroughly. Then the mixture was spread evenly and smoothly across the clean surface of the PEPP specimen. The specimen was left overnight at room temperature for drying. The thickness of silver paste on the specimen was measured to be 0.4mm.

After the specimen was dried and ready to be tested, the specimen was set up on the Instron® to undergo a tensile test at a rate of 5mm/min. The specimen also was subjected to the FPP test with constant input current of 32mA. Since the exact value of the volume resistivity of the silver paste was

not provided, a conservative current of 21.3mA was applied, which is close to but somewhat lower than the recommended range of 100mA [9] for volume resistivity of semiconductors of  $>0.3 \Omega \cdot \text{cm}$ . The recommended value is for semiconductive materials such as silicon wafers, but not metallic materials. Therefore, caution was exercised in selecting the current input to make sure damage to the FPP was avoided.

Another specimen of HDPE was used for a different surface preparation. A small amount of CERAC silver epoxy cement was well mixed with ethanol solvent. The solution was then brushed on the surface of the HDPE specimen, which was left at room temperature overnight to ensure the ethanol solvent was completely evaporated and the silver particles were left as a fine thin layer on the surface of the specimen. The thickness of the layer was so small that it can be neglected in the study of sheet resistivity.

After the specimen was dried and ready to be tested, the specimen was set up on the Instron<sup>®</sup> to undergo a tensile test at rate of 5mm/min. The specimen was also subjected to the FPP test with a constant current input of 32mA.



Figure 5.3: HDPE specimen with silver/ethanol evaporated coating

Last but not least, a dog-bone HDPE specimen was prepared with a layer of silver conductive paint. The silver conductive paint was purchased from RS Components, Northants, UK. The paint is specified to have an electrical resistivity of smaller than  $0.001 \Omega \cdot \text{cm}$ . The paint was easily applied on the surface of the sample using a small cotton swab or thin brush. The sample was then subjected to the same tensile and electrical test as described in previous experiments: 5mm/min strain rate and 32mA current input. Also, previous tests were done just up to 8% of strain for the purpose of acquiring the trend in resistivity changes. In this experiment, the tensile tests were carried up to 40% of strain or until the specimens

ruptured. The purpose of extending strain rate is to attain as many data as possible to produce an accurate characterization of the mechanical/electrical relationship.

## 5.2 Four-Point Probe Sensor

### 5.2.1 Four-Point Probe Characteristics

A four-point probe (FPP), also known as four-terminal sensing, is a simple apparatus for measuring the resistivity of semiconductor samples [53]. It can measure either bulk or thin specimens, in which different formulas apply to each different case [54]. The FPP technique was originally developed by Wenner in 1916 to measure the earth's resistivity used in geophysics. In 1954, Valdes adopted the technique to measure the resistivity of semiconductor wafers. The technique has also been applied to characterize electrolytes and to analyze gases [55].

The FPP has four needle-like electrodes in a linear arrangement. Current is delivered to the material via the outer two electrodes, and the resultant electric potential or voltage is measured via the two inner electrodes [57]. The four probe tips are set up in such a manner due to geometric factors. All of the current delivered across the two outer probes flows through the region between the two inner probes [58]. It is easier to interpret the data obtained by four-point probe measurements as compared to that of a two-point probe because by using different electrodes for current supply and electric potential measurement, the contact resistance between the metal electrodes and the material will not appear in the formulation for resistivity. Figure 5.4 shows how the four-point probe is arranged.

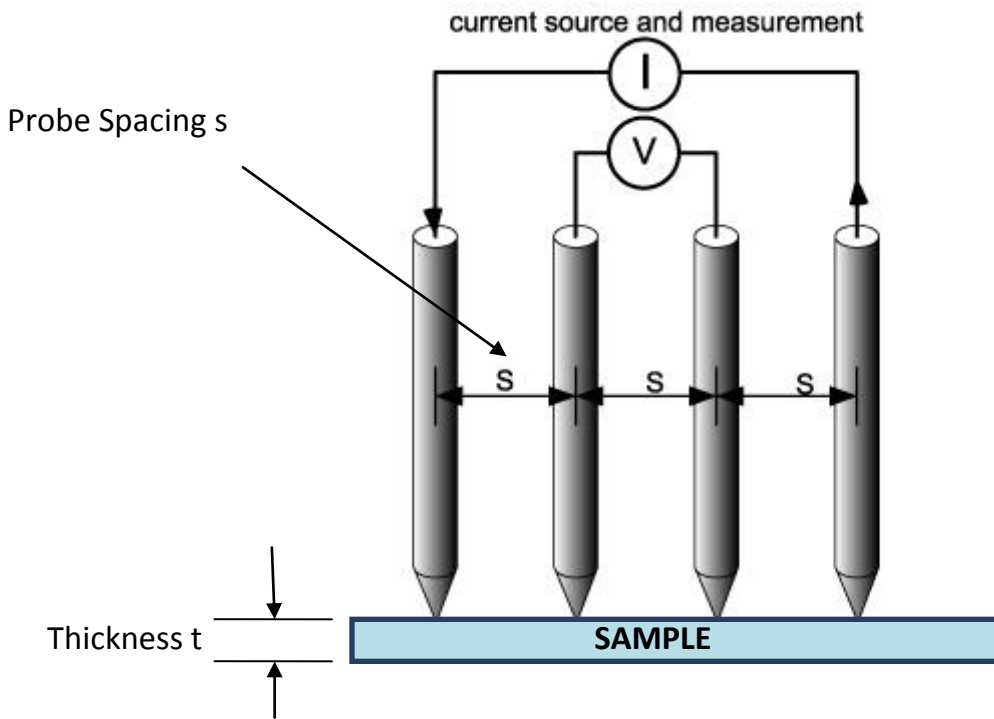


Figure 5.4: Four-point probe diagram [51]

There are several characteristics of the arrangement that can affect the measurement of the probe. These characteristics include probe spacing, probe tip material, probe tip radius, and spring pressure.

#### *Probe Spacing*

If  $\rho$  is the resistivity of a semi-infinite volume,  $I$  is the current flowing between the outer probes,  $V$  is the voltage measured between the two inner probes, and  $s$  is the distance consistent between each probe, then:

$$\rho = 2\pi s \frac{V}{I} \quad (6)$$

Probe spacing directly affects the measurement of resistivity. Common probe spacing ranges from 25Mils (0.635mm) to 62.6Mils (1.591mm).

#### *Probe Tip Material*

Two common materials used for probe tips are tungsten carbide and 50% osmium alloy with other platinum group metals such as platinum, rhodium, palladium, etc [58]. Osmium alloy tips are somewhat softer and less durable, and only in a few instances do they provide sufficiently superior contact to justify their usage. Osmium metal is lustrous, bluish white, extremely hard, and brittle even at high temperatures. Although diamond is much harder than osmium, osmium can withstand compression better than any known material. For those reasons, osmium alloy tips are more expensive than tungsten tips. Tungsten carbide is a crystalline material that is very hard and can be broken along the crystal boundaries with horizontal motion of the probe.

#### *Probe Tip Radius*

Depending on the materials being tested, the tip radius can be chosen from 1.6mils (40 $\mu$ ) to 20mils (500 $\mu$ ). The tip radius must be chosen carefully to correspond to the characteristics of the surface of the materials being tested, to make sure the tip is seated into the material deep enough to obtain the accurate properties of the material. It is recommended that for easily contacted films and thin films, one should use a 5-mil tip radius, 10-mil for very thin films, and less than 5-mil for other applications.

#### *Spring pressure*

The spring pressure is the pressure used to force each individual probe tip onto the sample surface to make electrical or Ohmic contact.

For easily contacted films such as metal films, soft films such as conductive polymers, or very thin films, the lowest spring pressure is desired to give satisfactory contact.

For difficult to contact samples such as high resistivity silicon or similar materials which naturally form a nonconductive layer when exposed to ambient air, high spring pressure is desired.

The range of 10 grams up to 200 grams spring load is commercially available.

#### *Probe configuration*

The configuration of the probe used in this study is described in Table 5.4.

**Table 5.4: Configuration of the Signatone Four-Point-Probe [35]**

Model	Spacing	Spring Pressure	Material	Tip Radius	Termination
Four-Point Probe	50 Mil	45Gram	Tungsten	1.6 Mil	38cm wire,
In-Line	(0.127cm)		Carbide	(0.0041cm)	flying lead

### 5.2.2 Four-Point Probe Theory

$\rho$  (Rho) is the resistivity parameter

V is the measured voltage between two inner probes

I is the current flow between two outer probes.

s is the spacing between each adjacent pair of probes. Ideally,  $s_1 = s_2 = s_3 = s$

If the sample is a semi-infinite volume, then, as described above [58]:

$$\rho = 2\pi s \frac{V}{I} \quad (7)$$

However, practical samples are of finite size. Therefore, correction factors are needed for the measurement:

$$\rho = \alpha 2\pi s \frac{V}{I} \quad (8)$$



where  $\alpha$  is the correction factor.

Valdes had derived correction factors for six different boundary configurations in 1954 [54]. Based on these findings, if the distance from any probe to the nearest boundary is at least 5 times the spacing, no correction is required. In other words, for samples whose thickness  $t$  is at least 5 times the probe spacing, no correction factor is needed; otherwise, the correction factor  $\alpha$  needs to be determined.

Case 1:  $\frac{t}{s} > 5$

$$\rho = 2\pi s \frac{V}{I} \quad \text{if } \frac{t}{s} > 5 \quad (9)$$

Case 2:  $\frac{t}{s} \leq 5$

The correction factor  $\alpha$  is calculated to be:

$$\alpha = 0.72 \frac{t}{s} \quad (10)$$

Substituting the factor into the basic equation, we have:

$$\rho = \alpha 2\pi s \frac{V}{I} = 4.53 t \frac{V}{I} \quad \text{if } \frac{t}{s} \leq 5 \text{ and } \frac{w}{s}, \frac{l}{s} > 5 \quad (11)$$

The value of  $\rho$  obtained is referred as bulk resistivity, and the units are  $\Omega \cdot \text{cm}$ .

Dividing both sides by the thickness  $t$  of the sample, we obtain:

$$R_s = \frac{\rho}{t} = 4.53 \frac{V}{I} \quad \text{if } \frac{t}{s} \leq 5 \text{ and } \frac{w}{s}, \frac{l}{s} > 5 \quad (12)$$

$R_s$  is referred as sheet resistivity.  $R_s$  does not depend on any geometrical dimensions. Sheet resistivity can be interpreted as the resistance of a square sample and has units of  $\Omega/\text{sq}$  or simply  $\Omega$ .

Equations (12) and (13) are valid under the assumption that the other two dimensions (width and length) of the sample are also very large compared to the probe spacing. However, if these other dimensions are not large enough, correction factors should be found in order to produce accurate measurements.

In general, to measure the sheet resistance of a small test area:

$$\rho = 4.53 t \frac{V}{I} F_1 F_2 \quad \text{if } \frac{t}{s}, \frac{w}{s}, \frac{l}{s} \leq 5 \quad (13)$$

where

(14)

$$F_1 = \frac{\ln 2}{\ln \left[ \frac{\sinh\left(\frac{w}{s}\right)}{\sinh\left(\frac{w}{2s}\right)} \right]}$$

and  $F_2$  is the finite width correction.

- $F_2 = F_{2C} d/s$  for a circular sample of diameter  $d$
- $F_2 = F_{2R}\left(l/w, d/s\right)$  for a rectangular sample of width  $w$  and length  $l$

The correction factor  $F_2$  can be found in [55].

### 5.2.3 Experimental Setup

The schematic of the FPP electrical circuit is similar to that described in Figure 5.4. As an inexpensive replacement for the current source, a resistor  $R$  is used with an ELC power supply to control the current  $I$  input to the FPP.

Depending on the material being tested (the anticipated range of resistivity), the value of R can be appropriately determined. Also, since the ELC power supply can provide up to only  $\pm 15\text{VDC}$ , the current input is limited.

**Table 5.5: Reading ranges of ELC power supply [48]**

Functions	Reading Range	Available Ranges
Volts	$\pm 10\mu\text{V}$ to $\pm 210\text{V}$	2V, 20V and 200V
Amps	$\pm 100\text{aA}$ to $\pm 21\text{mA}$	20pA, 200pA, 2nA, 20nA, 200nA, $2\mu\text{A}$ , $20\mu\text{A}$ , 200 $\mu\text{A}$ , 2mA, and 20mA
Ohms	10m $\Omega$ to 210 G $\Omega$	2k $\Omega$ , 20k $\Omega$ , 200k $\Omega$ , 2M $\Omega$ , 20M $\Omega$ , 200M $\Omega$ , 2G $\Omega$ , 20G $\Omega$ , and 200G $\Omega$

The method of FPP is an easy-to-apply procedure; however, there are important cautions that should be aware of to assure accurate results while operating the FPP test. The cautions include [57]:

- The probes must be able to make Ohmic contact with the material.
- Very low-resistance materials (e.g., aluminum, gold, platinum) require the maximum current from the current source to achieve a reading. Only very thin films (100s of Angstroms up to 1 micron thickness) can be measured. The current through the probe is best at 10mA, but not over 1A because of heating effects and excessive current density at the probe tips.
- Materials with high sheet resistivity (e.g., ion implanted silicon wafers, silicon on sapphire) can be measured using very low currents (values of  $1\mu\text{A}$  or less) and avoiding voltage indication greater than 200mV.

- An unclean sample or a sample that has surface doping will lead to inaccurate figures due to an impeded Ohmic contact or current leakage.
- *Ohmic Contact:*

$$V = IR \quad (15)$$

$$\leftrightarrow \log V = \log(IR) \quad (16)$$

$$\leftrightarrow \log V = \log I + \log R \quad (17)$$

$$\leftrightarrow y = ax + b \quad (18)$$

When graphing equation 17,  $\log V$  is presented as a function of the variable  $\log I$ . If the curve is linear and equation 15 holds true, the constant  $a$  should take a value very close to 1. Using this theory, we are checking to see whether the contact is Ohmic by comparing values of  $a$ .

### 5.3 Results and Discussions

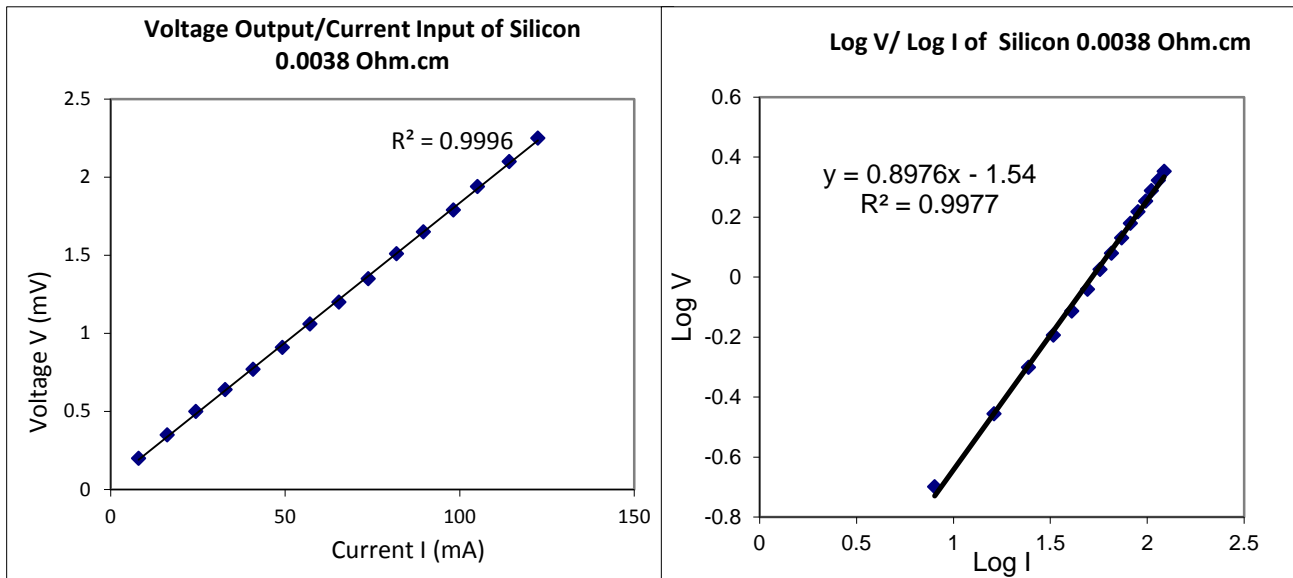


Figure 5.5: FPP test results of silicon  $0.0038\Omega\cdot\text{cm}$

Figures 5.5 -5.7 and Table 5.6 show the results of FPP tests with silicon wafers. The average bulk resistivity found for the nominal  $0.0038\ \Omega\cdot\text{cm}$  sample was  $0.0043\ \Omega\cdot\text{cm}$ , with 4.8% variation, as shown in Table 5.6. The data for this  $0.0038\ \Omega\cdot\text{cm}$  silicon wafer are graphed in Figure 5.5, showing that as the current input increases, the voltage output demonstrates a linear trend as expected. The linear fit has a high coefficient of determination  $R^2$ . Also, the result shows that the test was conducted in the range of Ohmic contact. The Ohmic contact coefficient was 0.89, which is close to the desired value of 1. In short, the result confirmed that the FPP is capable of giving a good resistivity test for materials that have bulk resistivity in the range of  $10^{-3}\ \Omega\cdot\text{cm}$ .

In a similar manner, the results obtained for the silicon wafer of  $3.45 \Omega \cdot \text{cm}$  (nominal) in Figure 5.6 were also to verify its compatibility with the FPP test. The Ohmic contact coefficient was slightly higher than that of the previous silicon wafer at 0.91. This result is acceptable to confirm that the test was in Ohmic contact. Therefore, the voltage/current curve is also expected to be linear. The average bulk resistivity was  $2.67 \Omega \cdot \text{cm}$  with 4.9% variation. We now can strongly conclude that the FPP test is good for the bulk resistivity range of  $10^{-3}$  to  $10^1 \Omega \cdot \text{cm}$ .

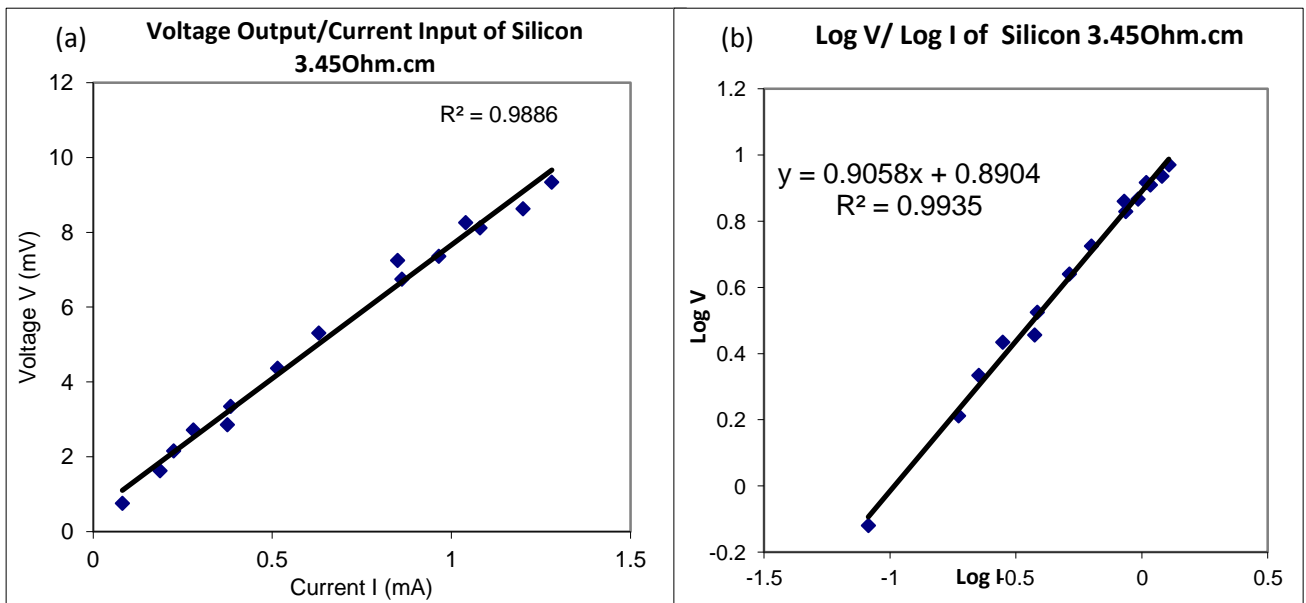


Figure 5.6: FPP test results of silicon  $3.45 \Omega \cdot \text{cm}$

A higher range of bulk resistivity was also tested with the  $3000 \Omega \cdot \text{cm}$  silicon wafer sample. However, the results for this test are not as favorable. As shown in Figure 5.7, the voltage/current curve does not follow a linear regression. Also, the average resistivity found for this sample was  $40,800 \Omega \cdot \text{cm}$ . This value is far from the target value of  $3000 \Omega \cdot \text{cm}$ . The coefficient of variation is 38%, which represents a very high random error of the test. The FPP thus appears incapable of measuring resistivity of  $3000 \Omega \cdot \text{cm}$  in this case. This phenomenon may be explained by the lack of protection among the wires and points of connections, which lead to major resistance leakage. As the result, the resistance of the system is now much smaller than the resistance of the sample, which tends to draw the current input

into the system, instead of passing by the sample. Thus, very small current or even no current was transferred to the sample so that the FPP test could be conducted. This is also a possible reason why there appears to be so much noise in this measurement.

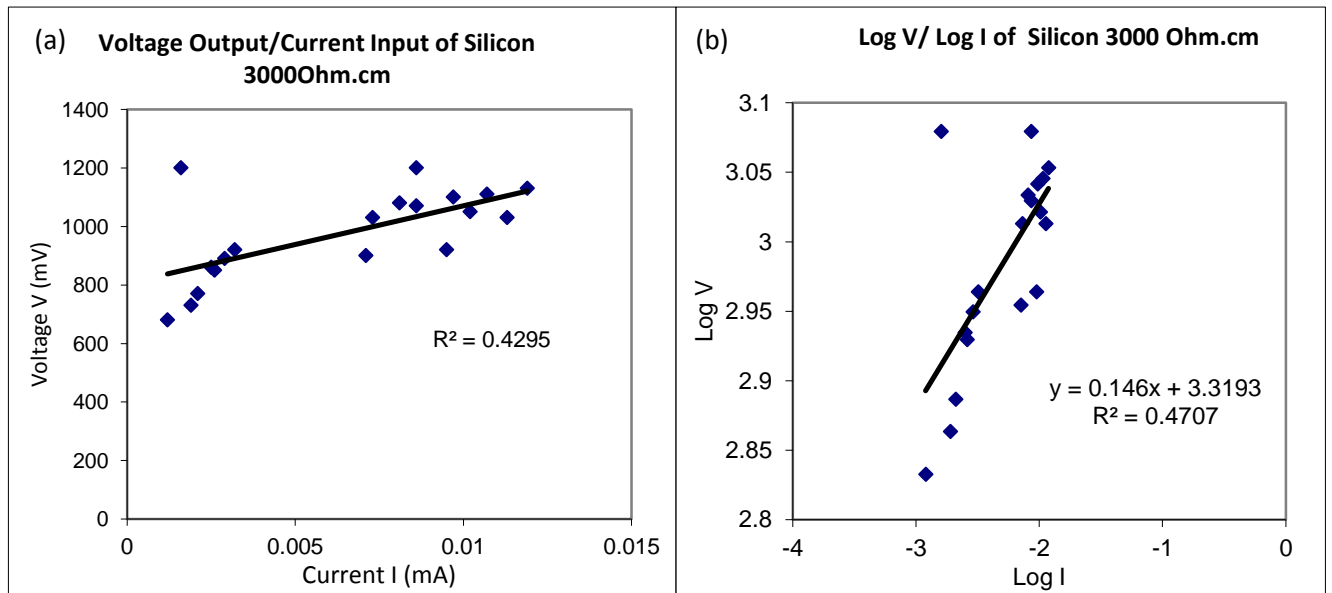


Figure 5.7: FPP test results of silicon 3000  $\Omega\cdot\text{cm}$

Table 5.6: Results of silicon wafers tests with FPP

Silicon Wafers	Measured bulk resistivity		Ohmic Coefficient	contact
	$\rho \pm \Delta \rho$ ( $\Omega\cdot\text{cm}$ )	$\gamma$ (%)		
0.0038 $\Omega\cdot\text{cm}$	$0.0043 \pm 0.0002$	4.8	0.897	
3.45 $\Omega\cdot\text{cm}$	$2.67 \pm 0.13$	4.9	0.906	
3000 $\Omega\cdot\text{cm}$	$40,800 \pm 13,800$	34	0.146	

In conclusion, the FPP test, using the equipment described, is valid in measuring electrical resistivity of semiconductors with bulk resistivity in the range of  $10^{-3}$  to  $10^1 \Omega\cdot\text{cm}$ . If a higher resistivity needs to be tested, system must be improved to prevent any resistance leakage.

A stress-strain curve was obtained for the PE specimen. The ultimate tensile strength observed for HDPE was 38MPa. The breaking point occurred at 13% deformation. The curve also displays HDPE's non-linear behavior. It is known that the non-linear stress/strain curves of HDPE and the modulus values derived from there are sensitive to rates of load application and are generally linear up to approximately 2% strain, also shown in Figure 5.8.

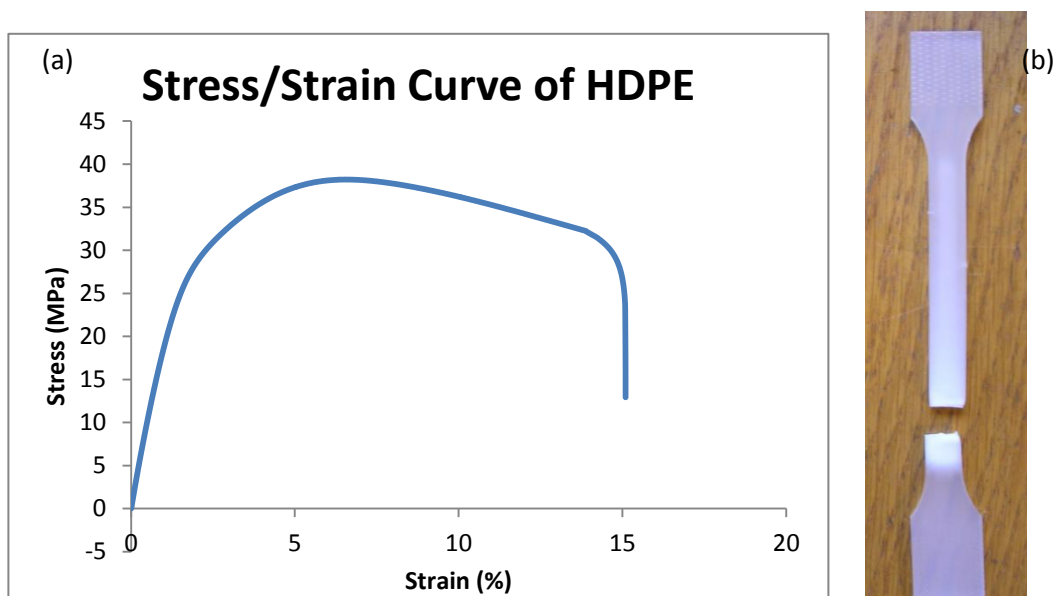


Figure 5.8: a ) Stress/strain curve for a HDPE specimen and b) the specimen ruptured after 15% of deformation.

These characteristics will be used as the control characteristics of HDPE for later comparison between plain HDPE specimens and HDPE specimens with surface preparation. The purpose of the comparison is to determine whether any surface deposit or modification would affect the original characteristics of HDPE.

For the FPP test, however, no useful measurements of the voltage output from the two inner pins were recorded. The readings were limited to noise. According to [77], the resistivity of HDPE is suggested to be  $10^{16}$  to  $10^{20} \Omega \cdot \text{cm}$ . Using equation 11 and this resistivity value, the voltage output was expected to



be on the order of  $10^{11}$  V, which cannot be captured by the Keithley ammeter. This explains why only noise was observed in this test.

As pertaining to the applicability of the method for testing high-resistivity materials, the FPP method is acceptable for materials (semiconductive and highly conductive) with a volume resistivity within a range of at least  $0.001\text{-}6000\Omega\cdot\text{cm}$  [62]. Thus, with the limitation of current input of the power supply and voltage range detection of the ammeter as well as the leakage of resistance, within the practical constraints of the FPP method, measuring the resistivity of HDPE is not feasible.

An alternative solution to make the polymer more conductive such that the FPP method can be appropriately applied is necessary. A first possible solution is to introduce conducting particles into the polymer mixture. Particulate and fibrous carbon materials such as graphite, black carbon, carbon/graphite fibers, and recently, carbon nanotubes, are widely used as conductive fillers for fabricating electrically conductive polymer composites [60, 63-65].

However, no readable voltage output measurements from the two inner pins were recorded. The observed data were limited to noise. The experiment was also carried out at different values of input current to see if some reading could be distinguished; however, no positive result was found. The current input was set from the smallest possible

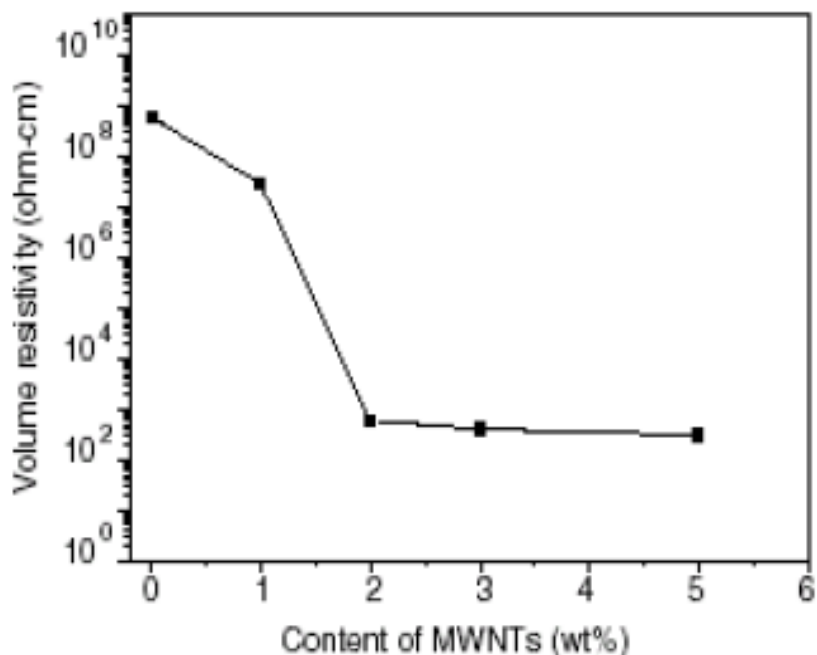


Figure 5.9: Electrical resistivity of a composite with different content of CNTs [67]

value of 1 $\mu$ A to the maximum recommended current of 1A (currents higher than 1A are not recommended for the FPP because they can heat up the FPP and damage it).

The influence of CNT contents on electrical properties of CNT-reinforced polypropylene (PP) composites was studied in [60]. The volume resistivity of the composites was shown to decrease with increasing CNT content [67]. The electrical percolation threshold was identified between 1 and 2 wt% CNT, which was caused by the formation of conductive chains in the composites.

According to this finding, the electrical resistivity of composite PP with 0.25 wt% CNTs is about  $10^9 \Omega \cdot \text{cm}$ .

A recent study conducted by Wen *et al.* published in early 2012 also mentioned the electrical conductivity of composites of carbon nanotubes/polypropylene (CNTs/PP) [66]. The study used CNTs as conductive fillers in PP composites to study the conductivity differences of the composites using a processing method of laminating-multiplying elements (divide and recombine polymer melts). They have shown the volume resistivity of CNT/PP as a function of CNTs concentration as in Figure 5.10:

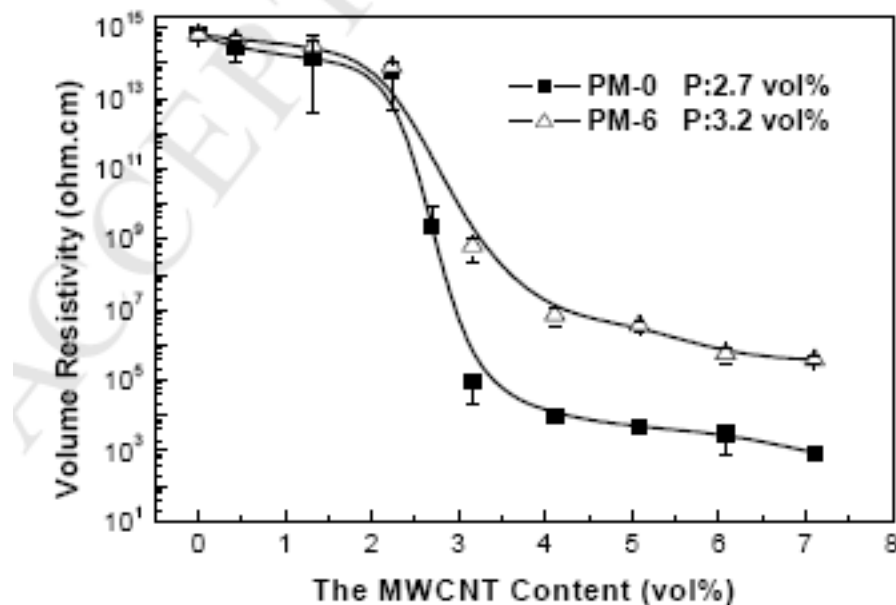


Figure 5.10: Electrical resistivity with different content of CNTs [66]

PM-O in Figure 5.10 corresponds to the CNT/PP composite processed without the laminate-multiplying element method and PM-6 is that with the method applied 6 times. The graph shows that using the new processing method, the percolation threshold of CNT/PP is increased to 3.2 wt%. Also, this study agrees with [67] that the percolation threshold of CNT/PP without any special processing method is at about 2-2.7 wt% with volume resistivity of more than  $10^3 \Omega \cdot \text{cm}$ . At a CNT concentration of 0.25 wt%, the volume resistivity is suggested to be in the range of  $10^{14} \Omega \cdot \text{cm}$ .

The findings of [66] and [67] seem to be applicable for the PE/CNT composite of 0.25 wt% that was manufactured for this study. That means the composite we have prepared may also still have very high resistivity ( $10^9$  to  $10^{14} \Omega \cdot \text{cm}$ ) due to its low percentage of CNTs. The only way to decrease the resistivity of our PE/CNT composite so that the FPP method can be successful is to increase the concentration of CNTs in the composite. However, in order to manufacture and process composites involving CNTs, a special laboratory setting is required to provide appropriate and safe conditions for handling CNTs, due to their carcinogenic nature [61].

Based on these limitations, it is necessary to find a material that can be tested with our currently available equipment. Moreover, the most important goal first and foremost in this project is to prove that the developed system is capable of studying the relationship between electrical and mechanical behaviors of a material. Although limitations prevent carrying out the proof of concept using normal polymers, the next solution undertaken is to use polymer specimens which have surface preparations of conductive materials (metals). This solution resolves the need for a conducting sample that fits with the measurement range of our system, and also provides an opportunity to study the threshold of electrical conductivity of the conductive surface with respect to applied deformation.

Chromium (Cr) has an electrical conductivity of  $7.9 \times 10^6$  S/m [78] or resistivity of  $1.27 \times 10^{-5}$   $\Omega \cdot \text{cm}$ . That means Cr is considered a conductive material. It was expected that a layer of Cr would lead to measurable data in the FPP test because the FPP test is considered valid for measuring conductivity of semiconductive or metallic materials. However, no discernible data were obtained. The experiment started with the specimen with the 10nm Cr deposit, and when the test turned out negative, the Cr layer was increased to 200nm. This test also resulted in a lack of any stable measurements. The suspected reason was that the pins of the FPP penetrated the layer of Cr, such that the tips of the probes

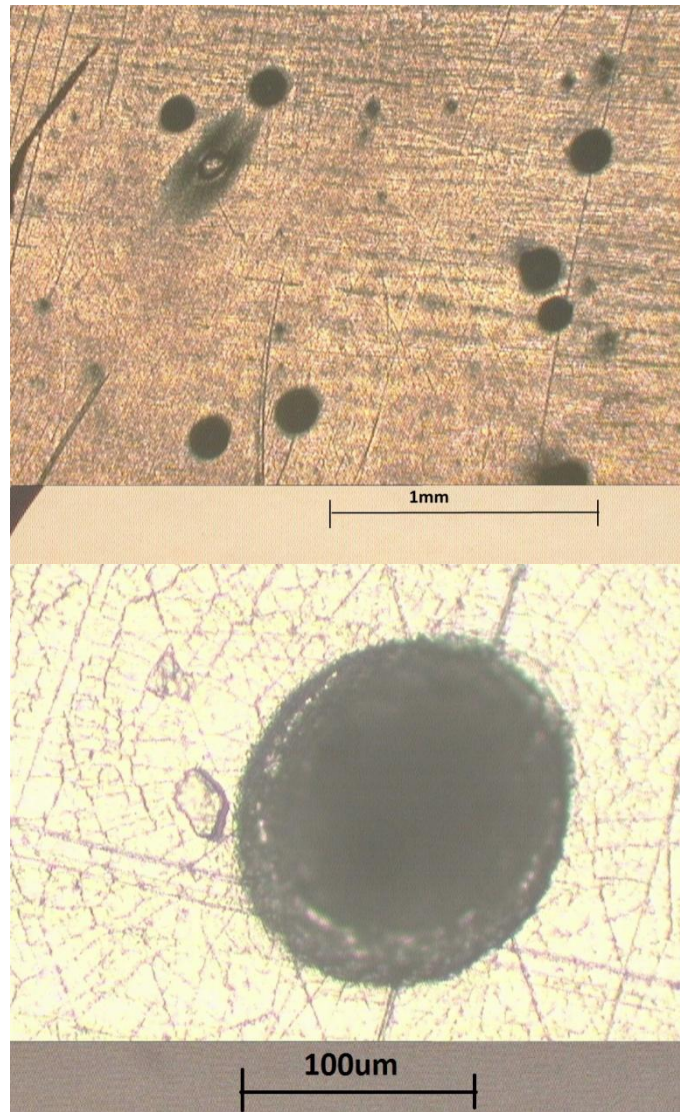


Figure 5.11: Surface of chromium deposited specimen after FPP test under Optic Microscopy

were in contact with the polymer, but not with the Cr layer. An optical microscopic observation was performed to understand this. As shown in Figure 5.11, the pins of the FPP did penetrate through the layer of Cr, leaving indentations in the surface of the PEPP specimen. The black spots on the image present the polymer portions which were exposed after the FPP test. Therefore, it is concluded that a 200nm layer of Cr on a polymeric specimen is too thin to be tested under the FPP. An increase in thickness of the layer is desired; however, the time and cost required are prohibitive. The next

approach is to use an easier method of depositing silver particles in a cement paste form. This method gives a thicker layer of the metallic material, and the preparation process is not very time consuming.

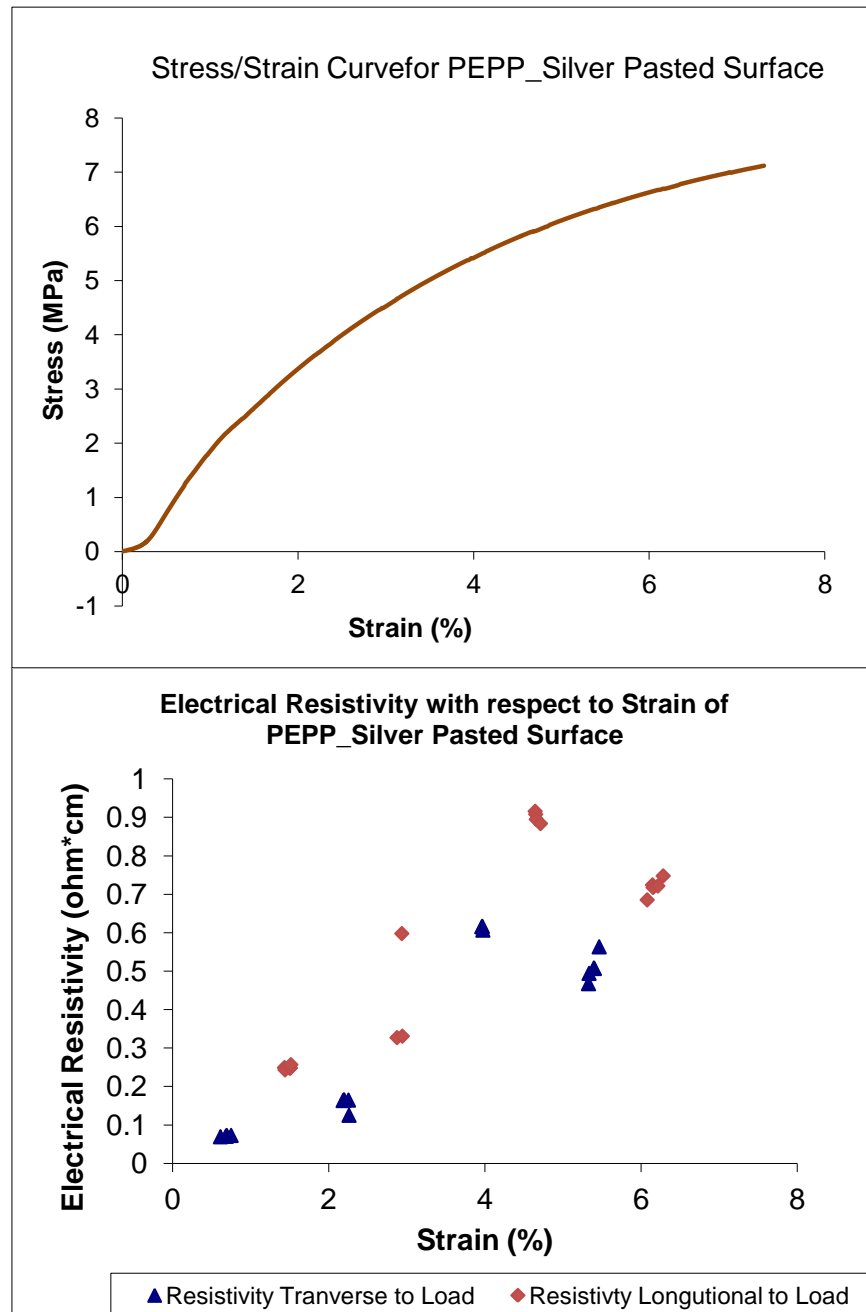


Figure 5.12: Results for PEPP silver pasted surface

The result shown in Figure 5.12 describes the general trend of electrical resistivity of the silver pasted surface increasing from  $0.069 \Omega \cdot \text{cm}$  to highest observed resistivity of  $0.91 \Omega \cdot \text{cm}$ . That is a gain of  $0.84 \Omega \cdot \text{cm}$  in resistivity after approximately 7% of strain, assuming the strain is uniform throughout the specimen. This preliminary result gives a first look at the relationship between the electrical and mechanical properties of the specimen. However, there are a couple of shortcomings associated with the results.

The first drawback shown in Figure 5.12 is that the electrical resistivity found in this study started with  $0.069 \Omega \cdot \text{cm}$ , which is too high compared to the suggested value. The manufacturer suggested the value of electrical resistivity of CERAC silver cement is less than  $0.001 \Omega \cdot \text{cm}$ . The difference can be explained by the value of current supplied to the inner pins of the FPP during the test. For such a conductive material as silver, a higher current input should have been provided to ensure the measurements are in Ohmic contact. However, since there is no defined value of the electrical resistivity of the silver paste, it is difficult to determine the necessary value of current input.

As described in Figure 5.12, directional measurements are also shown. The resistivity in the direction transverse to the direction of stress is always smaller than that along the direction of stress, in both cases of before and after the deformation increases. That could be explained by the fact that when the paste was applied to the specimen surface, the direction of spreading could affect the amount of silver deposited in each direction. Since the direction of spreading was transverse to axis of stress, more silver particles are deposited in the transverse direction compared to the longitudinal direction, causing the conductivity to be higher (or lower resistivity). Also, as the strain increases, the layer of silver is stretched anisotropically causing silver particles spreading more in the direction longitudinal to the stress axis than in the transverse direction, leading to the rapid increase in resistivity observed between 3% and 5% of strain along the axis of stress. Initially, it was expected to observe a decrease in resistivity

(increase in conductivity) in transverse direction to loading due to the Poisson's effect; however, the opposite result was seen. The resistivity in the transverse direction to the axis of stress also increases. No exact explanation has been made to depict this phenomenon.

One other observation found to be undesirable is that during the strain test, the silver surface tended to detach from the PEPP specimen. The reason could be that that epoxy is not adhesive or strong enough to keep the paste stable on the surface of the polymeric specimen. This observation leads to our next solution of using the method of evaporation deposit.

The tensile test at 5mm/min was terminated after 10% strain for the sample with ethanol coating silver. The electrical resistivity of the silver coated surface was found to be in the range of 0.010 to 0.0136  $\Omega\cdot\text{cm}$  as seen in Figure 5.13. Compared to the electrical resistivity in the range of 0.069 to 0.91  $\Omega\cdot\text{cm}$  found in the previous PEPP test, even though both specimens used the same silver epoxy cement, the resistivity found in the silver/ethanol coating was much lower. This could be due to the different methods of surface preparation; whereas in one method, the silver particles were applied directly on the surface, the silver was mixed with ethanol prior to the application in the other method.

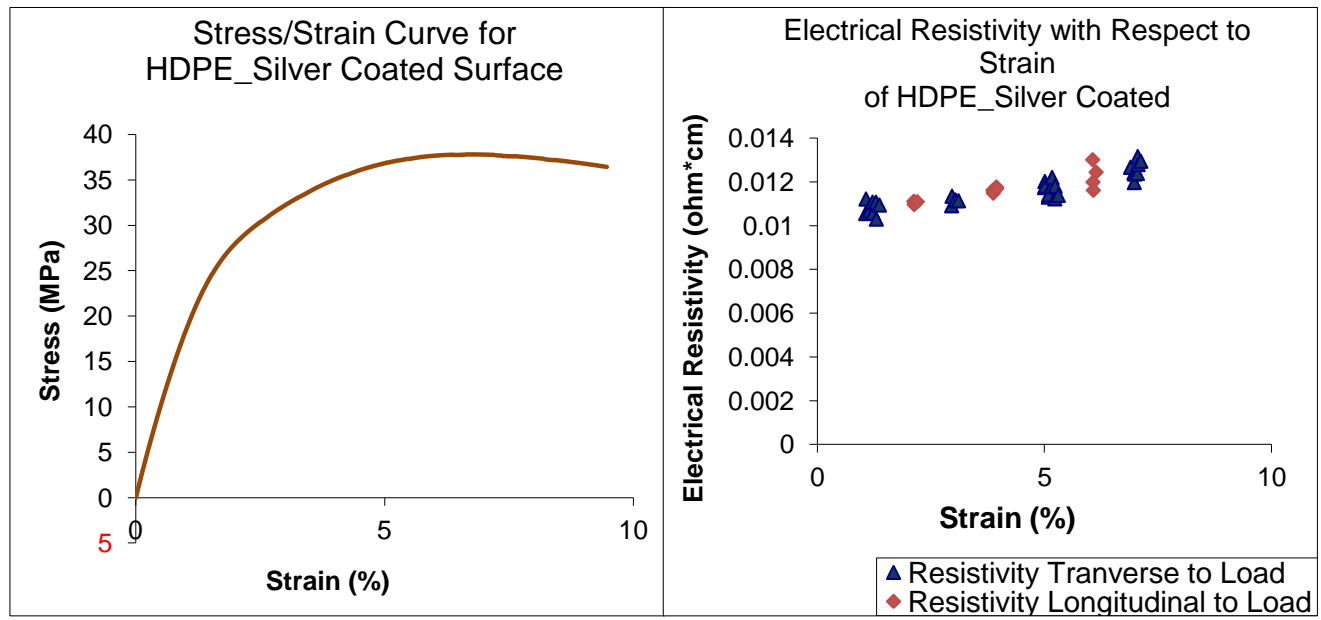


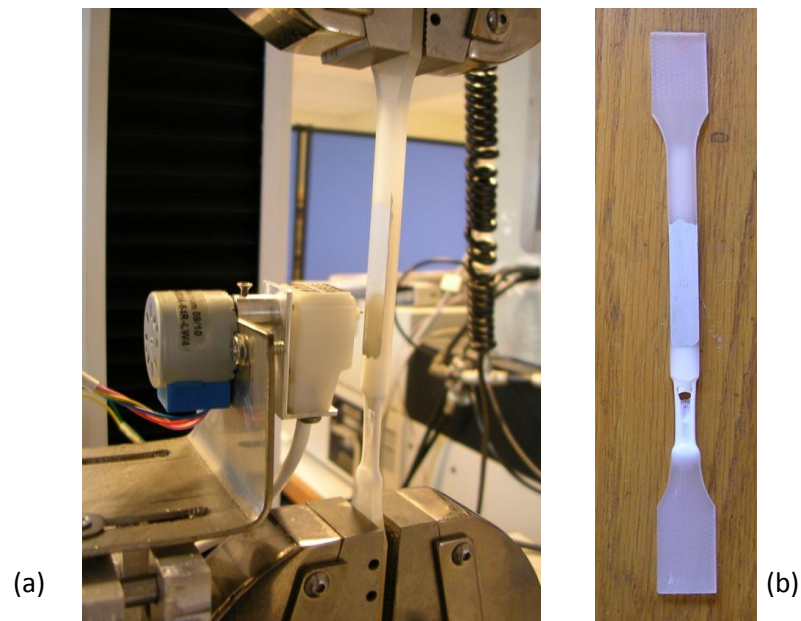
Figure 5.13: FPP test results for HDPE silver coated specimen

It was found that the surface layer of silver has an increase in electrical resistivity as the strain increases. The resistivity gains  $0.0036 \Omega \cdot \text{cm}$  after 10% of strain. This result is consistent with the previous result found in PEPP 5% specimen with silver paste, in which there is an increase in electrical resistivity with an increase in tensile strain, although the rate of gain in resistivity is different in the two experiments. As discussed in the previous section, the rate of gain in resistivity in PEPP 5% with silver pasted surface after about 7% strain is  $0.84 \Omega \cdot \text{cm}$  compared to  $0.0036 \Omega \cdot \text{cm}$  after 10% in the current case. The difference in the resistivity increase rate can be, again, due to the different methods of applying silver particles. More than that, it could be due to the difference in mechanical properties between PEPP and HDPE samples. At the same strain rate at 7%, the stress required to elongate the sample of PEPP was much smaller (7MPa in Figure 5.12) than the stress required to elongate the HDPE sample (about 38MPa in Figure 5.13). That means it is more difficult to stretch the HDPE sample than the PEPP 5% sample, leading to less change in resistivity of HDPE sample compared to that observed in PEPP 5%.



Via the preliminary results that we have found in the two experiments above, we are confident to say that we are capable of tracking the changes in electrical resistivity of surface metallic deposited polymers with respect to mechanical manipulations using our innovative CTS and FPP theory. The next set of experiments are performed to achieve a further goal, in which we are interested in characterizing the relationship between the mechanical and electrical properties of such specimens by empirically fitting obtained data. We also introduce another type of silver deposit, which is silver conductive paint. This paint is easy to apply. Also, since the silver/ethanol evaporation method did not always produce uniform drying even after overnight open air drying, and sometimes gave residues around the testing area, the paint can tackle these drawbacks.

The tensile test at a rate of 5mm/min was terminated at 40% strain for the sample with surface silver paint. As seen in the stress/strain curves for the test in Figure 5.14a, necking occurred at the range of 20% strain. Necking occurred at the area close to the bottom grips in Figure 6.14; however, the area of measurement was above the affected area in both cases. No significant elongation occurred in the local vicinity of the FPP test unfortunately, and that is the reason why the tests were terminated at the mentioned strain.



**Figure 5.14: Specimen under FPP and tensile test: (a) specimen position while loading with necking occurred below the testing area, and (b) specimen after the test**

A specimen of HDPE with silver painted surfaces underwent FPP tests while being subjected to tensile tests with strain rate of 5mm/min. The result is shown in Figures 5.15. The result agrees with what had been found in previous experiments with the evaporation-coated specimen, that as the strain increases, the electrical resistivity obtained also increases. Also, the resistivity in the direction longitudinally to loading seems to be always higher than that transverse to the loading direction. This finding also agrees to the result of the HDPE silver coated specimen shown in Figure 5.13. Similarly, this phenomenon could be explained by the fact that when the specimen is stretched longitudinally, silver particles are moving farther away from each other as the fibers stretch. Therefore, particles of silver are further apart in the longitudinal orientation compared to the direction transverse to the fibers, causing the decrease in conductivity or increase in resistivity (Figure 5.15).

Via this particular experiment, we can also observe another important phenomenon. As shown in Figure 5.15, the stress was homogeneously applied to the specimen until it reached 20% strain. At this position necking occurred, which theoretically alters the amount of stress and strain applied to different locations of the specimen. Consequently, the test should have been characterized by changes in the electrical resistivity. However, we observed no significant variation in electrical resistivity of the silver paint surface. The resistivity remains in a linearly increasing manner as the strain rate increases. No observation for changes in molecular structures has been displayed via the resistivity test. Therefore, we can conclude that the FPP test conducted only provides a good inspection of surface modification, not bulk molecular structure modifications.

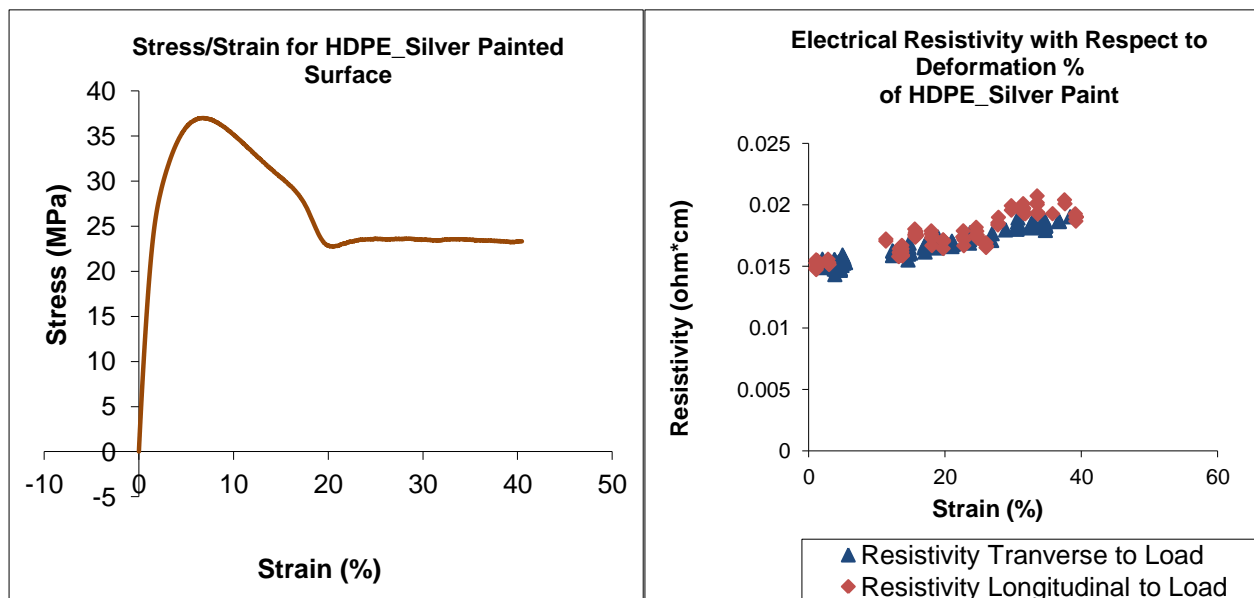


Figure 5.15: FPP test results of HDPE silver painted

The result represented in this study is significant and potentially responds to many current issues of conducting polymers in a variety of applications. For example, metal electrode materials used in active polymeric implantable devices are often reported to have poor long-term stimulation and recording performance. Researchers are looking for solutions to modify these materials for improving the tissue-electrode interface and increasing the effective lifetime of the implants [20-21]. The outcomes of this study offer a beneficial insight of how metallic surface modification on a polymer specimen changes its electrical properties as the polymer undergoes long-term mechanical stimulation. It is essential information that can assist in studies of biomedical applications involving conducting polymers or polymers with conductive surfaces such as in therapeutic body-machine interfaces, artificial muscles, controlled drug release, or even neural recording [21].

There was an attempt to modify the physical configuration of the specimen so that necking/elongation would occur at the FPP testing area. The attempt was done by decreasing the thickness of specimen

where the FPP was in contact. However, rupture of the specimen took place immediately after stress was applied. No further deformation happened to the specimen. Therefore, were not able to study the electrical resistivity changes of necking area.

One additional set of experiments was performed in order to understand what type of modification happened to the metallic layer while being loaded. The experiment was done by measuring the electrical resistivity of the silver paste layer during loading and reloading. The process took place within the elastic region to create hysteresis loops, which for HDPE are presented in Figure 5.8a, from 0% up to 5% strain. The schematic of this experiment is presented in Figure 5.16.

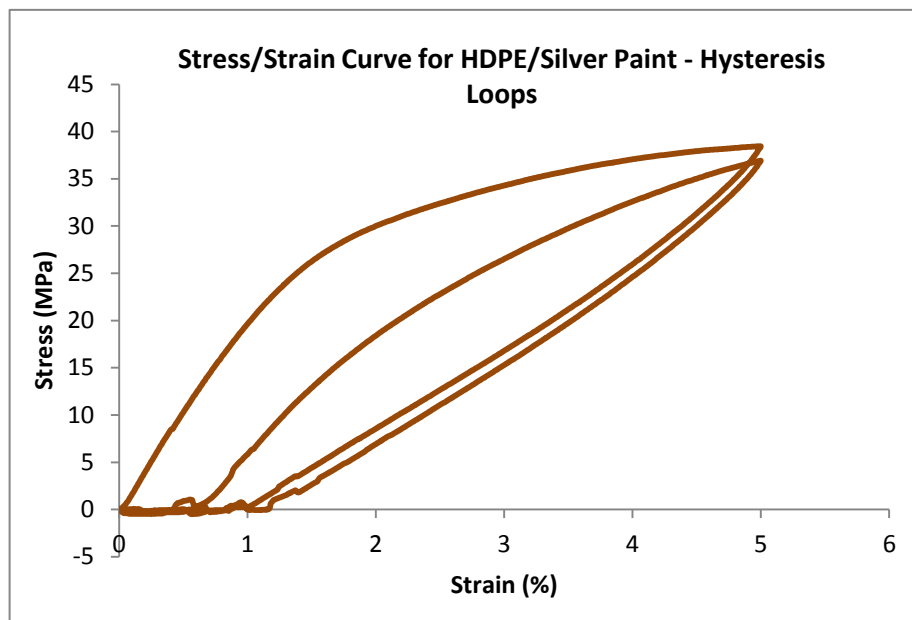


Figure 5.16: Reload test for HDPE/Silver paint

Two hysteresis loops were created. The specimen was loaded up to 5% strain, then unloaded back to 0% strain and another loop was done in the same manner. Figure 5.17 describes the electrical resistivity of the specimen for loading and unloading portions, explicitly.

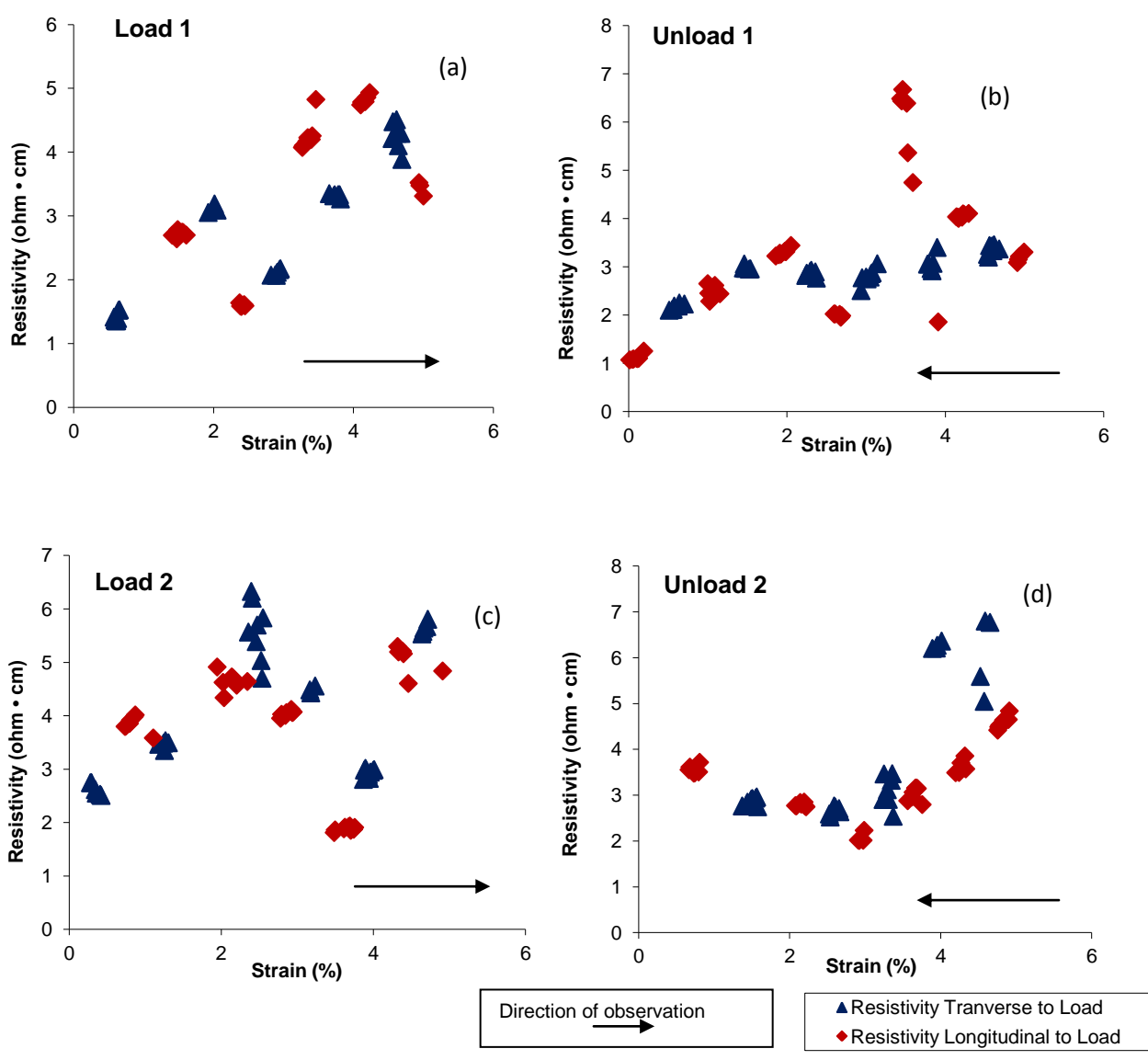


Figure 5.17: Result of FPP for hysteresis loops

There is an increase in resistivity for the 1<sup>st</sup> loading as shown in Figure 5.17a. This result is expected as we have seen the same trend observed in previous experiments. However, after the 1<sup>st</sup> loading, there are no particular trends observed in the 1<sup>st</sup> unloading and the 2<sup>nd</sup> loop. Figure 5.17b even shows a slight decrease in resistivity as the strain decreases; however, it is most likely that the silver layer could already form cracks, which leads to unpredictable changes in resistivity. In fact, the 2<sup>nd</sup> loading in Figure 5.17c does not follow the common trend of increasing strain leads to increasing resistivity. Instead, there is no particular relationship is formed here as well as in the 2<sup>nd</sup> unloading shown in Figure 5.17d.

In short, via the hysteresis loop experiment, we can conclude that it is most likely that stretching the specimen with silver paste surface layer tends to form cracks or fractures on the layer. This surface modification can be seen via changes in surface electrical resistivity.

## CHAPTER 6: CONCLUSION AND FUTURE WORK

A CTS was designed and built to couple with the Instron® 3365 universal testing machine to understand the relationship between the mechanical and electrical properties of mechanically loaded polymeric specimens. The system provides an innovative method allowing a pioneering study in material behavior. Uses of polymers include biomaterial applications, space applications including composite overwrapped pressure vessels, and recently as target materials incorporated in plastic electronic devices. Polymers in those applications come in different forms, sizes, shapes, and compositions. However, one of the most common conditions that the polymers experience is subjection to loading. Studies of polymer behavior under mechanical loading have been widely performed using universal tensile testing machines. However, none of the studies have been done to study a critical property of materials in relation to mechanical loadings: electrical conductivity.

The CTS was designed to attach on the Instron® 3365. The system was controlled using C programming via an Arduino microcontroller and a data acquisition system integrated with TestPoint™ software. The CTS consists of a four-point probe (FPP) sensor to conduct the electrical resistivity (conductivity) test on loaded samples on the system enables study of electromechanical behavior in both transverse and longitudinal orientations of the specimen.

The FPP test was first conducted on silicon wafers to verify the accuracy of the method, and to find the valid range of measurements. The result suggested that with the particular equipment resources available, the range of resistivity that the FPP can accurately measure is  $10^{-3}$  to  $10^1 \Omega \cdot \text{cm}$ .

Next, the FPP test was performed on specimens of polyethylene and other polymers. However, no useful measurements were obtained via this method due to very high resistivity that the polymers possessed. Carbon nanotubes (CNTs) were then incorporated into the polymers to create a conducting

composite so that the FPP can produce readable measurements. Within the current laboratory setting, we were able to produce a PE composite of 0.25% CNTs. The FPP test of this sample turned out to be unsuccessful. Literature suggested increasing the volume weight of CNTs up to 3 wt% to produce manageable readings for the FPP test. However, due to the carcinogenicity of CNTs, we were forced to abandon this method of applying CNTs in our polymeric composites.

Our next approach was to deposit metallic materials on the surface of polymer specimens. Even though this method does not guarantee an accurate understanding of the electrical behavior of polymers, the method provides an opportunity to understand the relationship of electrical and mechanical behaviors of a material in real time, which no studies have allowed before.

Specimens of polyethylene with 5% polypropylene (PEPP) and high density polyethylene (HDPE) were prepared with a thin layer of metallic material on their surfaces. The metallic materials included chromium and silver. A 200nm layer of chromium was deposited on a PEPP specimen, but the FPP penetrated through the layer, resulting in no useful data. Silver particles were then deposited using three separate methods: silver epoxy cement, silver cement/ethanol evaporated coating, and conductive silver paint. All specimens with silver layers produced readable measurements. These experiments allowed identification of a common behavior: as the deformation increases in the specimens, the resistivity of the metallic surface also increases. We suggest that due to breakdown of the metallic layer as it is stretched, silver particles move away from each other, causing a decrease in conductivity or increase in resistivity detected by the FPP. Also, the resistivity longitudinal to the direction of stress on specimens was always higher than that in the transverse direction. This phenomenon could be due to the method of applying the silver particles on the specimen's surface. But more importantly, it could be due to the local strain in the longitudinal direction being different from that in the transverse direction.



A hysteresis loop also was carried out with a specimen of HDPE with silver painted surface. The specimen underwent loading and unloading while surface electrical conductivity was being measured. The result possibly confirmed that applying stress on the specimen did alter the surface structure, in other words, forming cracks on the silver, which is depicted with random and inconsistent observations in surface electrical resistivity.

In the long run, microscale experiments could also be performed to determine the underlying cause of changes in resistivity and whether the change relates to the degree of disorder in material structures. Another interesting approach would be studying the mechanical-electrical relationship in conducting polymers (or conducting carbon-based polymer composites). To study conducting polymer composites using CNTs, an increase of CNT volume in the composite to at least 2% is desirable. Also, there are many other carbon-based materials such as black carbon, graphite powders, etc., that can be incorporated into the composite to increase the electrical conductivity. The potential for future studies using the basic concept of this study is great.

A few modifications are suggested to benefit future studies. First, it is necessary to implement a more advanced data acquisition system, in particular the current source and voltage meter. If studying polymeric materials is desired, a current source that can provide a direct low current in the range of micro to even picoamperes is critical. A low current is best to understand electrical properties of polymers which have very high resistivity values. A more sensitive and advanced voltage meter would also be beneficial. A voltage meter that can detect smaller changes in current input and give a stable reading is preferred in the study of FPP methods. Also, in relation to hardware system, more protection should be applied to all the electrical components to ensure that there would be no leakage of resistance occurring during testing. This step assures the current input would be directly applied on the sample and not to the system.

A second approach is to use a commercial test fixture according to ASTM D 991 – Rubbery Property - Volume Resistivity of Electrically Conductive and Antistatic Products. This method is used to evaluate the electrical behavior of nonconductive materials such as rubber products. In particular, model 831 D 991 Test Fixture [79] from Electro-Tech System Inc., is one of several commercial systems that can measure volume resistivity of non-conducting materials up to 10 MΩ in resistance.

In summary, the presented work has been shown to prove that the CTS is capable of measuring the electrical conductivity of a specimen while being mechanically stimulated under a tensile test. Specimens can potentially be different types of materials including polymeric materials, but limited to polymers with metallic surface modifications due to constraints in available testing equipment and protection for electronic components. However, we are optimistically anticipating that CTS would be able to perform experiments on desired materials subsequent to improvements that have been suggested throughout this paper.

## REFERENCES

- [1] Mark, J.E. "Part I – Structure." *Physical Properties of Polymers Handbook*. Springer Science + Business Media, LLC, 2007. 2-43. EPrint
- [2] Lovell, M.C., Avery, A.J. & Vernon, M.W. "Mechanical Properties of Materials." *Physical Properties of Materials*. Berkshire, Great Britain: Van Nostrand Reinhold Company Ltd, 1977. 87-123. Print.
- [3] Askeland, D.R. "Mechanical Testing and Properties." *The Science and Engineering of Materials*. London: Chapman & Hall, 1988. 145-185. Print.
- [4] Miller, E. & Rothstein, J.P. Control of the sharkskin instability in the extrusion of polymer melts using induced temperature gradients. *Rheol Acta* 44. 160-173 (2004).
- [5] Allal, A., Lavernhe, A., Vergnes, B. & Marin, G. Relation entre structure moléculaire et défaut de peau de requin pour les polymères linéaires à l'état fondu. *Rheologie* 8. 31-43 (2005).
- [6] Lovell, M.C., Avery, A.J. & Vernon, M.W. "Electrical Properties." *Physical Properties of Materials*. Berkshire, Great Britain: Van Nostrand Reinhold Company Ltd, 1977. 124-152. Print.
- [7] Schiefelbein, S.L., Fried, N.A., Rhoads, K.G. & Sadoway, D.R. A high-accuracy, calibration-free technique for measuring the electrical conductivity of liquids. *Review of Scientific Instrument* 69. 3308-3313 (1998).
- [8] "Electrical conductivity in materials –Measuring technique." Danish Technological Institute. Retrieved 12 Feb, 2012 at <http://www.dti.dk/27779,2>.
- [9] [ASTM-F84] ASTM Committee F-1 Standard Test Method for Measuring Resistivity of Silicon Wafers With an In-Line Four-Point Probe. Philadelphia: ASTM. 2000.

- [10] Meaden, G.T. *Electrical Resistance of Metals*. London: Heywood Books, 1966. Print.
- [11] Dugdale, J.S. *The Electrical Properties of Metals and Alloys*. London: Edward Arnold, 1977. Print.
- [12] Sutter, J.K., Jensen, B.J., Thomas, S.G., Morgan, R.J., Thesken, J.C. and Phoenix, S.L. Material Issues in Space Shuttle Composite Overwrapped Pressure Vessels. NASA 2006.
- [13] National Aeronautics and Space Administration. *2011 NASA Strategic Plan*. 5-34 (2011).
- [14] Ramakrishna, S., Mayer, J., Wintermantel, E. & Leong, K.W. Biomedical Applications of Polymer-Composite Materials: A Review. *Composites Science and Technology* 61. 1189-1124 (2001).
- [15] Nair, L.S. & Laurencin, C.T. Polymers as Biomaterials for Tissue Engineering and Controlled Drug Delivery. *Adv Biochem Engin/Biotechnol* 102. 47-90 (2006).
- [16] Wintermantel, E., Mayer, J. Anisotropic biomaterials strategies and developments for bone implants. *Encyclopedic Handbook of Biomaterials and Bioengineering*. Part B-1. Marcel Dekker: New York, 1995. P. 3-42.
- [17] Thull, R. Physicochemical principles of tissue material interactions. *Biomolecular Engineering* 19. 43-50 (2002).
- [18] Al-Ahmad, A., Wiedmann-Al-Ahmad, M., Carvalho, C., Lang, M., Follo, M., Braun, G., Wittmer, A., Mulhaupt, R. & Hellwig, E. Bacterial and *Candida albicans* adhesion on rapid prototyping-produced 3D-scaffolds manufactured as bone replacement materials. *Journal of Biomedical Materials Research Part A* 87. 933-943 (2008).
- [19] Coquet, L., Cosette, P., Junter, G.A., Beucher, E., Saiter, J.M. and Jouenne, T. Adhesion of *Yersinia ruckeri* to fish farm materials: influence of cell and material surface properties. *Colloids and Surfaces B: Biointerfaces* 26. 373-378 (2002).
- [20] Ma, Z., Mao, Z. & Gao, C. Surface modification and property analysis of biomedical polymers used for tissue engineering. *Colloids and Surfaces B: Biointerfaces* 60. 137-157 (2007).

- [21]Bendrea, A.D., Cianga, L. & Cianga, I. Review paper: progress in the field of conducting polymers for tissue engineering applications. *J Biomateria Appl* 26. 3-84 (2011).
- [22]Wang, W., Ouyang, Y. & Poh, C.K. Orthopaedic Implant Technology: Biomaterials from Past to Future. *Ann Acad Med Singapore* 40. 237-244 (2011).
- [23]Ravichandran, R., Sundarranjan, S., Venugopal, J.R., Mukherjee, S. & Ramakrishna, S. Applications of conducting polymers and their issues in biomedical engineering. *J. R. Soc. Interface* 7. 559-579 (2010).
- [24]Loo, Y.L. Structural elucidation of active layers in organic electronic devices via NEXAFS. *Materials Science and Engineering* 14. 1-9 (2010).
- [25]Horowitz, G. Organic Field-Effect transistors. *Advanced Materials* 10. 365-377 (1998).
- [26] Singh, Th.B. & Sariciftci, N.S. Progress in Plastic Electronics Devices. *Annu. Rev. Mater. Res.* 36. 199-230 (2006).
- [27]Dodabalapur, A. Organic and polymer transistors for electronics. *Materials Today* 9. 24-30 (2006).
- [28]Horowitz, G. Organic thin film transistors: From theory to real devices. *J. Mater. Res.* 19. 2004.
- [29]Tsumura, A., Koezuka, K. & Ando, T. Macromolecular electronic device: Field-effect transistor with a polythiophene thin film. *Appl. Phys. Lett.* 49. (1986).
- [30]Davis, Joseph R. (2004), *Tensile testing* (2nd ed.), ASM International, ISBN 9780871708069.
- [31]Gedney, Richard. Tensile Testing Basics, Tips and Trends. *Admet Quality Test & Inspection.* 2005.
- [32]"Series Dual Column Tabletop Universal Testing Systems." Instron®. Retrieved 9 Sep, 2011 at <http://www.Instron®.us/wa/product/3300-Dual-Column-Testing-Systems.aspx>
- [33]"Reference Manual – Instron® Series 3300 Load Frames Including Series 3340, 3360, 3380". [www.Instron®.com](http://www.Instron®.com). 2004. Print.

- [34]“Ball-Bearing Carriages and Guide Rails.” McMaster-Carr. Retrieved 9 Sep, 2011 at <http://www.mcmaster.com/#catalog/118/1096/=g8pa0f>
- [35]“Lucas/Signatone Four Point Probe Part Numbers.” Lucas/Signatone Corporation. 2010.
- [36]“Permanent Magnet Stepper Gearotor.” Anaheim Automation. Retrieved at [www.anaheimautomation.com](http://www.anaheimautomation.com).
- [37]“Permanent Magnet Stepper Motor Actuator.” Anaheim Automation. Retrieved at [www.anaheimautomation.com](http://www.anaheimautomation.com).
- [38]“Black-Oxide Steel Partial-Thread T-Slot Nut M6 Screw Size, 1mmPitch, for 8mm Slot Width.” McMaster-Carr. Retrieved at [www.mcmaster.com](http://www.mcmaster.com).
- [39]“Metric 18-8 SS Precision Socket Shoulder Screw Hex, 10mm Shoulder Dia, 8mm Shoulder L, M6 Thread.” McMaster-Carr. Retrieved at [www.mcmaster.com](http://www.mcmaster.com).
- [40]“The Ruggeduino.” Rugged Circuits. Retrieved 13 Jan, 2012 at <http://ruggedcircuits.com/html/Ruggeduino.html>
- [41]“Arduino – Introduction.” Arduino. Retrieved 13 Jan, 2012 at <http://arduino.cc/en/Guide/Introduction>
- [42]“Motor shield.” Ladyada. Retrieved 12 Jan, 2012 at <http://www.ladyada.net/make/mshield/solder.html>
- [43]“25W Single Output Switching Power Supply.” Mean Well. 2010. Retrieved at [www.meanwell.com](http://www.meanwell.com).
- [44]“LCA710 Single Pole, Normally Open OptMOS®Relay.” Clare – an IXYS Company. Retrieved at [www.clare.com](http://www.clare.com).
- [45]“Subminiature Snap Action Switch D3M.” OMRON. Retrieved at <http://www.components.omron.com>.

- [46]“Honeywell Part Number 11SM1 SWITCH-BASIC.” Honeywell. Retrieved at [www.honeywell.com](http://www.honeywell.com).
- [47]“Keithley Model 6514 System Electrometer Instruction Manual.” Keithley Instruments, Inc. 2003. Print.
- [48]“ELC DC Power Supply AL 991S.” Testoon. Retrieved at [www.testoon.com](http://www.testoon.com)
- [49]“TestPoint® QuickStart.” Capital Equipment Corporation. 2001. Print.
- [50]Bautista, Kevin. “Four-Point Probe Operation”. University of Texas at Dallas. 2004.
- [51]“The measurement of Sheet Resistivity.” PVEducation. Retrieved at <http://pvcdrom.pveducation.org/CHARACT/4pp.HTM>
- [52]Chan, James. “Four-Point Probe Manual.” EECS 143 Microfabrication Technology. 2002.
- [53]Schuetze, Andrew.P. A laboratory on the four-point probe technique. Am. J. Phys. 72. 149-153 (2004).
- [54]Valdes, L. G., Proc. I.R.E., 42, pp. 420-427 (February 1954)
- [55]Smits, F. M., "Measurements of Sheet Resistivity with the Four-Point Probe," Bell System Technical Journal 37, 711-718 (1958).
- [56]“Four-Probe Resistivity and Hall Voltage Measurements with the Model 4200-SCS.” *Keithley Application Note Series* Number 2475. 2011
- [57]“Lab Manual - Four-point Probe Resistivity Measurement.” Marvell Nanofabrication Laboratory Chapter 8.01 pg 1-4.
- [58]“Four Point Probes – Technical Information.” Bridge Technology. Retrieved at <http://www.four-point-probes.com/article.html>
- [59]Holtzknecht, L.J., Mark, H.B.JR., Ridgway, T.H. & Zimmer, H. Design and characterization of a four point probe for conducting polymer electrode studies. Analytical Instrumentation 18. 23-35 (1989).

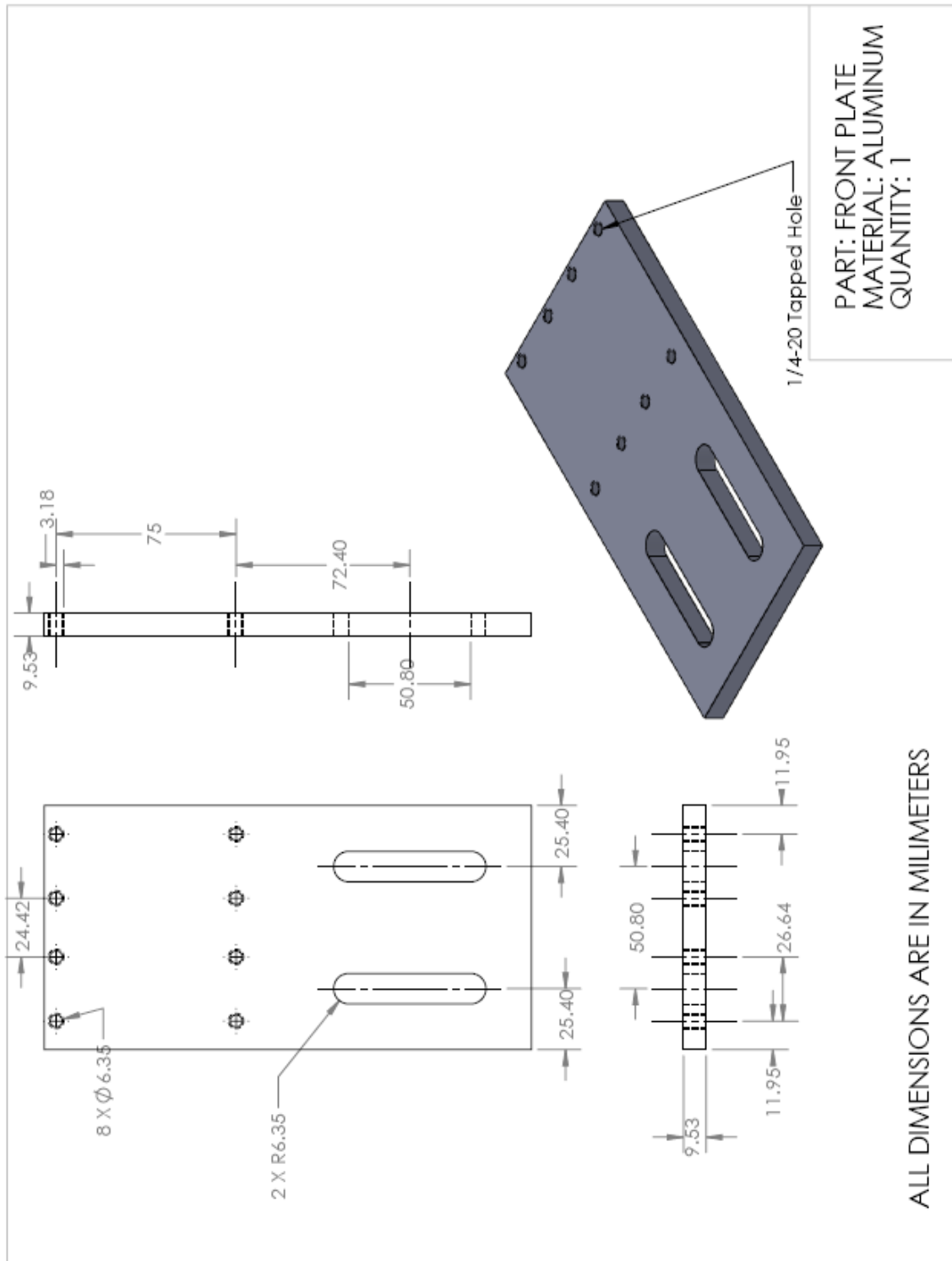
- [60]Khare, R. & Bose, S. Carbon Nanotube Based Composites – A Review. *Journal of Minerals & Materials Characterization & Engineering* 4. 31-46 (2005).
- [61]Kostarelos, K. The long and short of carbon nanotube toxicity. *Nature Biotechnology* 7. 774-776 (2008)
- [62]Mironov, V.S., Kim, J.K., Park, M., Lim, S. & Cho, W.,K. Comparison of electrical conductivity data obtained by four-electrode and four-point probe methods for graphite-based polymer composites. *Polymer Testing* 26. 547-555 (2007).
- [63]Shanov, V., Yun, Y.H. & Schulz, M.J. Synthesis and characterization of carbon nanotube materials (Review). *Journal of the University of Chemical Technology and Metallurgy* 41. 377-390 (2006).
- [64]Keivani, M.B., Zare, K., Aghaie, M., Aghaie, H. & Monajjemi, M. Synthesis of Nano Conducting Polymer Based Polyaniline and its composite: Mechanical Properties, Conductivity and Thermal Studies. *E-Journal of Chemistry* 7. 105-110 (2010).
- [65]Daenen, M., de Fouw, R.D., Hamers, B., Janssen, P.G.A., Schouteden, K. & Veld, M.A.J. The Wondrous World of Carbon Nanotubes “a review of current carbon nanotube technologies. Eindhoven University of Technology. 2003.
- [66]Wen, M., Sun, X., Su, L., Shen, J., Li, J. & Guo, S. The electrical conductivity of carbon nanotube/carbon black/polypropylene composites prepared through multistage stretching extrusion. *Polymer* (2012).
- [67]Seo, M.K. & Park, S.J. Electrical resistivity and rheological behaviors of carbon nanotubes-filled polypropylene composites. *Chemical Physics Letters* 395. 44-48 (2004).
- [68]“Silver-Filled Epoxy Cement.” NEYCO. Retrieved at [www.neyco.fr](http://www.neyco.fr).
- [69] Yue, J.J. “Energy Concepts for Fracture.” Virginia Tech. Retrieved at [http://www.sv.vt.edu/classes/MSE2094\\_NoteBook/97ClassProj/anal/yue/energy.html](http://www.sv.vt.edu/classes/MSE2094_NoteBook/97ClassProj/anal/yue/energy.html)

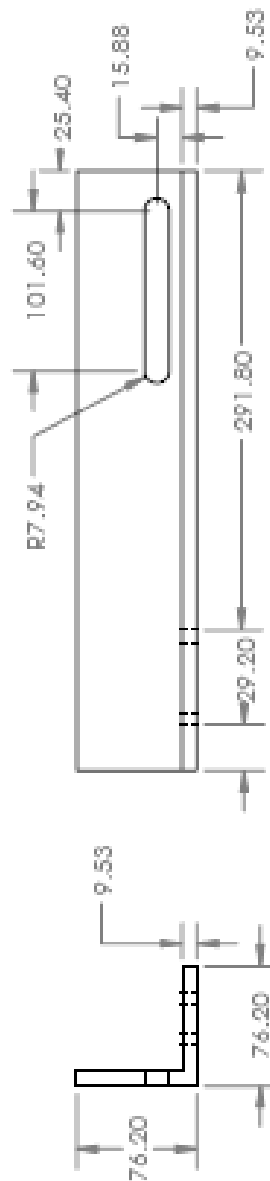
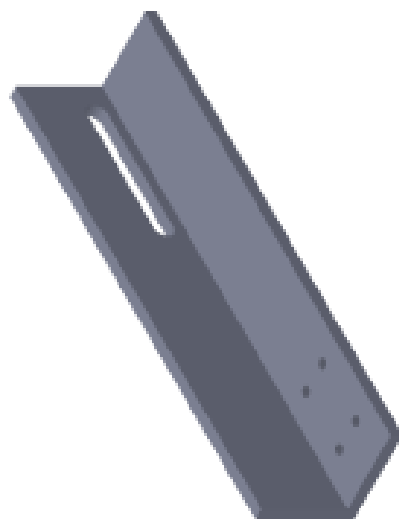


- [70] Mathers, G. "Creep and Creep Testing." TWI. Retrieved at <http://www.twi.co.uk/services/technical-information/job-knowledge/job-knowledge-81-creep-and-creep-testing/>
- [71] "Tensile Test." ENGINEERING ARCHIVES. Retrieved at [http://www.engineeringarchives.com/les\\_mom\\_tensiletest.html](http://www.engineeringarchives.com/les_mom_tensiletest.html)
- [72] Askeland, D.R. "Mechanical Testing and Properties." *The Science and Engineering of Materials*. London: Chapman & Hall, 1988. 5<sup>th</sup> Edition at [www.ius.edu.ba/csarioglu/ENS205/ch6.pdf](http://www.ius.edu.ba/csarioglu/ENS205/ch6.pdf)
- [73] "Knowledge-Based Risk on Composite Overwrapped Pressure Vessel Technology." NASA. Retrieved at <http://www.nasa.gov/centers/wstf/laboratories/composite/index.html>
- [74] Hadlington, S. "Nanotube mesh boosts plastic electronics." RSC. Retrieved at <http://www.rsc.org/chemistryworld/News/2008/July/24070801.asp>
- [75] "Conductive Polymers: Plastic Electronics." Dickinson College. Retrieved at <http://blogs.dickinson.edu/mindmeetsmatter/category/conductive-polymers-plastic-electronics/>
- [76] Abernathy, J.H. "New Coating For Joint Replacements Kills Germs." AQUAPOUR. Retrieved at <http://aquapour.com/new-coating-for-joint-replacements-kills-germs/554671/>
- [77] "HDPE." MATBASE. Retrieved at <http://www.matbase.com/material/polymers/commodity/hdpe/properties>
- [78] "Chromium Element Facts." CHEMICOOOL. Retrieved at <http://www.chemicool.com/elements/chromium.html>
- [79] "ASTM D991 Test Fixture Model 831." Electro-tech system, inc. Retrieved at [www.electrotechsystems.com](http://www.electrotechsystems.com).

**APPENDIX A:**

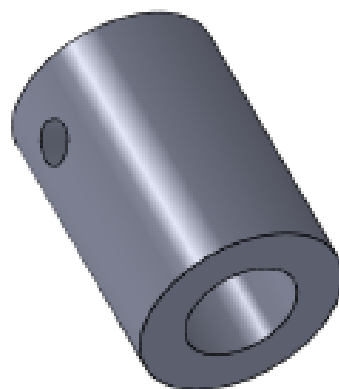
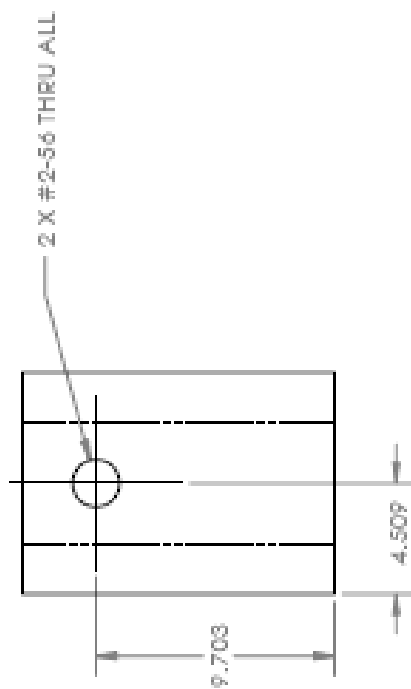
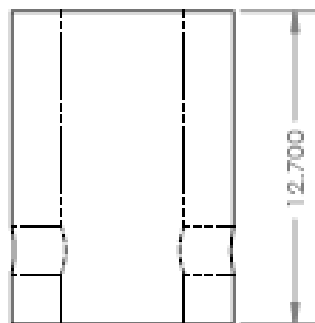
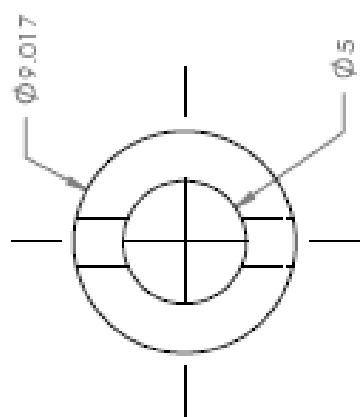
**Engineering Drawings**





PART: BACK PLATE  
 MATERIAL: ALUMINUM  
 QUANTITY: 1

ALL DIMENSIONS ARE MILLIMETERS



TITLE:

Bracket Coupler  
- Thao Nguyen -

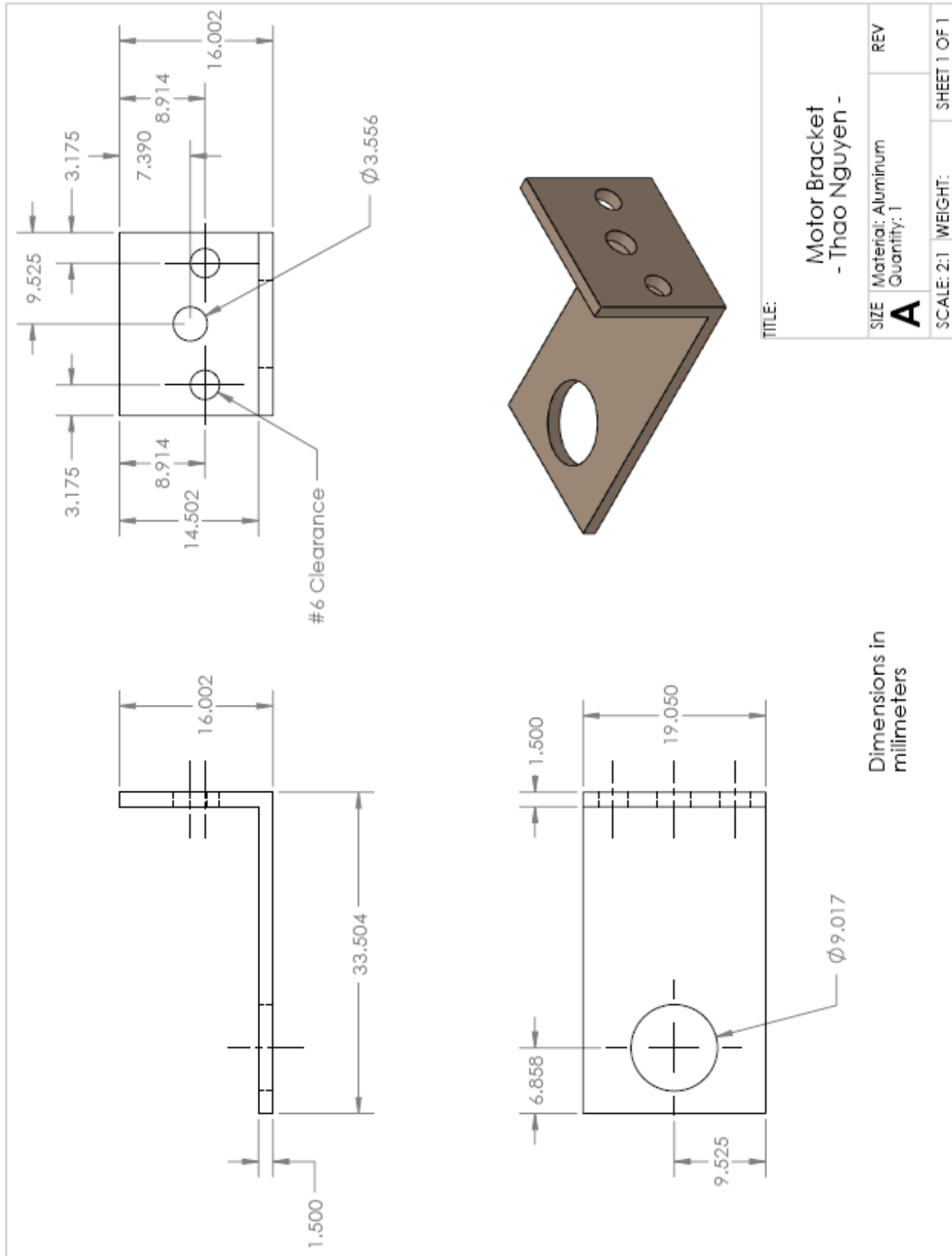
SIZE: Material: Aluminum  
Quantity: 1

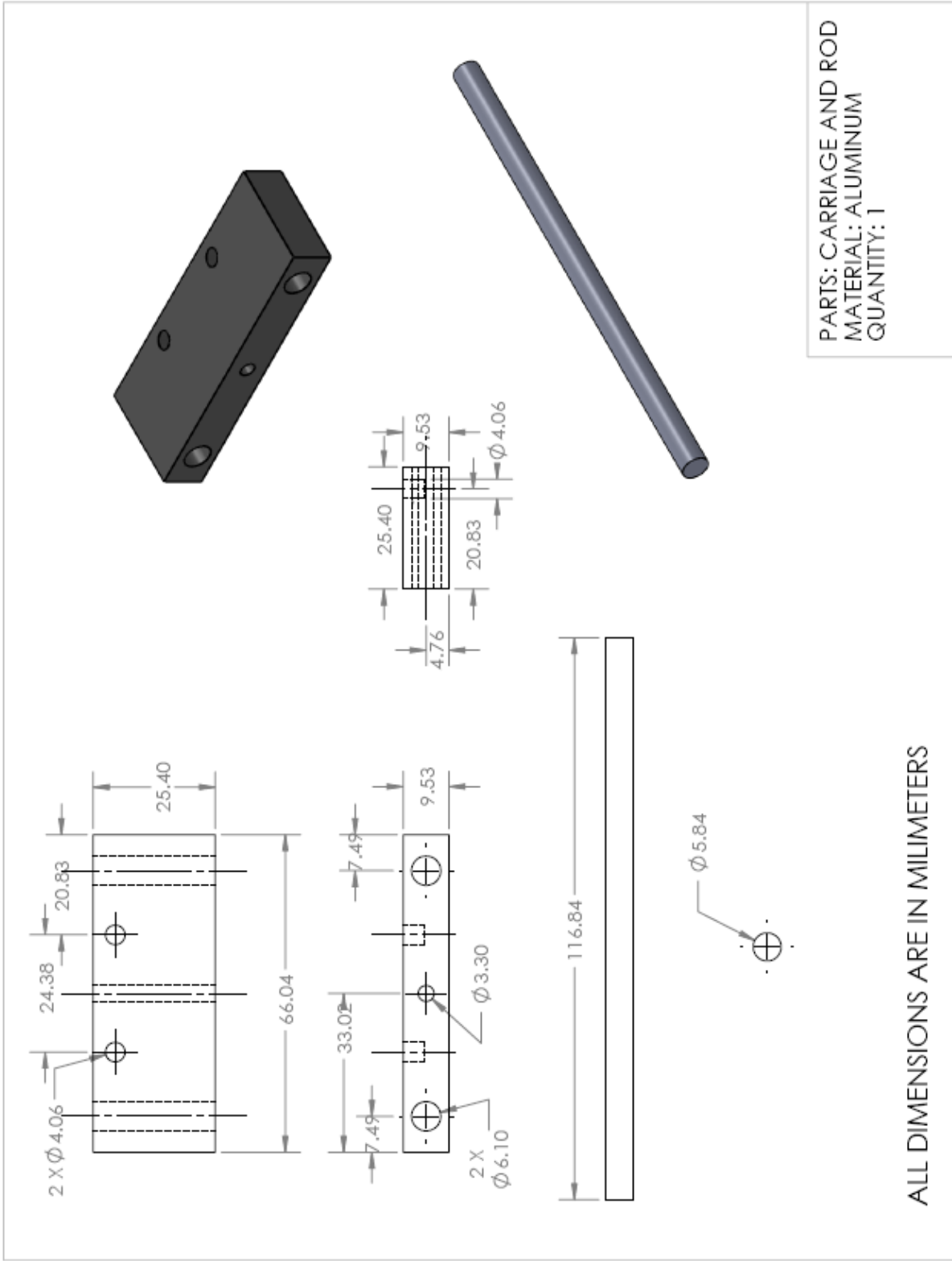
**A**

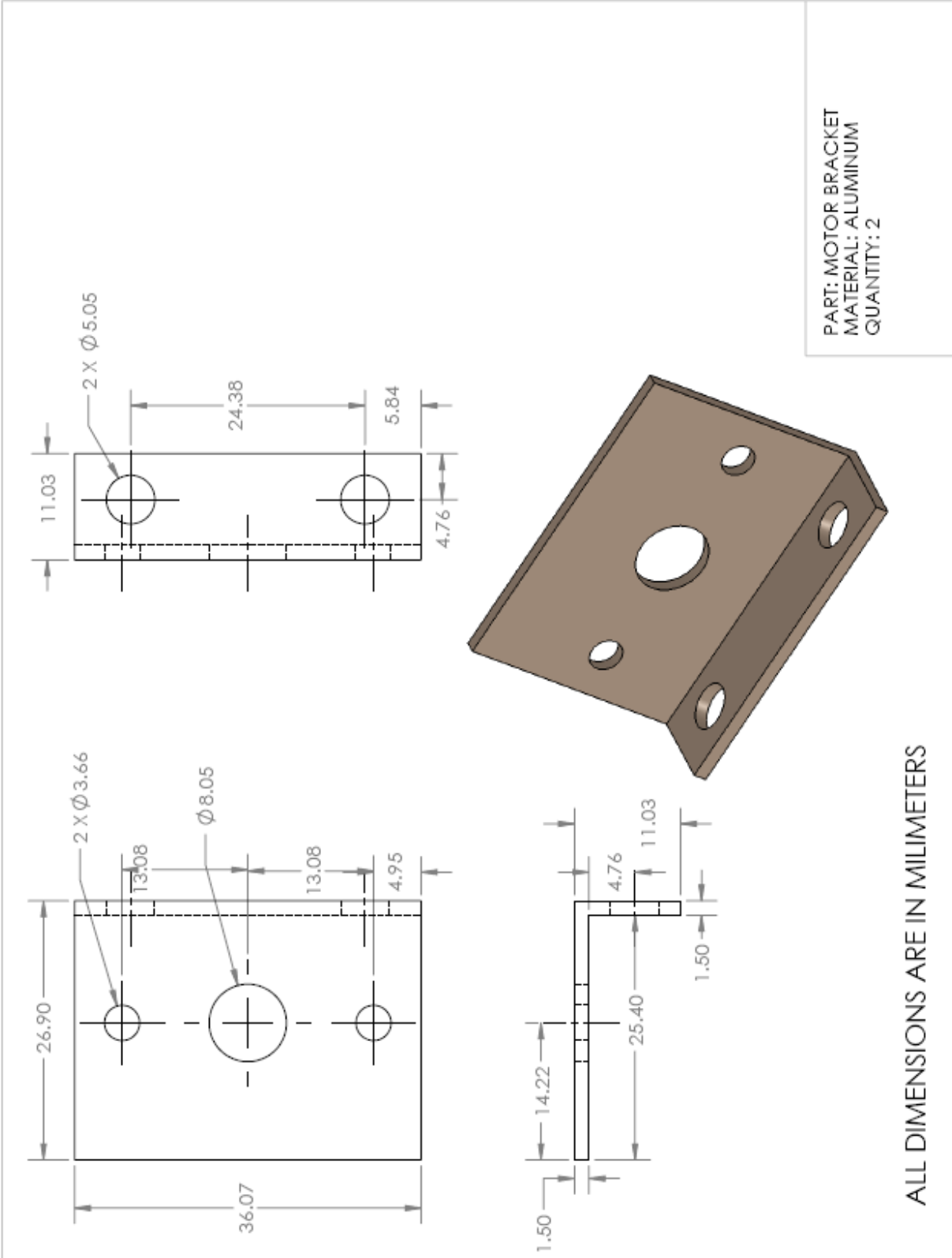
REV

SCALE: 4:1 WEIGHT: SHEET 1 OF 1

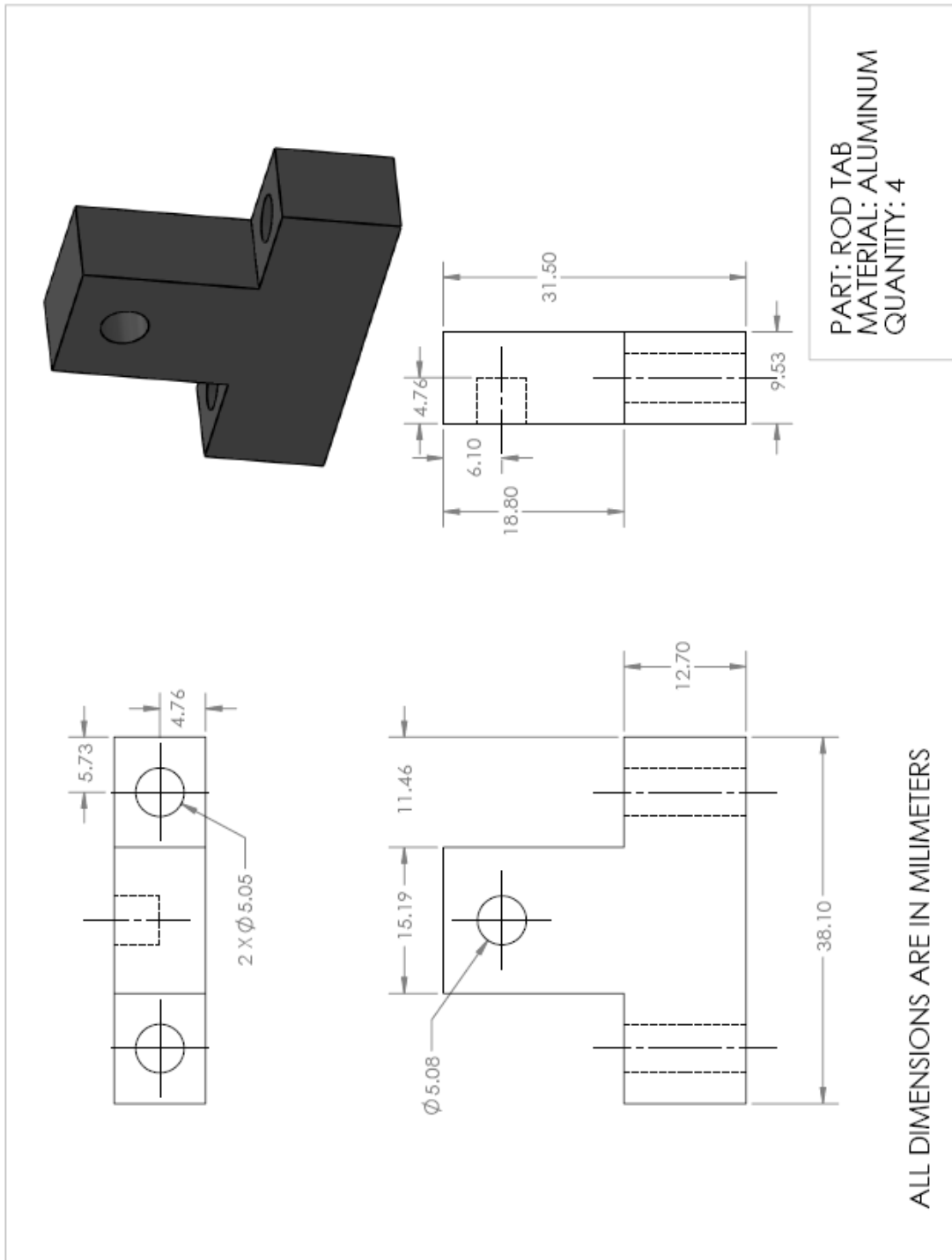
Dimensions in millimeters











**ARDUINO CODING:**

```
#include <AFMotor.h>

AF_Stepper motor1(64, 1);

AF_Stepper motor2(100, 2);

int moveCnt = 0;

int stepCnt = 0;

int done = 0;

int pause = 0;

int forward = 1;

int newMove = 1;

const int buttonPin = 2;

const int ledPin = 10;

const int backupPin = 9;

//-----

void setup()
{

  Serial.begin(9600);    // set up Serial library at 9600 bps

  Serial.println("Stepper test!");

  pinMode(buttonPin, INPUT);

  pinMode(backupPin, INPUT);

  pinMode(ledPin, OUTPUT);
```

```
motor2.setSpeed(100);  
motor1.setSpeed(200);  
motor2.release();  
motor1.release();  
  
}  
  
void loop()  
{  
  
if (!done)  
{  
    if (digitalRead(buttonPin))  
    {  
        digitalWrite(ledPin, HIGH);  
        delay(2000);  
        Serial.println("Button Pin");  
        digitalWrite(ledPin, LOW);  
        motor2.step(100, BACKWARD, SINGLE);  
        stepCnt = stepCnt - 100;  
        newMove = 1;  
        forward = 0;  
  
    }  
}
```

```
else if (digitalRead(backupPin))
{
  Serial.println(moveCnt);
  delay(2000);
  if (newMove)
  {
    moveCnt = moveCnt + 1;
  }      if (moveCnt%2)
  {      motor1.step(530, BACKWARD, SINGLE);
  }
  else
  {
    motor1.step(530, FORWARD, SINGLE);
  }
  forward = 1;
  motor2.step(150, FORWARD, SINGLE);
  stepCnt = stepCnt + 100;
  if(moveCnt == 4)
  {
    done = 1;
    Serial.println("STOP!");
  }
  newMove = 0;
}
```

```
    else if (forward)
    {
        Serial.println("FORWARD");
        motor2.step(100, FORWARD, SINGLE);
        stepCnt = stepCnt + 100;
    }
    else
    {
        Serial.println("BACKWARD");
        motor2.step(100, BACKWARD, SINGLE);
        stepCnt = stepCnt - 100;
    }
}
}
```

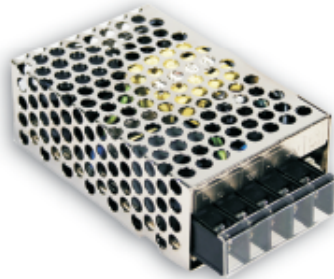
**APPENDIX B:**

**Technical Details of Commercial Components**



## 25W Single Output Switching Power Supply

## RS-25 series



## ■ Features :

- Universal AC input / Full range
- Protections: Short circuit / Overload / Over voltage
- Cooling by free air convection
- LED indicator for power on
- 100% full load burn-in test
- All using 105°C long life electrolytic capacitors
- Withstand 300VAC surge input for 5 second
- High operating temperature up to 70°C
- Withstand 5G vibration test
- No load power consumption < 0.5W
- High efficiency, long life and high reliability
- 3 years warranty



## SPECIFICATION

MODEL	RS-25-3.3	RS-25-5	RS-25-12	RS-25-15	RS-25-24	RS-25-48	
OUTPUT	DC VOLTAGE	3.3V	5V	12V	15V	24V	48V
	RATED CURRENT	6A	5A	2.1A	1.7A	1.1A	0.57A
	CURRENT RANGE	0 ~ 6A	0 ~ 5A	0 ~ 2.1A	0 ~ 1.7A	0 ~ 1.1A	0 ~ 0.57A
	RATED POWER	19.8W	25W	25.2W	25.5W	26.4W	27.36W
	RIPPLE & NOISE (max.) Note.2	80mVp-p	80mVp-p	120mVp-p	120mVp-p	120mVp-p	200mVp-p
	VOLTAGE ADJ. RANGE	2.85 ~ 3.6V	4.75 ~ 5.5V	10.8 ~ 13.2V	13.5 ~ 16.5V	22 ~ 27.6V	42 ~ 54V
	VOLTAGE TOLERANCE Note.3	±3.0%	±2.0%	±1.0%	±1.0%	±1.0%	±1.0%
	LINE REGULATION Note.4	±0.5%	±0.5%	±0.5%	±0.5%	±0.5%	±0.5%
	LOAD REGULATION Note.5	±2.0%	±1.0%	±0.5%	±0.5%	±0.5%	±0.5%
	SETUP, RISE TIME	1800ms, 23ms/230VAC      4000ms, 30ms/115VAC at full load					
HOLD UP TIME (Typ.)	80ms/230VAC      14ms/115VAC at full load						
INPUT	VOLTAGE RANGE	88 ~ 264VAC      125 ~ 373VDC (Withstand 300VAC surge for 5sec. Without damage)					
	FREQUENCY RANGE	47 ~ 63Hz					
	EFFICIENCY (Typ.)	73.5%	78.5%	81.5%	83.5%	86%	85%
	AC CURRENT (Typ.)	0.7A/115VAC      0.4A/230VAC					
	INRUSH CURRENT (Typ.)	COLD START 30A/230VAC					
LEAKAGE CURRENT	<2mA / 240VAC						
PROTECTION	OVERLOAD	110 ~ 180% rated output power Protection type : Hiccup mode, recovers automatically after fault condition is removed					
	OVER VOLTAGE	3.8 ~ 4.45V	5.75 ~ 6.75V	13.8 ~ 16.2V	17.25 ~ 20.25V	27.6 ~ 32.4V	55.2 ~ 64.8V
ENVIRONMENT	WORKING TEMP.	-20 ~ +70°C (Refer to output load derating curve)					
	WORKING HUMIDITY	20 ~ 90% RH non-condensing					
	STORAGE TEMP., HUMIDITY	-40 ~ +85°C, 10 ~ 95% RH					
	TEMP. COEFFICIENT	±0.03%/°C (0 ~ 50°C)					
	VIBRATION	10 ~ 500Hz, 5G 10min./cycle, period for 60min. each along X, Y, Z axes					
SAFETY & EMC (Note 6)	SAFETY STANDARDS	UL60950-1, TUV EN60950-1 approved					
	WITHSTAND VOLTAGE	I/P-O/P: 3KVAC    I/P-FG: 1.5KVAC    O/P-FG: 0.5KVAC					
	ISOLATION RESISTANCE	I/P-O/P, I/P-FG, O/P-FG: 100M Ohms / 500VDC / 25°C / 70% RH					
	EM CONDUCTION & RADIATION	Compliance to EN55022 (CISPR22) Class B					
	HARMONIC CURRENT	Compliance to EN61000-3-2, -3					
OTHERS	EMS IMMUNITY	Compliance to EN61000-4-2, 3, 4, 5, 6, 8, 11; ENV50204, light industry level, criteria A					
	MTBF	309.7Khrs min.    ML-HDBK-217F (25°C)					
	DIMENSION	78*51*28mm (L*W*H)					
	PACKING	0.2Kg, 60pcs/13Kg/0.46CUFT					
NOTE	<p>1. All parameters NOT specially mentioned are measured at 230VAC input, rated load and 25°C of ambient temperature.</p> <p>2. Ripple &amp; noise are measured at 20MHz of bandwidth by using a 12" twisted pair-wire terminated with a 0.1µf &amp; 47µf parallel capacitor.</p> <p>3. Tolerance : Includes set up tolerance, line regulation and load regulation.</p> <p>4. Line regulation is measured from low line to high line at rated load.</p> <p>5. Load regulation is measured from 0% to 100% rated load.</p> <p>6. The power supply is considered a component which will be installed into a final equipment. The final equipment must be re-confirmed that it still meets EMC directives. For guidance on how to perform these EMC tests, please refer to "EMI testing of component power supplies." (as available on <a href="http://www.meanwell.com">http://www.meanwell.com</a>)</p>						



**Mechanical Specification** Case No.931A Unit:mm

Pin No.	Assignment	Pin No.	Assignment
1	ACL	4	DC OUTPUT -V
2	AC IN	5	DC OUTPUT +V
3	FG $\perp$		

**Block Diagram** fosc: 60KHz

**Derating Curve** **Static Characteristics (24V)**

File Name:RS-25-SPEC 2010-10-18

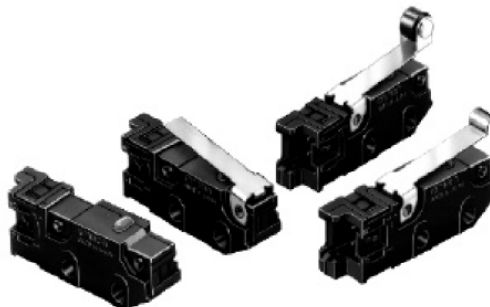


OMRON


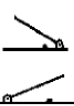
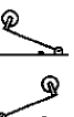
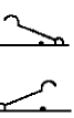
## Subminiature Snap Action Switch D3M

### Saves Wiring Effort, Production Steps, and Time

- Easy wiring ensured through the Quick-Connect Terminals
- External actuator mounts in either of two directions
- Horizontal layout of terminals saves mounting space
- Same internal mechanism as the OMRON SS Subminiature Snap Action Switch
- RoHS Compliant



### Ordering Information

Actuator	Actuator mounting position	Contact type	Model
Pin plunger 	—	SPST-NC	D3M-01
		SPST-NO	D3M-01-3
Hinge lever 	High ratio operating position	SPST-NC	D3M-01K1
		SPST-NO	D3M-01K1-3
	Standard operating position	SPST-NC	D3M-01L1
		SPST-NO	D3M-01L1-3
Hinge roller lever 	High ratio operating position	SPST-NC	D3M-01K2
		SPST-NO	D3M-01K2-3
	Standard operating position	SPST-NC	D3M-01L2
		SPST-NO	D3M-01L2-3
Simulated roller lever 	High ratio operating position	SPST-NC	D3M-01K3
		SPST-NO	D3M-01K3-3
	Standard operating position	SPST-NC	D3M-01L3
		SPST-NO	D3M-01L3-3

### ■ Connectors

Refer to *Wiring* under the Precautions section of this data sheet.

## Specifications

### ■ Characteristics

Permissible operating speed (see note 1)		0.1 mm/s to 1 m/s
Permissible operating frequency	Mechanical	400 operations/min max.
	Electrical	60 operations/min max.
Insulation resistance		100 M $\Omega$ min. at 500 VDC
Contact resistance (initial value)		100 m $\Omega$ max. including connector and 50-mm AWG28 lead wire resistance
Dielectric strength	Between terminals of the same polarity	1,000 VAC at 50/60 Hz for 1 min
	Between charged metal part and ground	1,500 VAC at 50/60 Hz for 1 min
	Between non-charged metal part and each terminal	1,500 VAC at 50/60 Hz for 1 min
Vibration resistance	Malfunction (See Note 2.)	10 to 55 Hz, 1.5-mm double amplitude for 1 ms max. with contacts closed or open.
Shock resistance	Destruction	1,000 m/s <sup>2</sup> (approx. 100G)
	Malfunction (See Note 2.)	300 m/s <sup>2</sup> (approx. 30G) for 1 ms max. with contacts closed or open.
Life expectancy	Mechanical	500,000 operations (at full-stroke operating speed of 10 mm/s at a frequency of 60 operations/min)
	Electrical	200,000 operations (at full-stroke operating speed of 10 mm/s at a frequency of 30 operations/min)
Enclosure rating		IP00
Degree of protection against electric shock		Class I
Proof tracking index (PTI)		175
Ambient temperature	Operating	-25°C to 85°C (with no icing)
Ambient humidity	Operating	85% max.
Weight		Approx. 2 g (pin plunger model)

- Note: 1. The permissible operating speed applies to pin plunger models.  
 2. If a lever actuator model is used, the above vibration resistance conditions will apply when the actuator is in the maximum over-travel position.

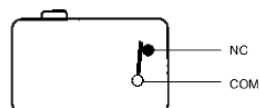
### ■ Operating Characteristics

Characteristics	Part number						
	D3M-01 D3M-01-3	D3M-01K1 D3M-01K1-3	D3M-01L1 D3M-01L1-3	D3M-01K2 D3M-01K2-3	D3M-01L2 D3M-01L2-3	D3M-01K3 D3M-01K3-3	D3M-01L3 D3M-01L3-3
Max. operating force (OF)	153 gf	51 gf	102 gf	51 gf	102 gf	51 gf	102 gf
Min. reset force (RF)	25 gf	6 gf	10 gf	6 gf	10 gf	6 gf	10 gf
Min. pretravel (PT)	0.6 mm	—	—	—	—	—	—
Min. overtravel (OT)	0.4 mm	1.2 mm	0.7 mm	1.2 mm	0.7 mm	1.2 mm	0.7 mm
Max. movement differential (MD)	0.1 mm	0.8 mm	0.6 mm	0.8 mm	0.6 mm	0.8 mm	0.6 mm
Max. free position (FP)	—	14.0 mm	11.5 mm	19.7 mm	17.2 mm	16.2 mm	13.6 mm
Operating position (OP)	8.4 $\pm$ 0.3 mm	10.0 $\pm$ 0.8 mm	9.2 $\pm$ 0.6 mm	15.7 $\pm$ 0.8 mm	14.9 $\pm$ 0.6 mm	12.2 $\pm$ 0.8 mm	11.3 $\pm$ 0.6 mm

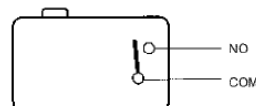
- Note: 1. A tolerance of  $\pm$ 0.4 mm applies to all of the above dimensions unless otherwise specified.  
 2. The operating characteristics apply when each actuator is moved in the direction indicated by the arrow and "A."

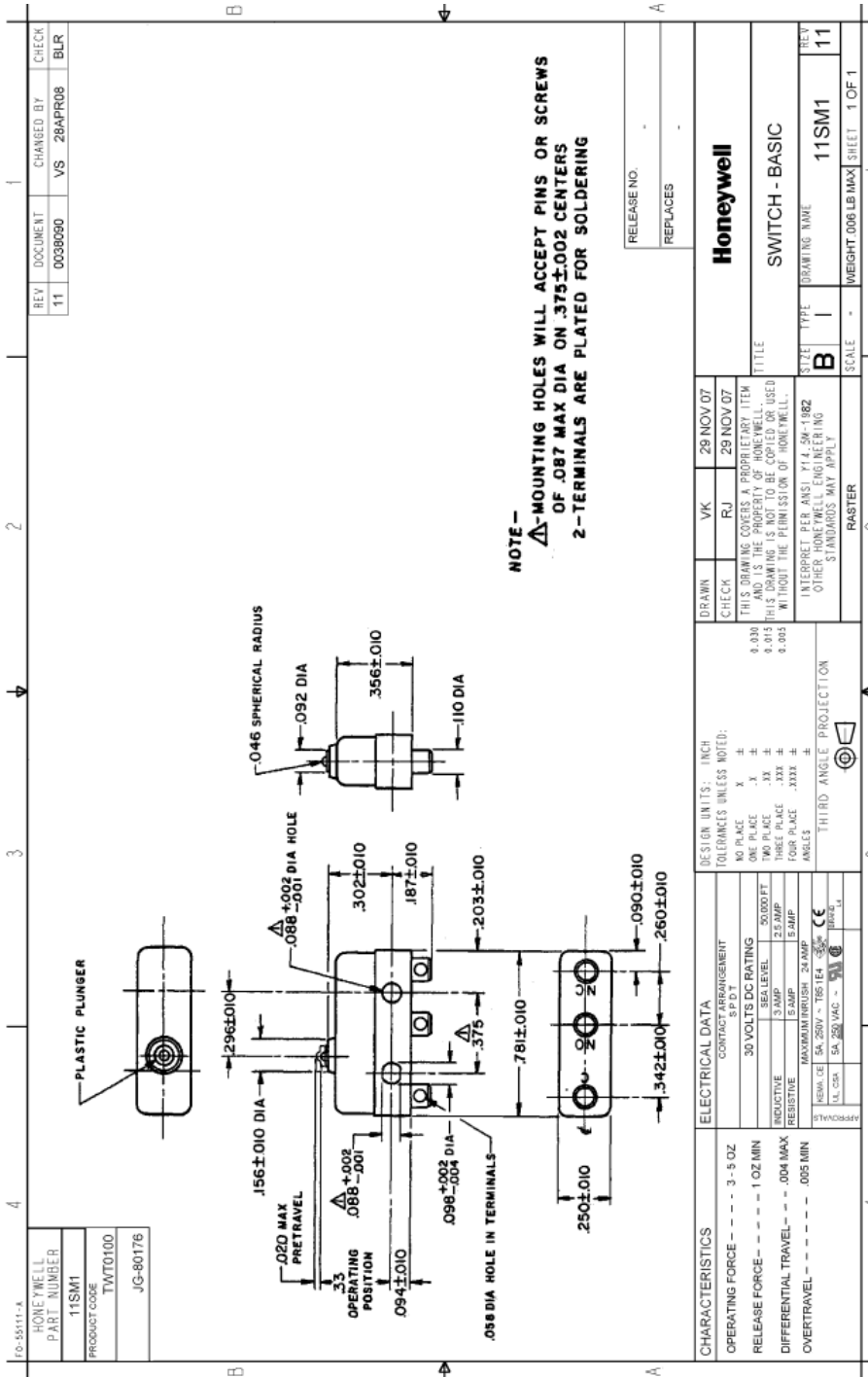
### ■ Contact Form

SPST-NC



SPST-NO





REV	DOCUMENT	CHANGED BY	CHECK
11	0038090	VS 28APR08	BLR

10-55511-4
HONEYWELL
PART NUMBER
11SM1
PRODUCT CODE
TWV0100
JG-80176

RELEASE NO.	
REPLACES	

DESIGN UNITS: INCH	TOLERANCES UNLESS NOTED:	0.030	0.015	0.005
NO PLACE	.X ±			
ONE PLACE	.X ±			
TWO PLACE	.XX ±			
THREE PLACE	.XXX ±			
FOUR PLACE	.XXXX ±			
ANGLES	.XXX ±			
THIRD ANGLE PROJECTION				

CHARACTERISTICS	OPERATING FORCE - - - - - 3 - 5 OZ
	RELEASE FORCE - - - - - 1 OZ MIN
	DIFFERENTIAL TRAVEL - - - .004 MAX
	OVERTRAVEL - - - - - .005 MIN

ELECTRICAL DATA	CONTACT ARRANGEMENT	30 VOLTS DC RATING	SEA LEVEL	50,000 FT
		2 AMP	2 AMP	2 AMP
		MAXIMUM BURST: 24 AMP		
		UL CQA 5A, 250VAC	UL CQA 5A, 250VAC	UL CQA 5A, 250VAC

DRAWN	VK	29 NOV 07
CHECK	RJ	29 NOV 07
THIS DRAWING COVERS A PROPRIETARY ITEM AND IS THE PROPERTY OF HONEYWELL. THIS DRAWING IS NOT TO BE COPIED OR USED WITHOUT THE PERMISSION OF HONEYWELL.		
INTERPRET PER ANSI Y14.5M-1982 OTHER HONEYWELL ENGINEERING STANDARDS MAY APPLY		

Honeywell
SWITCH - BASIC
11SM1
11
1 OF 1

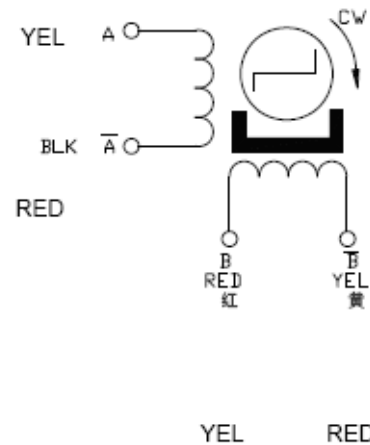
## TSFNA25-150-21-050-LW4



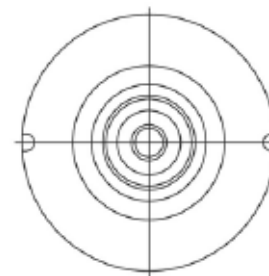
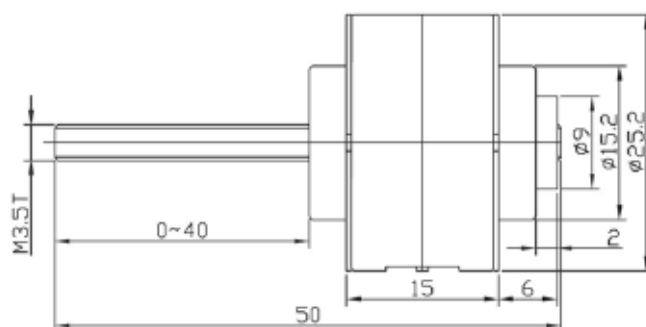
- Permanent Magnet Stepper Motor Actuator
- Precise Motion at a Low Cost
- 30 Newton of Force
- 25 mm diameter
- Screw travels through the motor
- Inexpensively create linear travel

### Specifications

Item	Specifications
Step Angle Accuracy	±8% (full step, no load)
Resistance Accuracy	±10%
Inductance Accuracy	±20%
Temperature Rise	80° C Max
Ambient Temperature	-20°C to +50°C
Insulation Resistance	100MΩMin. .500VDC
Dielectric Strength	500VAC for one minute
Shaft Radial Play	0.08Max. (450 g-load)
Shaft Axial Play	0.08Max. (450 g-load)
Screw Type	M3.5



Model	Step Angle (deg)	# of Wires	Voltage (V)	Current per Phase (A)	Resistance Per Phase (ohms)	Force (N)	Travel (mm)	Screw Type
TSFNA25-150-21-050-LW4	15	4	12	0.5	24	30	40	M3.5



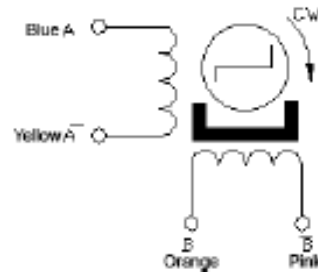
## TGM24-056-19-5V-020A-64R-LW4



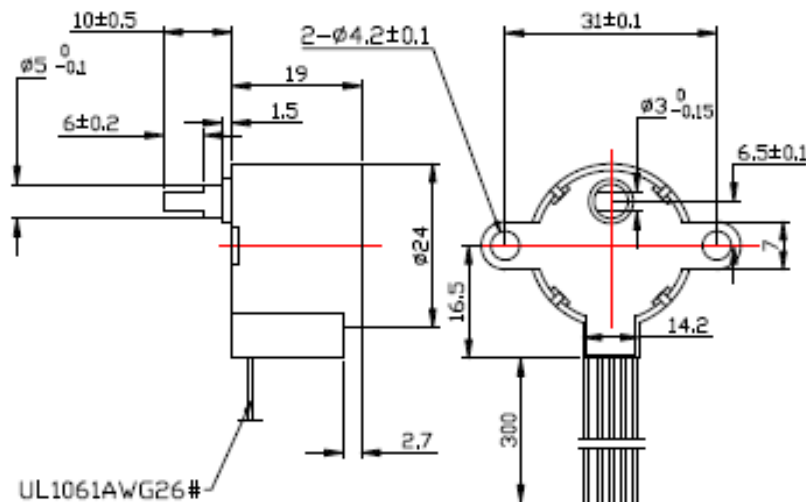
- Permanent Magnet Stepper GearMotor
- High torque in a Small Package at a Low Cost
- 300 g-cm of Torque
- 64:1 gear Ratio
- 24 mm diameter

### Specifications

Item	Specifications
Step Angle Accuracy	± 7% (full step, no load)
Resistance Accuracy	± 10%
Inductance Accuracy	± 20%
Temperature Rise	80° C Max
Ambient Temperature	-20°C to +50°C
Insulation Resistance	100MΩ Min., 500VDC
Dielectric Strength	500VAC for one minute



Model	Step Angle (deg)	Gear Ratio	# of Wires	Voltage (V)	Current per Phase (A)	Holding Torque (g.cm)	Detent Torque (g.cm)
TGM24-056-19-5V-020A-64R-LW4	5.625	64:1	4	5	0.20	300	150



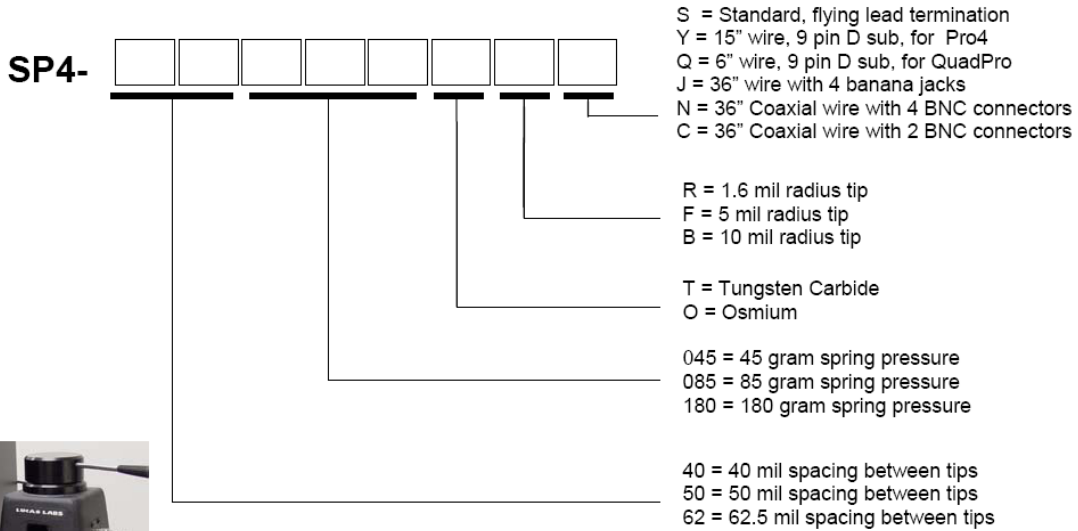
# SIGNATONE

Lucas / Signatone Corporation – Since 1968

393-J Tomkins Court • Gilroy, California 95020-3632 • USA  
 Tel: 408-848-2851 • Fax: 408-848-5763  
 e-mail: [sales@signatone.com](mailto:sales@signatone.com) web: [www.signatone.com](http://www.signatone.com)

## Lucas/Signatone Four Point Probe Part Numbers

### Standard Head (Delrin)

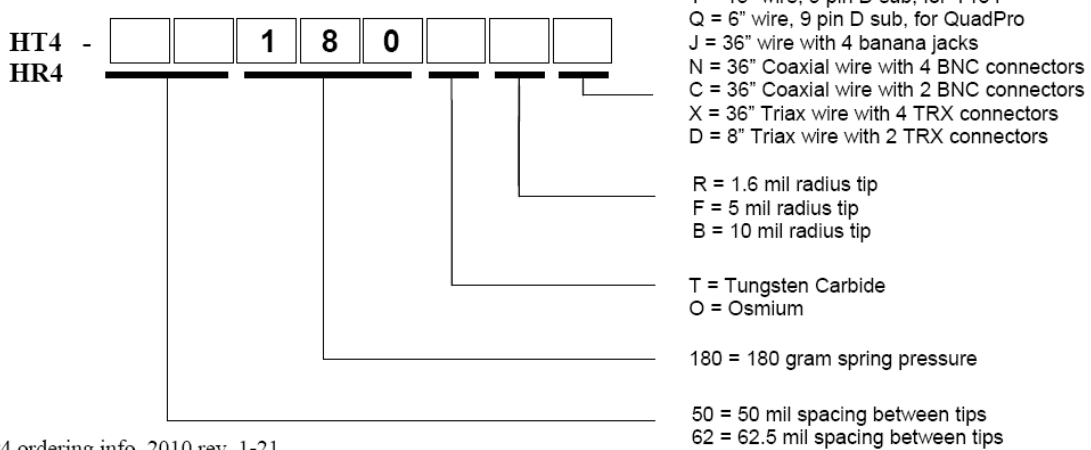


Sample Part Numbers:

SP4-62085TRY

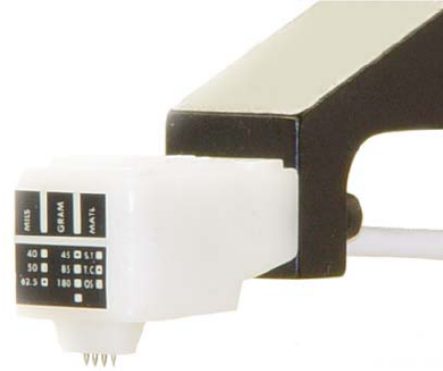
HT4-50180ORY

### High Temperature or High Resistance Head (Macor)



## SP4 Four Point Probe Head

The SP4 probe head is designed for use with Lucas/Signatone and other resistivity probing systems for the measurement of thin films and materials. The SP4 head has several configuration parameters permitting users to define the probe head best for their application.



### Spacing between tips

0.0625 inches (62)  
0.050 inches (50)  
0.040 inches (40)

### Pressure on each probe tip

45 grams (045)  
85 grams (085)  
180 grams (180)

### Probe tip material

Osmium (O)  
Tungsten Carbide (T)

### Tip radius

0.0016 inches [1.6mil] (R)  
0.005 inches [5 mil] (F)  
0.010 inches [10 mil] (B)

### Electrical Connection option

Flying lead termination, 15" wire (S)  
9 pin D sub with 15" wire (Y)  
9 pin D sub with 6" wire (Q)  
4 36" wires with Banana Jacks (J)\*  
4 36" coax wires with BNC (N)\*  
2 36" coax wires with BNC (C)\*  
4 36" Triax wire with TRX (HT4) (X)\*  
2 8" Triax wire with TRX (HT4) (D)\*

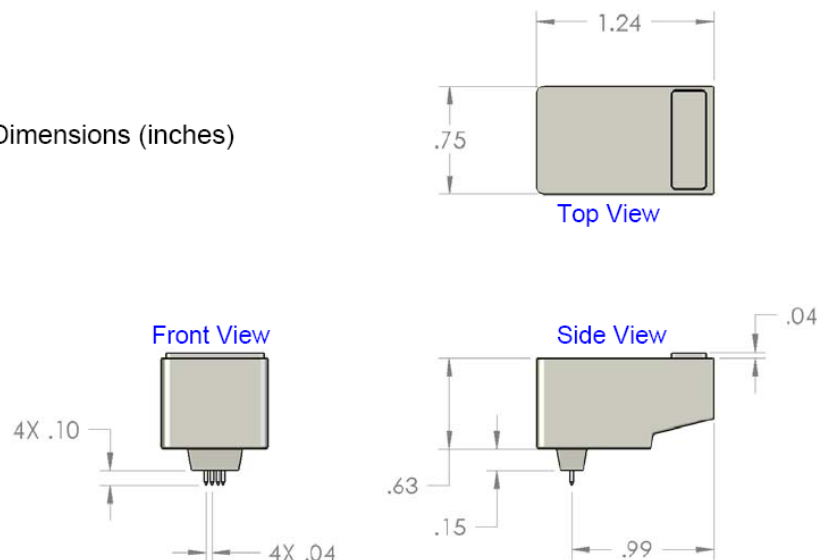
\* for direct connection to various meters

### Ordering Model Maker Information

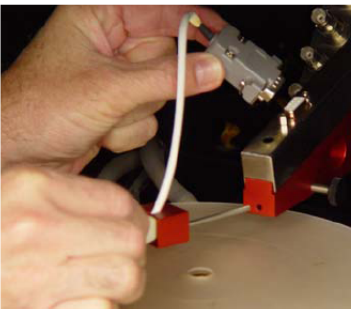
SP4-[Spacing][Pressure][Material][Radius][Termination]

Sample Part Number: [SP4-40085TRS](#)

Dimensions (inches)



### Mounting Options L-4PQM Quick Mounting Block



Use the L-4PQM to mount the SP4 and HT4 probe heads to any late model Lucas / Signatone Corp. resistivity test stand.

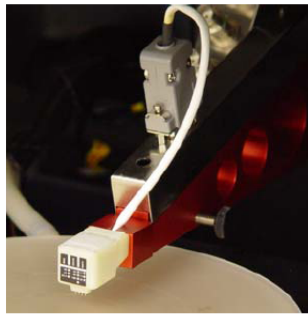
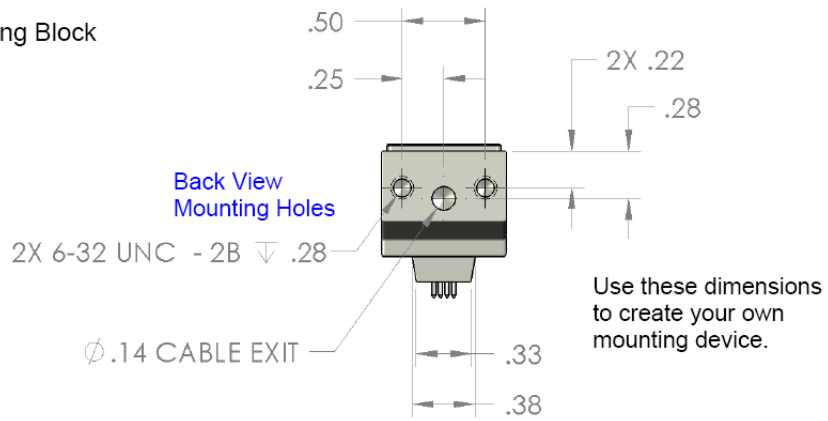


Photo: L-4PQM quick mounting block, holding SP4-62085TRQ mounted to our QuadProS-A8 resistivity test station.

### FAQ: How do I choose the best SP4 or HT4 for my application?

#### SELECTING THE BEST 4 POINT PROBE HEAD FOR YOUR APPLICATION

Choosing the right probe head is a matter of selecting the best spring pressure, probe tip radius, material and probe tip spacing for your application. The following is a guide for making the best selection; however, experience has shown best results are achieved by using guidelines to select the initial probe head, then experimenting with different spring pressures or materials to match the characteristics of your application.

**Spring Pressure:** The spring pressure is the pressure used to force each individual probe tip onto the sample surface to make electrical or ohmic contact. Lucas Signatone offers 45 gram, 85 gram and 180 gram spring pressures for standard probe heads (SP4 series) for testing below temperatures of 90 degrees C. Probe heads for use at higher temperatures (the HT4 series) have 180 gram spring pressures. The physical characteristics of the sample determine the correct spring pressure as follows:

- A. For easily contacted films such as metal films or soft films such as conductive polymers or very thin films, start with the lowest spring pressure that gives satisfactory contact, usually 45 grams.



- B. For difficult to contact samples such as high resistivity silicon or similar materials which naturally form a nonconductive layer when exposed to an air ambient, start with the high spring pressure of 180 grams. Note: Nonconductive layers may form when samples experience high temperatures; therefore, HT4 high temperature probes use 180 gram spring pressures.
- C. For intermediate or unknown films start with an 85 gram spring pressure probe.

**Probe Tip Radius:** Lucas Signatone probe tips are micro-machined to have the shape of a section of a sphere at the tip. 1.6 mil, 5 mil, and 10 mil tip radii are available. Generally the large tip radius probes are more robust, but it is more difficult to make good electrical contact with these probes. Use the following guide for the selection of tip radius:

- A. For easily contacted films and thin films start with a 5 mil tip radius.
- B. For very thin films start with a 10 mil probe tip radius.
- C. All other applications start with the standard 1.6 mil probe tip radius.

**Probe Tip Material:** Lucas Signatone offers 4 point probes with tips of either Tungsten Carbide or Osmium. Tungsten Carbide is a crystalline material that is very hard and can be broken along the crystal boundaries with horizontal motion of the probe. Osmium is an amorphous material and is also hard, but is more forgiving to small horizontal motion. It is believed that Osmium will give longer performance or more touch downs than Tungsten carbide, but it is slightly more expensive. Also, Osmium has the physical characteristic (work function) such that it can make better contact with some exotic materials. The following is suggested:

- A. For laboratory and low volume usage start with Tungsten Carbide.
- B. For production environment probing or contacting many points on the sample consider Osmium. Also, consider trying Osmium to improve contact.

**Probe Spacing:** The probes have a constant spacing, S, between each of the 4 tips. Lucas Signatone products use software with correction algorithms allowing for probing near the edge of the sample (to within a proximity of 4 x S) with 1% accuracy. Generally larger probe tip spacings give better results. Please use the following guide.

- A. For samples with geometry greater than 0.5 inch in diameter use 0.0625 inch (62.5 mils) spacing.
- B. For smaller samples or for probing closer than 0.25 inch to the edge use 0.040 (1mm or 40 mils) spacing.

<http://www.fourpointprobe.com/applications/resistivity.asp>

### \$\$\$ SP4 / HT4 Pricing \$\$\$

For pricing, please configure the part number by using the above information, then send us an e-mail at: [Sales@Signatone.com](mailto:Sales@Signatone.com)

## Four Point Probe Theory

Resistivity,  $Rho$ , is a particularly important semiconductor parameter because it can be related directly to the impurity content of a sample; the four point probe is the apparatus typically used to determine bulk Resistivity.

The mobility of the carriers depends upon temperature, crystal defect density, and ALL impurities present. Hall Effect Measurements can determine the mobility of the carriers in a given sample to allow for more accurate dopant concentration measurements, but Hall measurements are usually destructive to the sample.

The four point probe contains four thin collinearly placed tungsten wire probes which are made to contact the sample under test. Current  $I$  is made to flow between the outer probes, and voltage  $V$  is measured between the two inner probes, ideally without drawing any current. If the sample is of semi-infinite volume and if the inter-probe spacing is  $s1 = s2 = s3 = s$ , then it can be shown that the Resistivity of the semi-infinite volume is given by:

$$Rho = (\pi s) V/I \quad (1)$$

The subscription in the preceding equation indicates the measured value of the Resistivity and is equal to the actual value,  $Rho$ , only if the sample is of semi-infinite volume. Practical samples, of course, are of finite size. Hence, in general,  $Rho \neq Rho$ . Correction factors for six different boundary configurations have been derived by Valdes (1). These show that in general, if  $l$ , the distance from any probe to the nearest boundary, is at least  $5s$ , no correction is required. For the cases when the sample thickness is  $5s$ , we can compute the true Resistivity from:

$$Rho = a \pi s V/I = Rho \quad (2)$$

Where  $a$  is the thickness correction factor which is plotted (on page 3). From an examination of the plot we see that for values of  $t/s \geq 5$  times the probe spacing, no correction factor is needed. Typical probe spacings are 25-60 mils and the wafers used in most cases are only 10-20 mils, so unfortunately we cannot ignore the correction factor. Looking again at the plot, however, we see that the curve is a straight line for values of  $t/s \leq 0.5$ . Since it is a log-log plot the equation for the line must be of the form:

$$a = K (t/s)^m \quad (3)$$

where  $K$  is the value of  $a$  at  $(t/s) = 1$ , and  $m$  is the slope. Inspection of the plot shows that in this case  $m = 1$ .  $K$  is determined to be 0.72 by extrapolating the linear region up to the value at  $(t/s) = 1$ . (The exact value can be shown to be  $1/(2 \ln 2)$ .) Hence for slices equal to or less than one half the probe spacing  $a = 0.72 t/s$ .

When substituted into the basic equation we get:

$$Rho = a \pi s V/I = 4.53 t V/I, (t/s) \leq 0.5 \quad (4)$$

All samples we will be using in the lab satisfy the one-half relationship so we can use the above formula to determine  $Rho$ . We will perform Resistivity measurements on the starting material for each experiment. The value of  $r$  obtained will be referred to as the bulk Resistivity, and the units are Ohm-cm.

If both sides of the Equation (4) are divided by  $t$  we get:

$$Rs = Rho/t = 4.53 V/I \text{ for } t/s \leq 0.5 \quad (5)$$

which we refer to as sheet resistance. When the thickness  $t$  is very small, as would be the case for a diffused layer, this is the preferred measurement quantity. Note that  $Rs$  is independent of any geometrical dimension and

is therefore a function of the material alone. The significance of the sheet resistance can be more easily seen if we refer to the end-to-end resistance of a rectangular sample. From the familiar resistance formula:

$$R = \text{Rho } l/wt \quad (6)$$

we see that if  $w = l$  (a square) we get:

$$R = \text{Rho}/t = R_s$$

Therefore,  $R_s$  may be interpreted as the resistance of a square sample, and for this reason the units of  $R_s$  are taken to be ohms-per-square or ohm/sq. Dimensionally this is the same as ohms but this notation serves as a convenient reminder of the geometrical significance of sheet resistance.

So far in our discussion of Resistivity measurements we have assumed that the size of our sample is large compared to the probe spacing so that edge effects could be ignored. This is usually the case for the bulk Resistivity measurement. However, our sheet resistance measurements will be made on a "test area" on our wafer and the test area dimensions (nominally 2.9 by 5.8mm) are not that large compared to the probe spacing (25 mils). In order to get accurate measurements we will need to correct for the edge effects. In general then:

$$R_s = C V/I \quad (7)$$

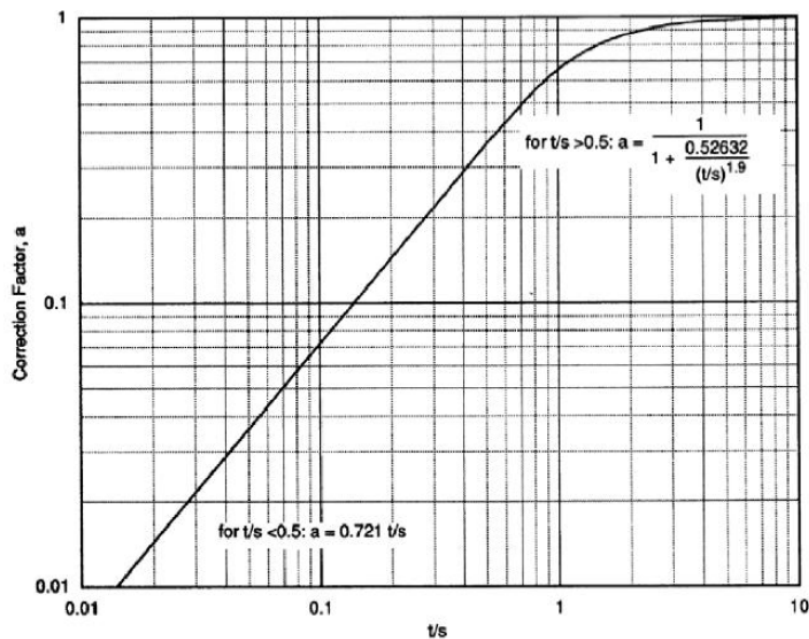
where  $C$  is the correction factor. Note that for  $d/s > 40$ ,  $C = 4.53$ , the value we had as the multiplier in Equation (5).

References:

1. Valdes, L.G., Proc. I.R.E., 42,pp. 420-427 (February 1954)
2. Smits, F. M., "Measurements of Sheet Resistivity with the Four Point Probe," BSTJ, 37, p. 371 (1958). (Same as BT Monograph, 3894, Part 2).

Courtesy of:

ECE344: Theory and Fabrication of Integrated Circuits  
Electrical and Computer Engineering  
University of Illinois – Urbana/Champaign





## LCA710

### Single Pole, Normally Open OptMOS<sup>®</sup> Relay

	LCA710	Units
Blocking Voltage	60	V <sub>p</sub>
Load Current	1	A
Max R <sub>ON</sub>	0.5	Ω

#### Features

- Low On-Resistance: 0.5Ω
- High Current Handling Capability: 1A
- 3750V<sub>peak</sub> Input/Output Isolation
- Small 6-Pin Package
- Low Drive Power Requirements (TTL/CMOS Compatible)
- No Moving Parts
- High Reliability
- Arc-Free With No Snubbing Circuits
- No EMVFI Generation
- Machine Insertable, Wave Solderable
- Surface Mount and Tape & Reel Versions Available

#### Applications

- Instrumentation
  - Multiplexers
  - Data Acquisition
  - Electronic Switching
  - I/O Subsystems
  - Meters (Watt-Hour, Water, Gas)
- Medical Equipment—Patient/Equipment Isolation
- Security
- Aerospace
- Industrial Controls

#### Description

The LCA710 is a 60V, 1A, 0.5Ω, normally open (1-Form-A) solid state relay featuring low on-resistance and high current handling capability. It uses optically coupled MOSFET technology to provide 3750V<sub>peak</sub> of input to output isolation. The efficient MOSFET switches and photovoltaic die use Clare's patented OptoMOS architecture. The optically coupled output is controlled by a highly efficient GaAlAs infrared LED.

The LCA710 can be used to replace mechanical relays, and offers the superior reliability associated with semiconductor devices. Because it has no moving parts, it can offer faster, bounce-free switching in a more compact surface mount or thru-hole package.

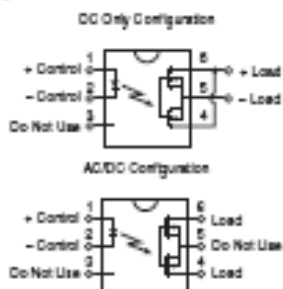
#### Approvals

- UL Recognized Component: File E76270
- CSA Certified Component: Certificate 1175739
- EN/IEC 60950-1 Certified Component: TUV Certificate B 09 07 49410 004

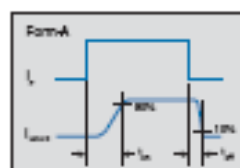
#### Ordering Information

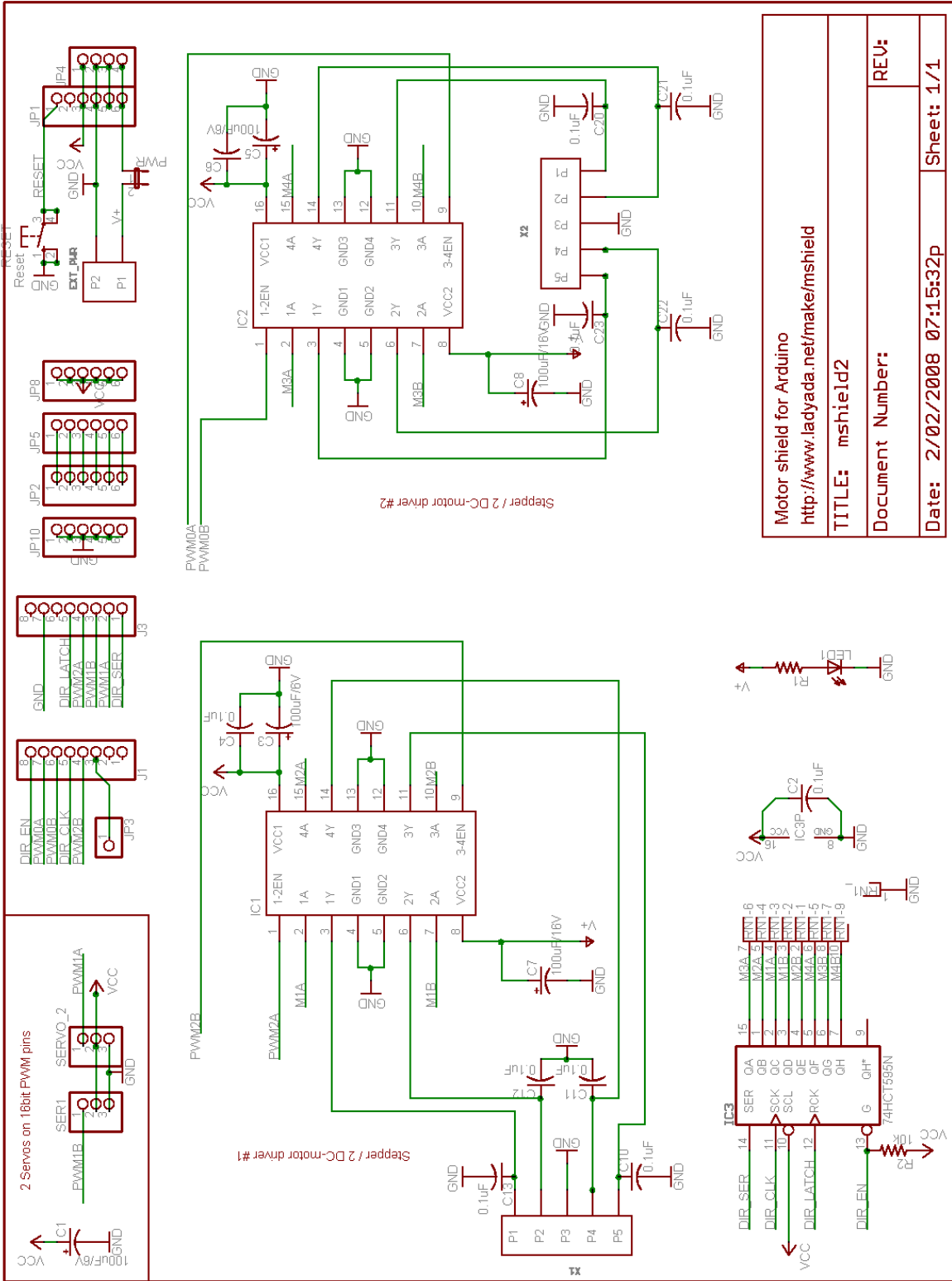
Part #	Description
LCA710	S-Pin DIP (50/Tube)
LCA710S	S-Pin Surface Mount (50/Tube)
LCA710STR	S-Pin Surface Mount (1000/Reel)

#### Pin Configuration



#### Switching Characteristics of Normally Open Devices





Motor shield for Arduino  
<http://www.ladyada.net/make/mshield>  
 TITLE: mshield2  
 Document Number:  
 Date: 2/02/2008 07:15:32p  
 Sheet: 1/1

REV:

Document Number:

Date: 2/02/2008 07:15:32p

Sheet: 1/1

